

En-ROADS Technical Reference

Table of Contents

[Introduction](#)

[Model Structure](#)

[Demand](#)

[Supply](#)

[Market Clearing and Utilization](#)

[Land Use, Land Use Change, and Forestry](#)

[Terrestrial Biosphere Carbon Cycle](#)

[Emissions](#)

[Carbon Dioxide Removal \(CDR\)](#)

[Well-Mixed Greenhouse Gas Cycles](#)

[Climate](#)

[Sea Level Rise](#)

[Damage to GDP](#)

[Other Impacts](#)

[Initialization, Calibration, Model Testing](#)

[References](#)

En-ROADS Technical Reference

Last updated August 2024

Lori S. Siegel¹, Chris Campbell¹, Adem Delibas¹, Sibel Eker¹, Tom Fiddaman³, Travis Franck¹, Khaled Gaafar¹, Jack Homer², Andrew P. Jones¹, Charles Jones¹, Joshua Loughman¹, Stephanie McCauley¹, Elizabeth Sawin¹, Chris Soderquist⁵, John Sterman⁴

¹ Climate Interactive

² Homer Consulting

³ Ventana Systems

⁴ Massachusetts Institute of Technology

⁵ Pontifex Consulting

Introduction

The [En-ROADS Climate Solutions Simulator](#) is a climate simulation tool for understanding how we can achieve our climate goals through changes in energy, land use, consumption, agriculture, and other policies. En-ROADS is a globally aggregated model of energy, economic, land use, and climate systems. The level of aggregation and several simplifying assumptions allow the model to return results in seconds and be accessible to policy makers and general audiences. En-ROADS is a simple climate model and complements the other, more disaggregated models addressing similar questions, such as integrated assessment models or general circulation climate models. Those larger disaggregated models are used for calibrating results in En-ROADS.

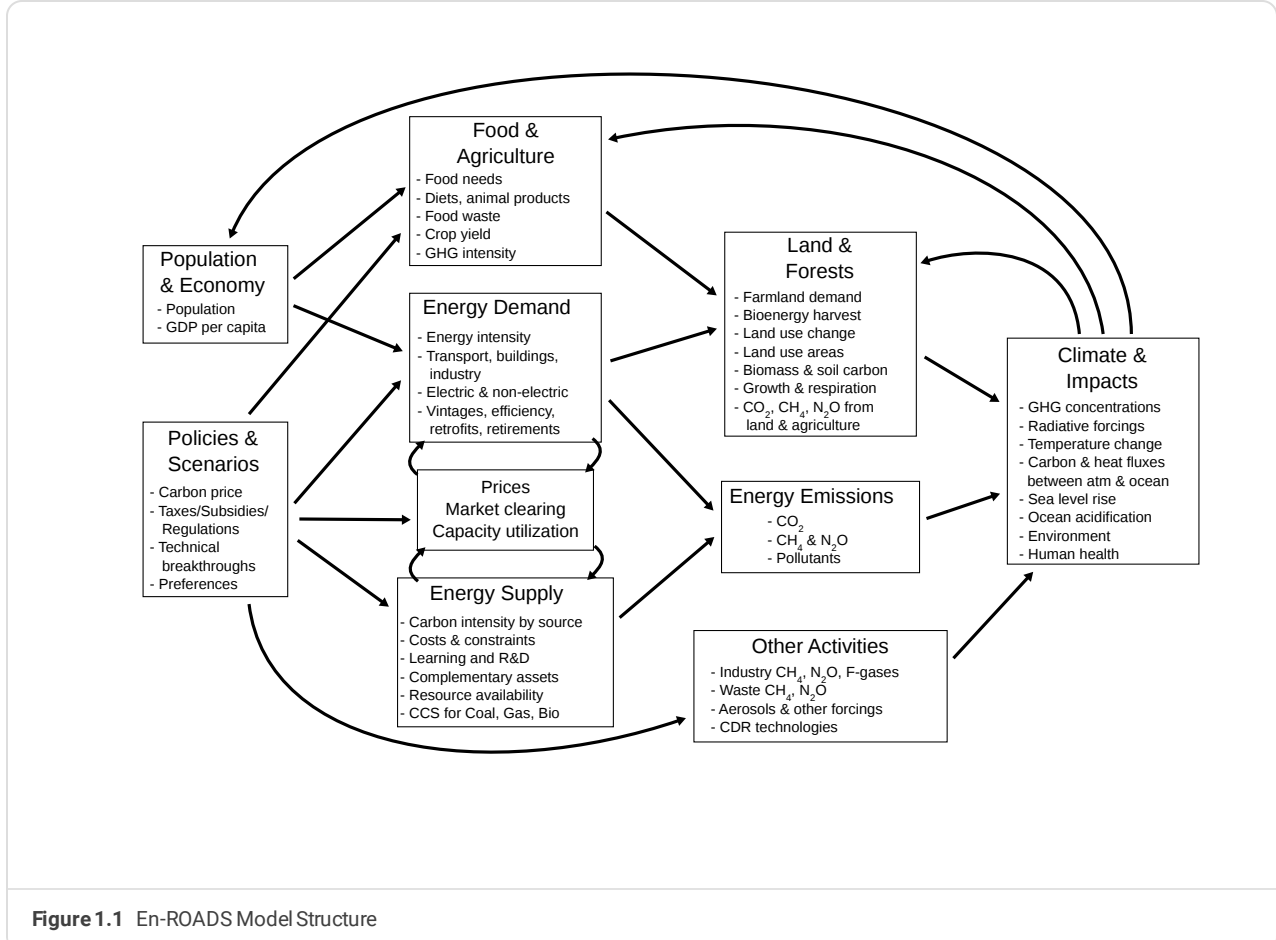


Figure 1.1 En-ROADS Model Structure

En-ROADS is being developed by [Climate Interactive](#), [Ventana Systems](#), [UML Climate Change Initiative](#), and [MIT Sloan](#).

This *En-ROADS Technical Reference* documents the En-ROADS model structure, equations, assumptions, and data sources. In addition, there is an [En-ROADS User Guide](#) more suited to general audiences. For a list of articles about the simulators see our [Peer-reviewed Research page](#). Climate Interactive also provides extensive training materials for En-ROADS at learn.climateinteractive.org.

Please visit support.climateinteractive.org for additional inquiries and support.

Purpose and Intended Use

En-ROADS is designed to be used interactively with groups as a basis for scientifically rigorous conversations about addressing climate change. It is not intended as a tool for prediction or projections, nor does it cover every impact of the economics, energy use, or land use decisions. It is suitable for decision-makers in government, business, and civil society; or for anyone who is curious about the choices of our world.

En-ROADS is also useful for learning about the dynamic behavior of systems in general by highlighting those impacting the climate:

- The differences between high and lower leverage actions
- The response to policies based on incentives, supply-side and demand-side interventions, mandates and technology
- Delays in the system, including capital turnover, momentum in the carbon cycle, social and technological transitions, and more
- Effective and conflicting combination of actions
- The scale of required action, and the unintended consequences of some actions
- The feedback between climate change and economic growth

En-ROADS allows users to adjust many of the assumptions underlying these dynamics.

Model Structure

En-ROADS is a system dynamics model. It consists of a set of ordinary differential equations in time. Variables calculated by integration are called “stocks” (also called “levels”); components of the rate of change of a stock are called “flows”; variables used for intermediate steps or calculating other values include auxiliary, constant, data, and initial variables.

Equations represent both physical processes and human decisions. There is no assumption of equilibrium or optimal decision making. The model represents the climate, environment, economy, and energy systems at the global level of aggregation and at the system-wide level of analysis.

En-ROADS is constructed using Vensim modeling software from Ventana Systems, and transformed into an online simulation via the SD Everywhere converter built by Climate Interactive and Todd Fincannon.

En-ROADS is calibrated to an extensive set of historical data, and its endogenous behavior is grounded in and made consistent with other models, in particular the Integrated Assessment Models used by the Intergovernmental Panel on Climate Change (IPCC).

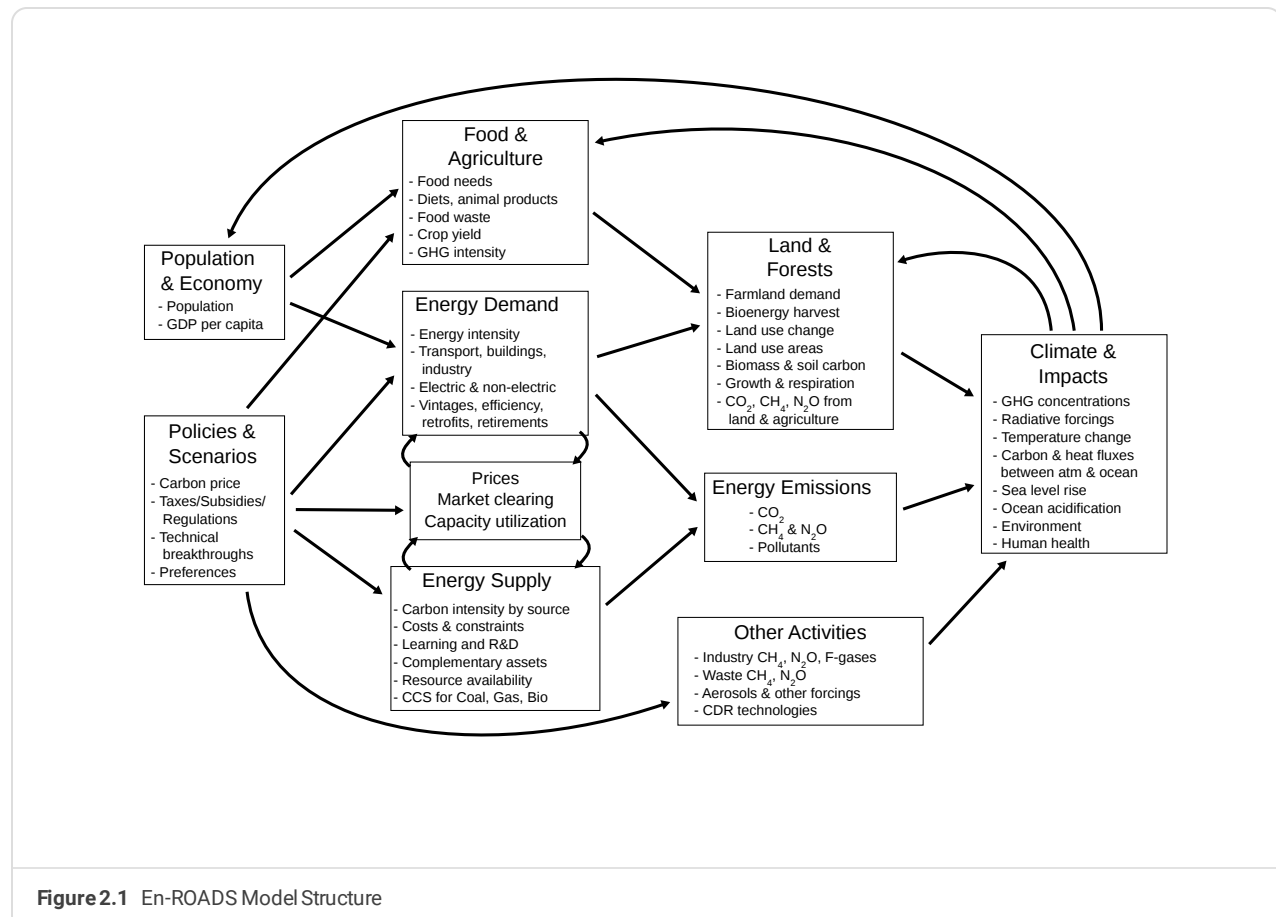
Simulation Method

The differential equations making up En-ROADS are non-linear and have no general closed form solution. Instead they are estimated numerically using the Euler method. At each time step (Δt), auxiliary and flow variables are calculated from previous values of stocks, along with constants and data as needed. Each stock is then computed by adding its previous value to the product of Δt times the sum of all its flows. A sufficiently small time step is required for good approximation - a value of one eighth (0.125) year is appropriate in En-ROADS given the characteristic times and delays in the system as modeled.

En-ROADS starts from initial values in the year 1990 and runs endogenously through 2100. The value of each variable is stored every year. Aside from a small number of exogenous values, the model runs free - calibrated to external data but not driven by data.

Causal Structure

At the highest level, En-ROADS calculates the concentration of each well-mixed greenhouse gas (CO_2 , CH_4 , N_2O , PFCs, SF_6 , and HFCs), in the atmosphere, and the resulting climate change and other impacts. Greenhouse gas concentrations of each gas depend on its global cycle, driven by natural emissions and by anthropogenic emissions from energy, industry, and land use. Energy and industry emissions depend on total consumption (population times consumption per person), energy intensity of consumption, and emission intensity of energy and industry. Agriculture emissions and the land needed for farming depend on population and diets. The impacts of climate change create feedbacks that reduce consumption (by slowing economic growth), increase the land needed for agriculture (by lowering yield), and alter the biosphere.



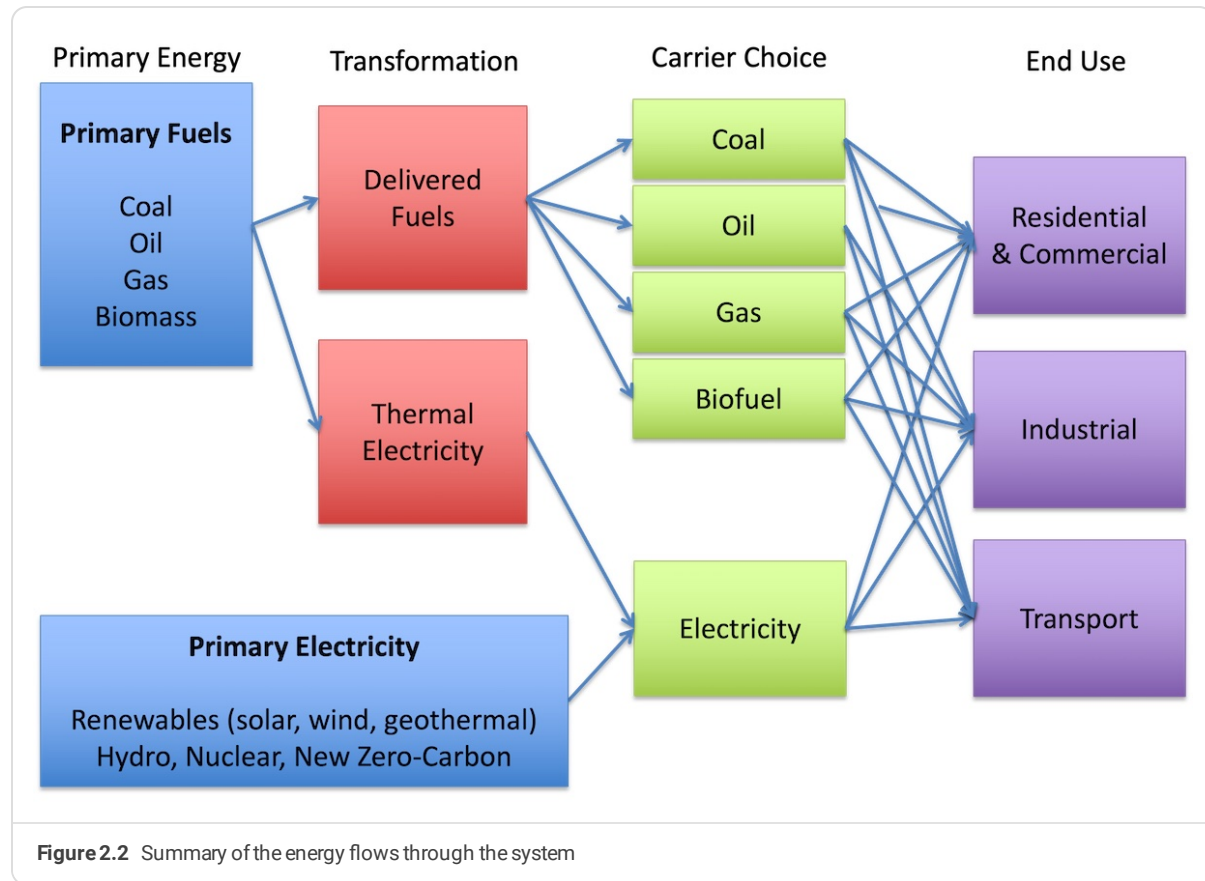
Scope & Detail

The model represents key processes in the energy system for a single, global region. Distinctions among regions are obviously important in the real world, but would considerably complicate the accounting framework of the model, particularly by introducing trade issues, and dilute the impact of any intervention, rendering it less useful for rapid scenario experimentation.

En-ROADS is dynamic, showing behavior over time, and does not find “optimal” results. There are a small number of exogenous inputs selected by the user. All other values are calculated endogenously using assumptions that can also be adjusted by the user.

- Exogenous (user inputs):
 - Population
 - Base GDP growth
 - Technology breakthrough
 - Policy choices
- Endogenous:
 - Energy source choice
 - Energy carrier choice
 - Energy intensity
 - Energy variable and capital costs
 - Price, capacity, and utilization of extracted fuels
 - Price, capacity, and utilization of delivered fuels
 - Price of electricity and capacity and utilization of each source
 - Energy technology (learning by doing)
 - Nonrenewable resource depletion
 - Renewable resource saturation
 - Energy Storage
 - Carbon capture and storage
 - GHG & climate dynamics
 - Agriculture and land use
 - Sea level rise and other climate impacts
 - GDP adjusted for climate impacts
- Excluded:
 - Inventories
 - Labor

The energy system is modeled in great detail, including price, technology and other factors that affect the dynamics of energy and emissions across the full lifecycle for all sources, including potential new technologies.



Organization

En-ROADS is made up of several interconnected submodels which hold the equations. Model sectors are functional and may span one or many submodels. A particular variable is always calculated in only one submodel, but the results are passed to other submodels, and each variable may participate in many model sectors. The submodel listing below describes what sectors each contributes to. A more detailed description of equations and dynamics is organized by model sector in the chapters that follow.

- **En-ROADS.mdl:** Collects and organizes model output for testing, includes all sectors.
- **Constants.mdl:** Holds constants used across multiple sectors and submodels, such as unit conversions.
- **Calibration.mdl:** Provides interfaces and data connections for calibrating to historical data and comparing to other model projections under different scenarios.
- **Population.mdl:** User selected scenarios for population, part of the demand sector.
- **GDP.mdl:** User selected base economic growth, and slowed growth due to feedbacks, part of the demand sector.
- **EnergyDemand.mdl:** Desire for and choice between types of capital, and the use of capital. Part of the demand and market clearing and utilization sectors.
- **EnergySupply.mdl:** Investment, construction, use, and retirement of capacity in the energy sector, including fuel extraction and delivery and electricity generation. Part of the supply and market clearing and utilization sectors.
- **EnergyCostsRevenues.mdl:** Calculates cost dynamics of energy sources for learning, technology, and policies such as taxes and subsidies. Some cross-cutting energy technologies, such as efficiency and energy storage. Parts of demand, supply, and market clearing and utilization sectors.
- **EnergyPricing.mdl:** Adjusts prices to balance supply and demand, Part of the market clearing and utilization sector.
- **Emissions.mdl:** Calculates emissions from energy, end-use capital, and waste; and sums, accumulates and categorizes emissions. Emissions include CO₂, CH₄, N₂O, and F-gases.
- **CDR.mdl:** Calculates the amount of carbon dioxide removal (CDR), afforestation, and carbon capture and storage (CCS) indicated by policy and price signals.
- **BioenergyAgriculture.mdl:** Calculates food needs, land and CH₄ and N₂O emissions for agriculture, and the costs and land needed for bioenergy materials. Parts of Land Use, Land Use Change, and Forestry; Terrestrial Biosphere; Emissions; Demand and Supply sectors.
- **TerrestrialBiosphere.mdl:** Tracks the land area, carbon content in biomass and soil, and the transfers of carbon between air, biomass, and soil for each category of land use.
- **CarbonCycle.mdl:** Sums the carbon transfers from TerrestrialBiosphere.mdl, and tracks the stocks and flows of carbon and other greenhouse gases between emissions, removals, atmosphere, and oceans.
- **Climate.mdl:** Calculates radiative forcing, heat flows, and temperature changes in the atmosphere and oceans.
- **ClimateImpacts.mdl:** Calculates those impacts that depend directly on temperature, or use temperature change as a proxy for climate change impacts.
- **PM25.mdl:** Calculates pollution other than greenhouse gases produced from burning fuels.
- **SeaLevelRise.mdl:** Tracks thermal expansion in the oceans, water flows, and ice melt along with the acidification effects of dissolved CO₂.

In the model structure diagrams in the following chapters, there are four types of elements:

1. Variables with a box represent stocks, determined by integration.
2. Variables without a box are auxiliary variables.
3. Simple arrows indicate a causal relationship, one variable is a function of the other.

4. Pipes represent flows - the elements of the rate of change of stocks - shown flowing into, out of, and between stocks.

Demand

Population, GDP, and Capital

The demand sector defines the global energy demand for transport (transportation), residential and commercial, and industry end uses, all of which may be met by electric and non-electric carriers. The model determines the energy demand according to the stock of energy-consuming capital and its associated energy requirements.

Capital grows according to GDP as calculated by specified population scenarios and GDP per capita rates. GDP exogenously uses data reported by the World Development Indicators (2023) for each region. Projections assume GDP per capita growth rates converge from what they are in the period leading up to the last historical year and converge to 1.5% through 2100. Population uses the UN historical data through 2021, followed by their projections for different fertility scenarios. By default, En-ROADS assumes the medium fertility projections, but the model can vary continuously between the lower and upper 95% confidence intervals.

National Aggregation

En-ROADS calculates actions and outcomes for the entire globe as a single region, with the exception of population and GDP, which are calculated for seven smaller regions. These are the same regions used in C-ROADS.

Table 3.1 Regional Aggregation

Regions	Individual Nations
United States (US)	United States (US)
European Union (EU)	Austria, Belgium, Bulgaria, Cyprus, Czech Republic, Denmark, Estonia, Finland, France, Germany, Greece, Hungary, Ireland, Italy, Latvia, Lithuania, Luxemburg, Malta, the Netherlands, Poland, Portugal, Romania, Slovakia, Slovenia, Spain, Sweden
Other Developed Countries	Albania, Andorra, Armenia, Australia, Azerbaijan, Belarus, Bosnia and Herzegovina, Canada, Faeroe Islands, Fiji, Georgia, Gibraltar, Greenland, Holy See, Iceland, Japan, Kazakhstan, Kyrgyzstan, Macedonia, Moldova, Montenegro, New Zealand, Norway, Russian Federation, Serbia, South Korea, Switzerland, Tajikistan, Turkmenistan, Ukraine, United Kingdom, Uzbekistan
China	China
India	India
Other Developing A Countries	Brazil, Indonesia, Hong Kong, Malaysia, Mexico, Pakistan, Philippines, Singapore, South Africa, Taiwan, Thailand
Other Developing B Countries	Afghanistan, Algeria, American Samoa, Angola, Anguilla, Antigua and Barbuda, Argentina, Aruba, Bahamas, Bahrain, Bangladesh, Barbados, Belize, Benin, Bermuda, Bhutan, Bolivia, Botswana, British Virgin Islands, Brunei Darussalam, Burkina Faso, Burundi, Cabo Verde, Cambodia, Cameroon, Central African Republic, Chad, Chile, Colombia, Comoros, Congo, Cook Islands, Costa Rica, Côte d'Ivoire, Croatia, Cuba, Democratic People's Republic of Korea, Democratic Republic of the Congo, Djibouti, Dominica, Dominican Republic, Ecuador, Egypt, El Salvador, Equatorial Guinea, Eritrea, Ethiopia, Falkland Islands (Malvinas), Federated States of Micronesia, French Guiana, French Polynesia, Gabon, Gambia, Germany, Ghana, Grenada, Guatemala, Guinea, Guinea Bissau, Guyana, Haiti, Honduras, Hungary, Iceland, India, Iran, Iraq, Israel, Jamaica, Jordan, Kenya, Kiribati, Kuwait, Lao People's Democratic Republic, Lebanon, Lesotho, Liberia, Libya, Macao, Madagascar, Malawi, Maldives, Mali, Marshall Islands, Mauritania, Mauritius, Mayotte, Mongolia, Montserrat, Morocco, Mozambique, Namibia, Nepal, New Caledonia, Nicaragua, Niger, Nigeria, Niue, Oman, Palau, Panama, Papua New Guinea, Paraguay, Peru, Qatar, Réunion, Rwanda, Saint Helena, Saint Lucia, Samoa, São Tomé and Príncipe, Saudi Arabia, Senegal, Seychelles, Sierra Leone, Slovakia, Slovenia, Solomon Islands, Somalia, Sri Lanka, Sudan, Suriname, Swaziland, Syrian Arab Republic, Timor-Leste, Togo, Tokelau, Tonga, Trinidad and Tobago, Tunisia, Turkey, Turks and Caicos Islands, Tuvalu, Uganda, United Arab Emirates, United Republic of Tanzania, Uruguay, Uzbekistan, Vanuatu, Venezuela, Vietnam, Wallis and Futuna Islands, West Bank and Gaza, Western Sahara, Yemen, Zambia, Zimbabwe

Notes:

- *Other Developed Countries* includes the Annex I countries within the UNFCCC process; the US and EU are also in the Annex I.
- *Other Developing A Countries* consists of the large developing countries with rising emissions.
- *Other Developing B Countries* consists of smaller developing countries, including the least developed countries and the small island states.

Capital

The capital-output ratio is assumed to be fixed such that capital and GDP rates are equivalent. Damage functions relating to GDP impacts from temperature change are described in detail in [Damage to GDP](#). Energy requirements are embodied in the capital stock at the time of investment, which introduces a lag between the energy intensity of new capital and the average energy intensity of the capital stock.

The energy intensity of new capital is governed by a response to the total cost of ownership of each carrier for each end use and an exogenous user-specified technology trend. For each end use and carrier, two price effects, one based on energy costs and the other based on non-energy costs, also affect its energy intensity of new capital. Each price effect is formulated according to a distinct constant elasticity, such that as the cost relative to the reference increases, the energy intensity of that end use and carrier decreases. Likewise, as the cost relative to the reference decreases, the energy intensity of that end use and carrier increases.

The demand sector includes energy intensity of new and average energy consuming capital, which is disaggregated into three vintages, with energy requirements of each vintage, accounting for aging, early discarding and retiring, and retrofitting. Capital and energy requirements of that capital are disaggregated by end use (residential & commercial, industry, and transport), as well as by carrier (electricity and four fuels). The nonelectric carriers are coal, oil, gas, and biomass. The model carefully tracks final and primary energy demand, where the former is the energy consumed by the end use capital, and the latter is the energy needed to be generated to meet that demand accounting for thermal efficiency that is less than 100% and other losses.

Carrier Choice

Energy is delivered to end use capital via five potential carriers; there are four nonelectric carriers and one electric carrier. Each of the nonelectric carriers matches 1:1 with each of the fuels, i.e., coal, oil, gas, and bio. The choice between each carrier is made in the carrier choice sector.

Shares of each carrier are allocated on the basis of the relative attractiveness of options according to a logit-type choice function, e.g.:

$$Share[Carrier] = \frac{Attractiveness[Carrier]}{\sum Attractiveness[Carrier]}$$

Attractiveness is an exponential function of cost, complementary assets (for transport only), and other factors including phase-out policies, technical feasibility, and other effects. Cost attractiveness is determined according to the weighted average of attractiveness based on upfront capital costs and that based on the total cost of ownership (TCO), i.e., sticker price plus annual operation and maintenance costs plus energy costs. The weight reflects the value of how the buyers' attention is distributed between the sticker price and the TCO while making purchasing decisions and is specified for each end use.

Costs associated with the market price of energy are driven by the energy dynamics (e.g., extracted fuel commodity cycle, market clearing algorithms). Costs associated with the end use capital may be reduced by learning from end use experience, and for the electric carrier, adjusted with subsidies.

Complementary assets (CAs) reflect the availability of infrastructure to support the carrier; the effect applies only to transport end uses, reflecting fueling points/charging stations for vehicles. The installation of CAs is a function of the embodied carrier demand and, for the electric carrier, a policy to increase that. However, it is also constrained by a third order delay of the installation capacity. CAs have a normal lifetime but can also be retired early if the level exceeds the carrier demand. The level of CAs relative to that which is needed factors into the attractiveness of each carrier. Coal is assumed to have adequate availability for the relatively small amount of demand, notably for trains. The bio carrier uses the complementary assets of the oil carrier.

Fuel phase-out mandates also affect attractiveness, as described in [Drivers of Cost of Supply](#).

The logit-determined shares are also subject to policies of phasing out fuel-powered capital, thereby electrifying new capital. These policies are phased in over time. For transport, the logit and fuel phase-outs only apply to the 85% of capital that is road and rail. To electrify the remaining 15% that is for shipping and aviation, another policy must be implemented.

Energy Intensity of New Capital

In the demand sector energy requirements are embodied separately for each fuel and for electricity. Energy intensity of each new unit of capital drives the embodied long-term requirements. Technological improvements and price of energy affect the energy intensity of new capital. The technological effect defaults to the historically observed improvements, assuming those persist into the future. However, the user may change those rates of improvement. Price effects for each end use and carrier are determined according to the long-term demand elasticities to the price of energy and to the non-energy costs of capital. The indicated price effect for each, which is the product of the effect of energy costs and the effect of non-energy costs, is delayed over time. There is also a fraction of the residential and commercial sector that is by definition electric, e.g., lighting and electronics. The energy intensity of this share grows with the closure of the gap between the average GDP per capita of developing countries and the initial average of developed GDP per capita.

Long Term Energy Requirements

The energy demanding capital that is installed is a function of the desired capital and that which is lost through discarding and retiring. The long term energy requirements are a function of the energy intensity of the capital that is installed and tracked through the capital lifetime through each vintage. Retrofitting for each end use also occurs, with the retrofits at the capital share and intensity of new energy.

Model Structure

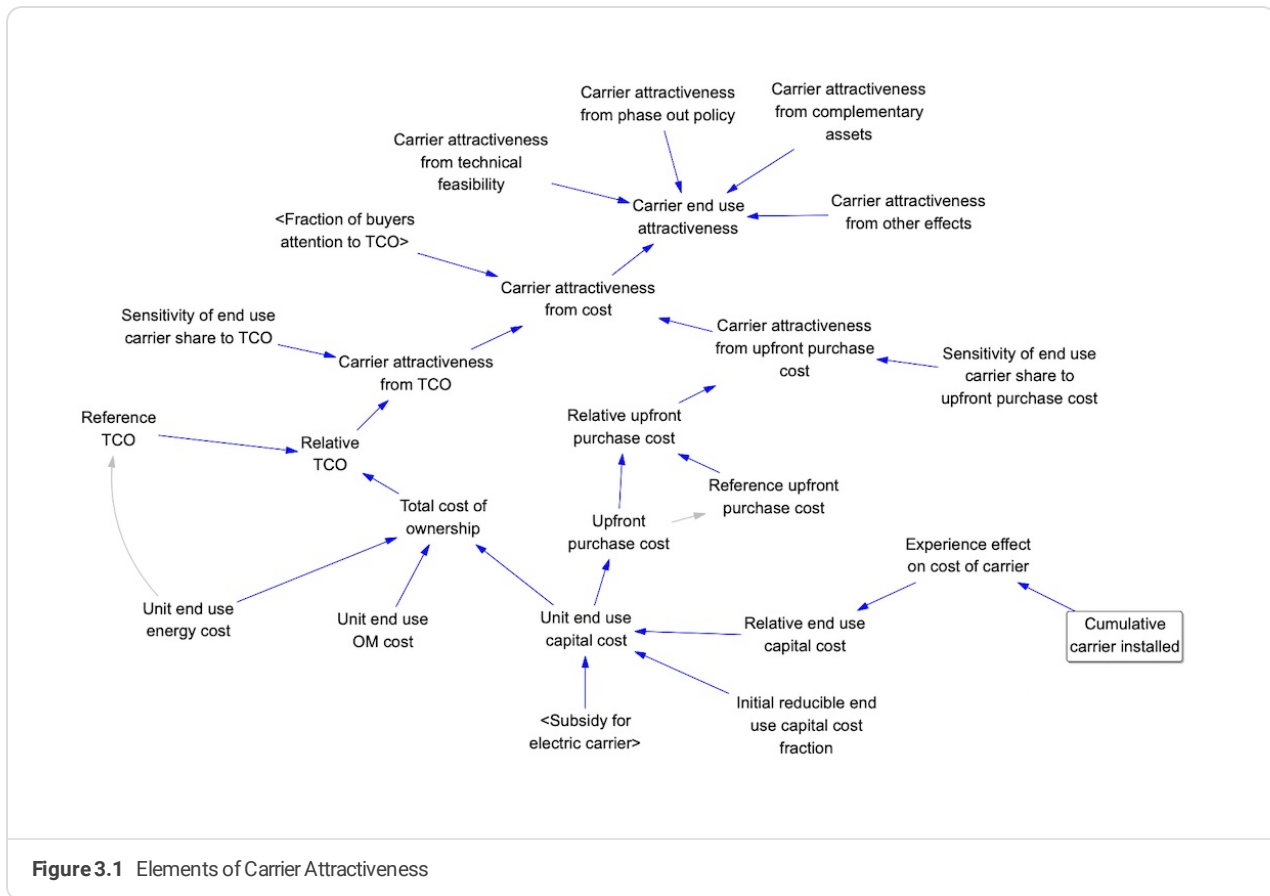


Figure 3.1 Elements of Carrier Attractiveness

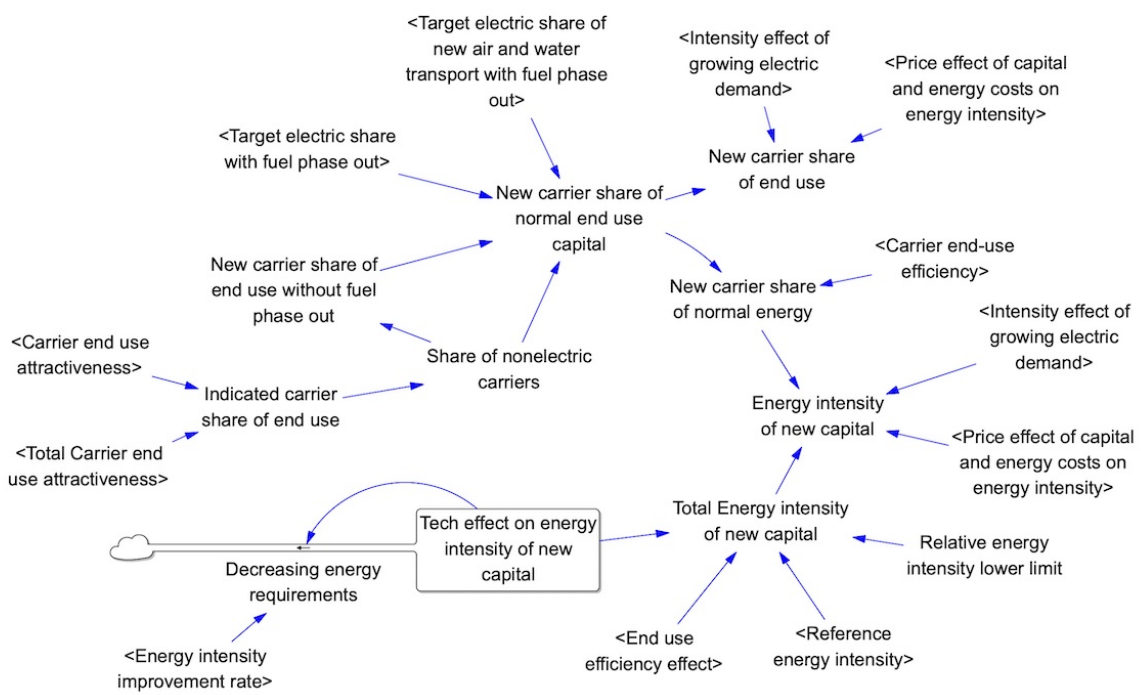


Figure 3.2 Carrier Choice

Supply

Supply of Extracted Fuels, Delivered Fuels, and Electricity Generation

There are three main supply chains to capture the stock and flow of supply capacity of extracted fuel (coal, oil, gas, and biofuel), delivered fuel (coal, oil, gas, and biofuel), and electricity production from each of the electric paths (coal, oil, gas, biofuel, nuclear, hydro, wind, solar, geothermal, other renewables, and new). The model assumes that each extracted fuel is available only for its respective delivered fuel type. All fuels plus nuclear, hydro, renewable types, and new zero-carbon are available for the electric carrier.

Table 4.1 Carriers

Carriers	Sources Used
Coal Carrier	Coal
Oil Carrier	Oil
Gas Carrier	Gas
Bio Carrier	Bio
Electric Carrier	Elec Paths

Each delivered fuel is available for nonelectric and electric use. The electric only paths are mapped to the primary source, where the renewable types are aggregated to Primary Renewables.

Table 4.2 Primary Energy Sources and Electric Paths

Primary Energy Sources	Primary Fuels	Elec Paths
Primary Coal	PCoal	ECoal
Primary Oil	POil	EOil
Primary Gas	PGas	EGas
Primary Bio	PBio	EBio
Primary Nuclear		Nuclear
Primary Hydro		Hydro
Primary Renewables		Wind Solar Geothermal Other Renewables
Primary New		New

Subscript ranges are grouped and mapped accordingly.

Table 4.3 Subscript Range Mapping

Range	Paths Included
Fossil Fuels	Coal: Primary Coal, PCoal, ECoal Oil: Primary Oil, POil, EOil Gas: Primary Gas, PGas, EGas
Elec thermal	ECoal, EOil, EGas, EBio
Electric Carrier	Elec thermal Nuclear Hydro Wind Solar Geothermal Other Renewables

The capacity and utilization and cost of extracted fuels affect the market price of extracted fuels, which feeds into the variable cost of delivered fuels. As such, the market price of extracted fuels affects the capacity, utilization, and market price of delivered fuels, which in turn feeds into the variable cost of electric producers using those fuels. Accordingly, the costs of delivered fuels affect the capacity and utilization of those electricity sources. [Market Clearing and Utilization](#) details the market clearing and utilization of delivered fuels and electricity sources.

For each of these phases, the capacity represents the installed base of usable capital. It depreciates via a constant fractional rate, without age vintaging of the stock. The profitability, however, affects the rate of depreciation. For delivered fuels and electric supply, capacity must go through the development phase and then constructed before it can be used, introducing a delay between initiating and completing the acquisition of new capacity. The amount of capacity that is planned for construction accounts for the total capacity needed to meet the energy demand, including transmission and delivery losses, plus a reserve margin and expected growth of energy requirements.

For capacities of extracted fuels and of delivered fuels for nonelectric consumption, the desired capacity of each depends in part on the centralized effect of expected growth and normal utilization, as well as on the profitability and current capacity of each fuel. Any non-cost policies banning new capacity adjust the resulting desired capacity. For electric generation, the desired capacity of each source depends on the demand of electricity and the Fraction invested in elec energy source , as well as the profitability and current capacity of each source. Desired capacities are adjusted by dividing by the capacity factor of each resource, requiring more of each energy path to be constructed to get the actual desired supply. The constructed supply is then multiplied by the capacity factor to yield the actual capacity. While the Actual Supply Capacity represents the amount of energy from each path that can be dispatched, the Energy Supply Capacity is the amount of energy that is constructed.

The rate of capacity completion is constrained by the capacity to do so. This structure captures supply chain constraints, for example the fact that if wind turbine orders double overnight, completion of new turbines cannot also double immediately. It takes time to acquire labor and machinery and build up other aspects of the necessary supply chain. This has two consequences: with increasing pressure to construct capacity, the effective lead time increases, and the cost of new capacity rises.

Drivers of Cost of Supply

Several factors affect the cost of each supply source, including,

- A baseline or reference cost
- a learning-by-doing effect from the accumulation of experience in capacity installation
- an exogenous user-specified cost reduction from technological breakthroughs achieved through research and development (R&D)
- cost of fuels as determined by the delivered fuel market price and efficiency of fuel use
- resource constraints
- source subsidies/taxes
- storage costs for variable renewables (solar and wind)
- soft costs for renewables
- emissions cost from carbon pricing
- qualifying electricity standards costs and penalties, [Qualifying Electricity Standards \(QES\)](#)
- a “pipeline overheating” premium from supply chain constraints on capacity installation, [Supply of Extracted Fuels, Delivered Fuels, and Electricity Generation](#)

Resource Constraints

The Resource Constraints sector addresses the potential limits to available energy resources and the effects those limits may have on supply costs. The resource effect cost is a function of the depletion effect on cost and the supply curve effect on cost.

The depletion effect is dynamic, with cost increasing as cumulative production grows. This captures cost escalation with the depletion of fossil fuels. It is possible to discover unconventional resources, thereby reducing the depletion effect; however, it is assumed that the unconventional resources have a different carbon intensity, adjusted by the user. Biomass is not limited by depletion but rather by the supply constraints of each feedstock, i.e., wood, crops, and others, which reflects the limit of production of energy from a source from the saturation of production opportunities. These resource constraints affect the extraction costs of fuels, resulting in a greater market price of extracted fuels. In turn, a greater market price of extracted fuels drives up the market price of delivered fuels for nonelectric use and increases the cost to produce electricity from the thermal paths with and without CCS.

The supply curve constraint can also affect the cost to produce the electric only paths, i.e., nuclear, hydro, renewable types, and new zero-carbon; of these sources, the model defaults to only affect hydro and renewables. Supply limitations for these paths affect the O&M and capital costs, capturing, for example, the escalation in cost of wind power that occurs as the cheapest sites are exploited first.

Parameters are based on IPCC 2007 and IEA 2022 estimates.

Storage for Renewables

Storage capacity for variable renewable energy (VRE) must meet its demand when the source is not available. Variable renewables include wind and solar, whereas geothermal and other renewables are more constant in their generation. Models of hourly, daily, and seasonal variability of demand and renewable generation determined the storage coverage, i.e., energy per variable renewable capacity (EJ per EJ/year), and the average power needed from storage per variable renewable capacity (EJ/year per EJ/year). Sensitivity analyses of each category of coverage determined the relationships between these parameters and the share of VRE capacity to total electric generation capacity. These analyses also confirmed the effect that round trip efficiency (RTE) has on the required coverage; it scales $1/RTE$ such that the lower the RTE to use storage, the higher the maximum storage capacity for storage required. The resulting relationship between hours of coverage versus VRE share is consistent with that found by others, including Solomon et al. (2017), Shaner et al. (2018), and Albertus (2020).

Storage coverage to balance the different time scales of variability is defined in the model by duration.

- **Hourly storage:** up to 12 hours of coverage.
- **Daily storage:** 12-72 hours of coverage.
- **Seasonal storage:** greater than 72 hours of coverage.

Long duration energy storage (LDES)—generally daily and seasonal storage coverage—is increasingly required at higher shares of variable renewables in the electric grid, and requires a breakthrough cost reduction to enable its growth.

Besides storage, other demand response technology, long-distance transmission, and behavioral load management can minimize storage needs but only for short and medium coverage. Learning and investment increases the percent effect these options have on the storage requirements.

While the model assumes that storage requirements will not limit utilization, costs of renewables account for those for storage. Comparable to the experience and breakthrough effects for energy, storage costs also decrease with cumulative capacity installation and potential technological breakthroughs.

Storage could be in the form of batteries, compressed air, pumped hydropower, and other more novel options, including hydrogen. NREL's Store-FAST: Energy Storage Financial Analysis Scenario Tool, version: 1.2 (2019), provides the inputs for power and energy costs, including RTE, for several storage options. The levelized cost of each type adds the cost of electricity for it, which is the market price of electricity divided by the storage RTE.

Other than hydrogen, these technologies all become limited and/or more costly with longer durations of coverage. Cost effective long duration coverage is critical when the share of VRE exceeds approximately 70-80%. Hydrogen, despite having a much lower RTE, approximately 36%, has the potential to provide more cost effective long duration coverage than the other technologies. This is because, although the power costs associated with hydrogen far exceed those other storage options, the costs to store each hour of energy coverage is far less than the other options. Despite that cost effectiveness for long-term coverage, ancillary costs currently associated with hydrogen storage constrain its use. A breakthrough in hydrogen also reduces these ancillary costs, thereby allowing it to take advantage of its cost attractiveness for long-term coverage.

Electricity for Storage

In addition to the power and energy costs, each storage option also requires electricity for charging and discharging. Electricity exceeding that which is generated from storage, determined from the sum of the average power needed from storage per variable renewable capacity from the hourly, daily, and seasonal models, is added to the industrial electric carrier demand. For example, an RTE of 100% requires no additional electricity; an RTE of 80% requires 0.25 times the power required; and an RTE of 36% requires 1.77 times the power required. By default, the electricity all comes from the grid.

Hydrogen Leakage

Hydrogen leakage, defaulted at 2%/year, releases hydrogen to the atmosphere. While there is no direct radiative forcing from hydrogen, the climate structure accounts for its indirect effects on the radiative forcings of CH₄, O₂, H₂O, and aerosols (Sand et al., 2023).

Soft Costs and Subsidies for Renewables

The levelized cost of electricity (LCOE) of renewables, particularly wind and solar energy, have decreased dramatically since 1990, especially over the past decade. Two opposing forces have contributed to those declines with the energy generated by them. There have been historical subsidies for solar and wind, defined as a fraction of their direct costs, stimulating their growth. While the fraction of solar subsidies declined over time until 2020, that fraction and the fraction for wind is expected to remain constant through 2100 as Baseline subsidies, comparable to the fossil fuel subsidies embedded in their costs. However, the user can end them sooner. There have also been soft costs, i.e., indirect costs, that have made the investment in these sources less attractive than direct cost alone would suggest. It captures the soft costs as an initial level that declines with experience at a rate determined by a progress ratio. The values defining these subsidies and soft costs were estimated from literature and set through optimization to fit historical cost (IRENA, 2020; Lazard, 2021; IEA, 2020) and energy data (IEA, 2022; BP, 2022).

Sources of LCOE data for renewables are not consistently presented and only available for some years, therefore requiring conversions and bridging between datasets.

- **IRENA**: All LCOE results are reported in \$2019 USD. Reported values calculated excluding any financial support and using a fixed assumption of a real cost of capital of 7.5% in OECD countries and China, and 10% in the rest of the world, unless explicitly mentioned. All LCOE calculations exclude the impact of any financial support. Converted to \$2017.
- **LAZARD 3.0-15.0**: All LCOE results reported in nominal dollars. Each analysis assumes 60% debt at 8% interest rate and 40% equity at 12% cost; Unless otherwise indicated, the analysis herein does not reflect decommissioning costs, ongoing maintenance-related capital expenditures or the potential economic impacts of federal loan guarantees or other subsidies; Lazard's unsubsidized LCOE analysis indicates significant historical cost declines for utility-scale renewable energy generation technologies. Converted to \$2017.
- **IEA Levelized Costs Data**: Global average LCOEs and auction results for utility-scale PV by commissioning date. Last updated 26 Oct 2022. Data shown = LCOE in \$2017.
- **IEA**: Evolution of solar **PV module cost** by data source, 1970-2020. Last updated 26 Oct 2022. While the LCOE data for solar PV is not readily available before 2009, IEA's cost per watt of solar PV from 1970-2020 provides data to estimate the LCOE from 1990. Using the ratio of annual costs per watt to that in 2010 and applying that ratio to the IRENA solar PV LCOE in 2010 provides an estimate of LCOE from 1990-2019.
- **Berkeley**. Median 30-Year LCOE without the ITC reported in \$2018. Converted to \$2017.

Utility vs distributed solar PV: There are differences between utility scale and distributed solar PV. According to [IEA \(2022\)](#), the fraction of PV that is utility scale grew from 24% to 50% of solar PV between 2010-2016, remaining at that level thereafter. Lazard provides utility scale and distributed cost data; accordingly, comparisons are made to the weighted average of these. The weights assume the trend of increasing utility scale relative to distributed increases at a comparable rate to history.

Onshore vs offshore wind: Likewise, there are differences between onshore and offshore wind. IRENA used the weighted average of the onshore fraction of wind, taken from [IEA Wind Electricity Report](#), to get the weighted average of wind LCOE. From regional graphs of onshore vs offshore wind, they estimated wind to be 100% onshore until 2010, when offshore wind starts to present, decreasing down to 95% by 2019.

Instant and Embodied Supply Costs and Efficiencies

The embodied costs of supply are modeled in the Embodied Supply Costs sector. These costs factor into the utilization of energy capacity in the Market Clearing and Utilization sector. Embodied costs represent the actual physically-imposed costs, which are locked in at the time of capacity investment, i.e., new capacity development. Variable costs include operation and maintenance (O&M), and fuel costs. The fuel costs for delivered fuels are the extracted fuel costs. The fuel cost for each electric source requiring fuel is the market price of extracted fuel, accounting for a markup, divided by the embodied thermal efficiency of the source; fuel prices for the primary electric paths are 0. Unit profit, which is the revenue less the variable costs, may be adjusted by a tax/subsidy and/or carbon tax to the producers of delivered fuels.

As in the [Demand sector](#), the construction pipeline is explicit but without vintaging of capital as there is in the demand side; costs are assumed to be well-mixed. All inputs to this sub-model are determined in other sub-models except for the Overheating cost sensitivity, which is set at 0.5. The embodied costs and efficiencies of supply are locked in at the time new capacity development.

The effects on costs apply to the leveled capital costs as well as to O&M and fuel costs.

Electric Supply Choice

As in the Carrier Choice sectors, the fraction of new investment allocated to each of the electric energy sources is a function of its attractiveness relative to that of the other sources. Attractiveness synthesizes cost effect and the effect of a performance standard.

The cost, adjusted by any source subsidies/taxes, drives the cost attractiveness of each electric path relative to the other electric paths.

The performance standard effect is a function of a specified carbon intensity threshold and the carbon intensity of each energy source resource, defined in [Emissions](#). The performance standard creates a soft threshold, beyond which sources with high emissions intensity (e.g., coal) are greatly diminished in attractiveness and are effectively eliminated from the investment mix. The effect of non-cost policies aims to capture any legislation or rule demanding no new investment in a specified source for a percentage of the global energy needs.

Model Structure

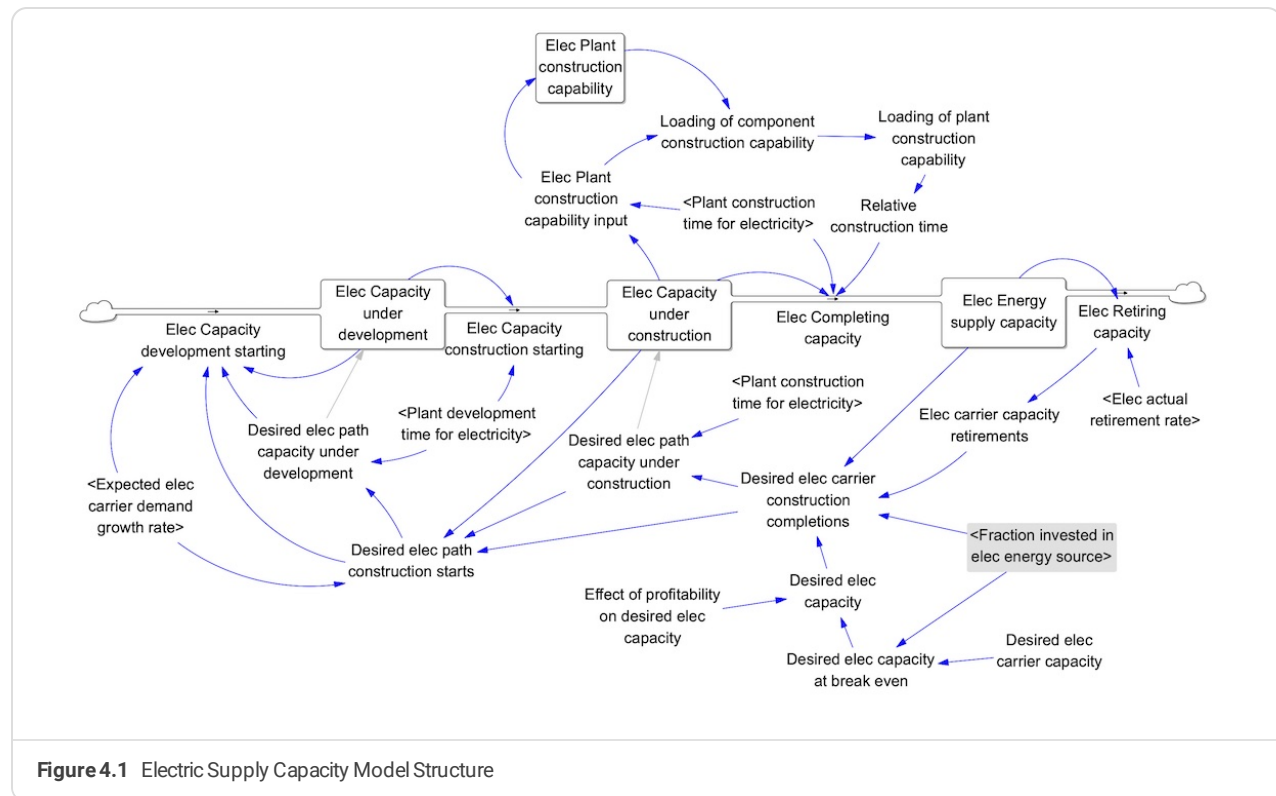


Figure 4.1 Electric Supply Capacity Model Structure

Market Clearing and Utilization

The Market and Utilization sector uses a market clearing theory to balance supply and demand given costs, prices, and assumed market attributes. In summary, the model includes the following:

- Extraction capacity and price of extracted fuels.
- Supply/demand/price of each fuel for nonelectric consumption. The variable costs include the extracted fuel price contracted over a period, adjusted by any taxes or subsidies.
- Supply/demand/price of electricity, where the variable costs include the extracted fuel price marked up by a ratio and contracted over a period, adjusted by any taxes or subsidies.
- For each delivered fuel for nonelectric consumption, the recent market price of each fuel relative to the reference market price of each fuel adjusts the actual demand from that at normal utilization. For each fuel, the normal demand is the sum of the long term demand for nonelectric consumption accounting for noncost phase-out policies.
- For electricity, the recent market price relative to reference market price adjusts the actual demand from that at normal utilization.

Market Price of Extracted Fuel

The market price of extracted fuels depends on the utilization and price effects as well as the cost of extraction, which depends on technological cost improvements and overheating of capacity, and resource constraints, all described in [Supply](#).

Market Clearing and Utilization

The market price and utilization of electricity and delivered fuels for nonelectric consumption depends on the long term demand, the supply capacity, and market price adjustments. Utilization of each source is a function of unit margins and the short term supply curves, defined by generalized logistics functions, but may be reduced by noncost phase-out policies. For nonelectric delivered fuels, the market price of each fuel is equivalent to the revenue for it. For electricity, the revenue is the market price of electricity less the transmissions and distribution (T&D) costs. The consumer pays the T&D costs, defaulted to \$0.02/kWh, to the utility regardless of the electricity generator. T&D costs are not subject to the learning or breakthroughs; they are assumed to remain constant throughout the simulation (see [EIA 2017](#) and [Fares & King 2016](#)). The generator's unit margin may also be increased according to qualifying credits, explained below in Clean Electricity Standards. Capacity of extracted fuels is utilized for electric generation and also processed for delivered fuels for nonelectric carriers.

Tax and Subsidy Adjustments to Costs

A carbon tax on fuels and source taxes reduce the margin and profit of that source; conversely, source subsidies increase the margin and profit of that source. Source taxes/subsidies can be applied either to capital costs or to variable costs, the fraction of which is determined by Fraction of fuel source adjustment for capital and Fraction of elec source adjustment for capital . For nonelectric consumption, the default is that all taxes/subsidies apply to the variable costs, whereas for electric consumption, the default is that they apply to capital costs. Carbon taxes, which depend on the carbon density of the fuel, increase the variable costs of that fuel. For fuel-generated electricity, the adjustment to the cost of fuel also depends on the thermal efficiency of that source.

Parameter values for source subsidy/tax inputs range from highly subsidized, defined to be 60% of the marginal cost in 2020, to very highly taxed, defined to be 200% of the marginal cost in 2020. For fuel-generated electricity, the percent thresholds apply to the marginal costs excluding those for fuel. Bounds are set to policy-relevant limits, which are source-dependent.

Clean Electricity Standards

Besides taxes and subsidies, market-driven credits or certificates are another mechanism to drive electricity to achieve target standards. En-ROADS allows the user to choose the sources to be counted as qualifying, the target percent of qualifying sources of electricity produced, the duration over which to achieve the target, and the base cost of the credits or certificates. The costs of buying certificates and potential fines for not reaching the standard are paid for by all sources, whereas only qualifying sources reap the revenue.

Model Structure

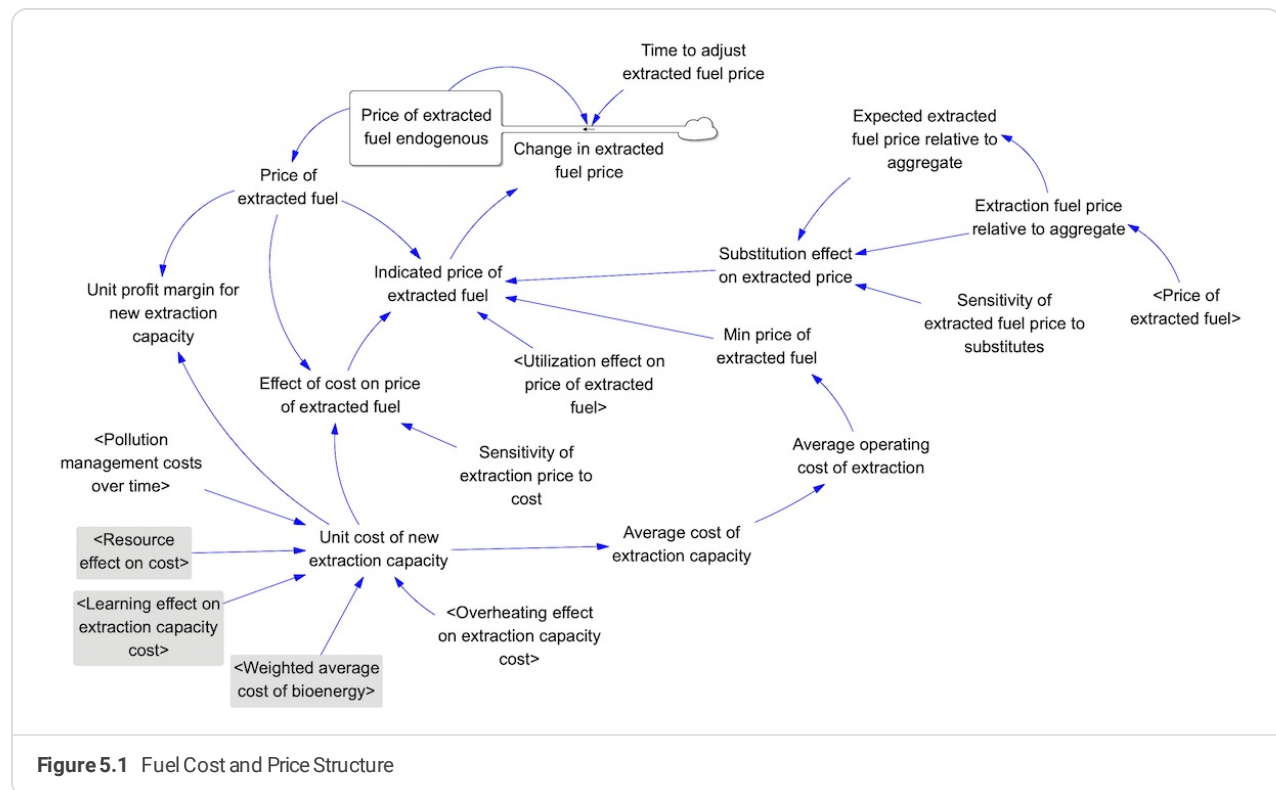


Figure 5.1 Fuel Cost and Price Structure

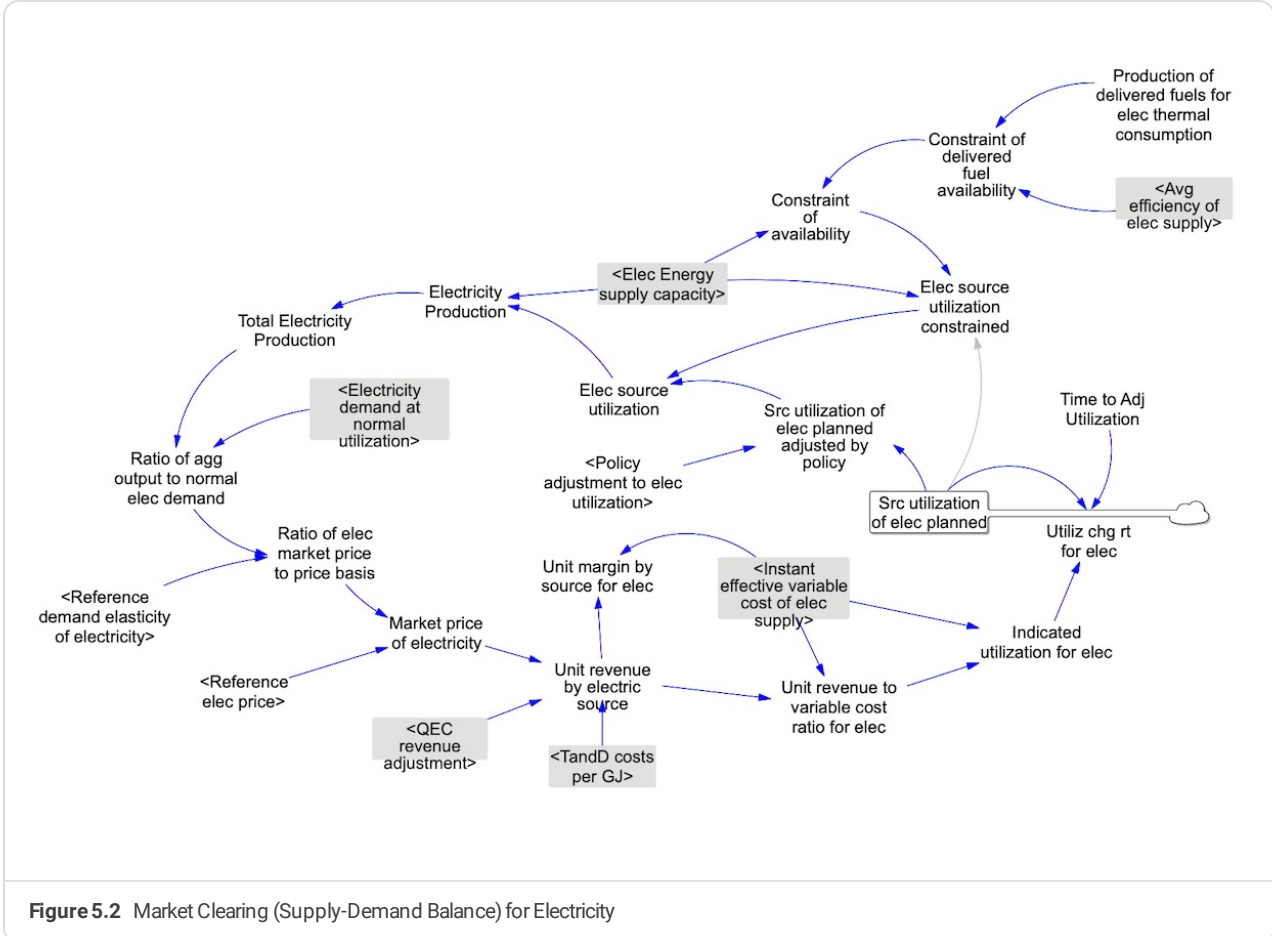


Figure 5.2 Market Clearing (Supply-Demand Balance) for Electricity

Land Use, Land Use Change, and Forestry

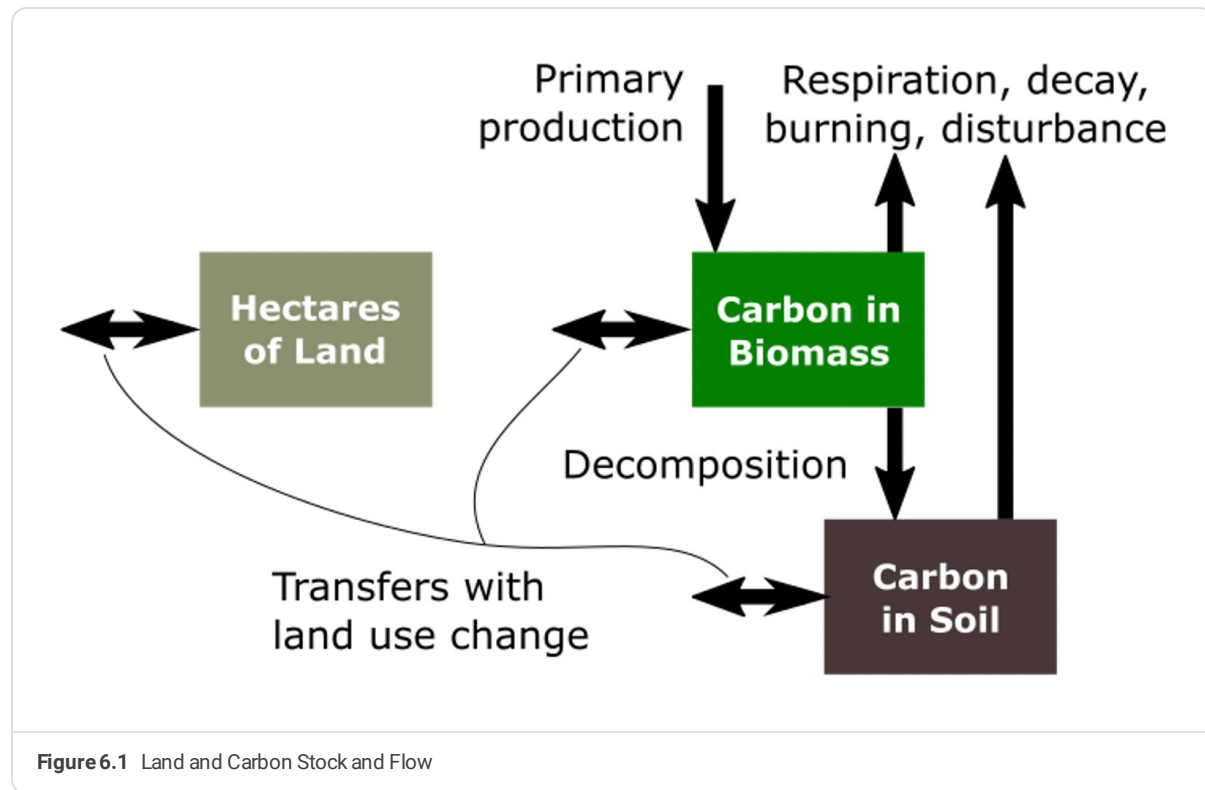
En-ROADS endogenously calculates the land use, land use change, and forestry (LULUCF) net C emissions by explicitly keeping track of each hectare of different land types; the fluxes of changing land types and the use of each land type due to land and energy demands and policies; and the coflow of carbon on the land. The terrestrial biosphere carbon (TBC) cycle accounts for these anthropogenic carbon emissions as well as natural emissions from biomass and soil respiration and releases as CH₄, accounted in the CH₄ cycle, and primary productivity of each land type.

The TBC cycle reflects that cutting down trees releases carbon and stops them from absorbing CO₂ from the atmosphere. While harvesting crops also releases carbon, the approximately annual or faster regrowth time allows the related carbon release to be considered net zero.

En-ROADS models different kinds of land that can be converted into the others, and the biomass and soil carbon on the land that can accumulate or be released. We have four different land uses: Forest, Agriculture, Other, Tundra; with Forest further divided into three cohorts (Young, 0-50 years; Medium, 50-100 years; and Mature, 100+ years) and whether or not it resulted from afforestation (9 total land uses).

Each type of land has carbon flows:

- From the atmosphere to biomass (primary production through photosynthesis)
- From biomass to soil (decomposition, etc.)
- From soil and biomass to the atmosphere (respiration, decay, burning)
- When land use changes, some of the carbon stays on the land and some is released to the atmosphere



We cut trees or remove biomass for two reasons: we want the material or we want the land (or both). The material is involved in concepts like bioenergy, wood products, and forest degradation. Needing the land means concepts like deforestation, afforestation, land use change, and agriculture. Those are the policies and scenarios where you can intervene in En-ROADS with each area described below.

Drivers of Deforestation and Degradation

Land that is converted from forest becomes either Farmland (driven by needs of the food system and bioenergy) or Other Land (non-farm deforestation). With six subcategories of forest (NonAF/AF, Young/Medium/Mature), the model assumes that the fraction of deforestation to farmland and to other is proportional to the land area of each to the total forest land.

The primary driver of deforestation has historically been to expand farmland, the need for which is driven by the [food system drivers](#) but also by the fraction of farmland expansion that comes from forest. Farmland needs that cannot come from forest comes from Other Land. Farm conversion from other land (mostly grasslands and scrub, but also deserts, barren, urban, etc.) has less effect on the carbon cycle than does deforestation. The fraction of farmland expansion that comes from forest is fixed (at 0.6) in the base case based on historical land use changes.

Non-farm deforestation is exogenous, a simple Baseline scenario based on the LUH data and projections. This reflects forest clearing for development and mining.

The fraction of farmland expansion coming from forests, and the rate of deforestation to other land may be modified by policy inputs. Those inputs come in two modes: from the main Deforestation slider, the input is a percent per year increase or decrease, which results in first order growth or decay relative to the Baseline scenario. In advanced settings, the user can set a year to halt which results in a linear transition to zero in the target year. The policies form reduction rates which are accumulated in a single stock called `Relative deforestation` which in turn multiplies each component of deforestation rate.

Forests are also harvested and allowed to regrow. The regrowing process can remove carbon from the atmosphere and is therefore often considered carbon-neutral. However, it can take decades to repay the carbon debt incurred with forest harvesting. All forests can be harvested for bioenergy or for wood products. The proportion of total harvest from each forest category is a function of available carbon on each category relative to the total carbon on all forests. A third element that is linked to the main deforestation slider is degradation of mature forest, i.e., forest of average age greater than 100 years. We include it because forest policies often link deforestation and degradation, as in REDD+. Although the terrestrial biosphere structure tracks removal and regrowth of biomass on all forest types, we limit the policies and graphs to degradation of mature forests. Harvest of mature forests is driven by the bioenergy structure, above, along with harvest for non-fuel wood. Non-fuel wood demand (lumber, paper, etc.) is a constant for each region times the population for each region. Structure exists for including a GDP per person effect but the sensitivity is zero.

The policy to directly control degradation is identical to the ones controlling the rate of non-farm deforestation (relative to Baseline) and farm expansion (fraction of expansion from forest), only it affects the fraction of mature forest available for harvest. The main deforestation slider increases or decreases degradation by a percent per year; the advanced view sets a year to halt degradation of mature forests, which also reduces the availability of wood for bioenergy and non-fuel harvest.

There are also command and control-type policies for land conservation; these limits do not address the drivers of deforestation or degradation, but rather prevent those drivers from affecting forest or mature forest. These policies represent the "year to halt" each component.

Food and Agriculture Drivers

Expanding farmland is a major driver of deforestation and other land use change. We start with the assumption that land will expand to meet food needs. We measure food in kilograms per year, and limit it to two types: crops and animal products. We model a single global food demand and a single global agriculture system. The variables involved in the causality from people to food to land are:

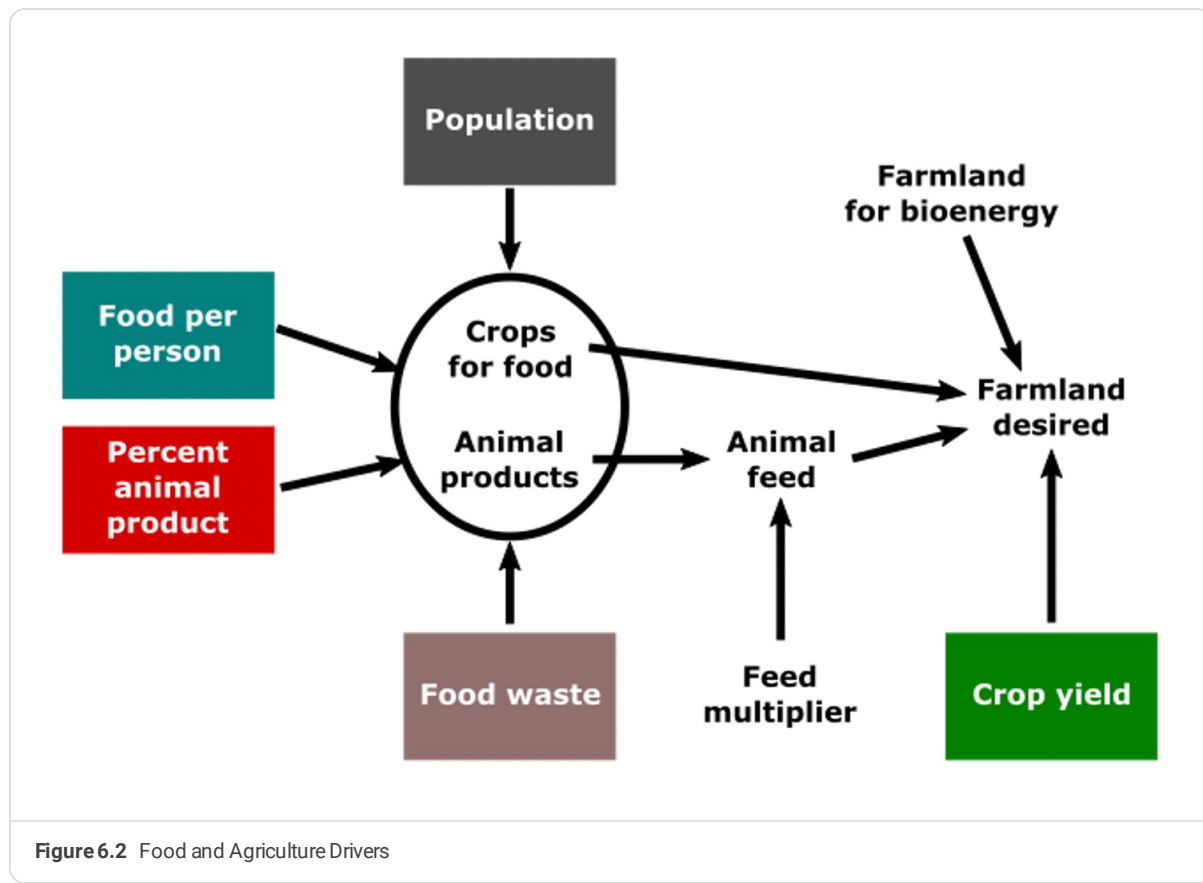


Figure 6.2 Food and Agriculture Drivers

Food per person is modeled as a simple function of GDP per person, fitted to the FAO food balance data, and approaches an upper limit of 900 kg/person/year. There are no user controls for food per person, based on our assumption of meeting food needs.

Percent animal product is the fraction of global diet met by milk, meat, eggs, etc. Consumption of animal product in kg/person/year is a function of global average GDP per person, calibrated to FAO food balance data, from which the fraction is calculated. Under baseline GDP scenarios, it rises from its current value (24%) to a peak of 30% as GDP rises, set by the [Food from livestock slider](#). The current consumption of milk, meat, etc. by region has range from 15% (China and Other Developing B) to over 40% (US), and not strictly arranged by GDP per person; traditional diets play a large part. It is still expected that global animal product consumption will grow over time as countries develop, but En-ROADS allows for users to vary that value between 10% to 40% to be reached in 2100.

Food waste is a single stock that is by default constant at 30%. 30% is the widely quoted but poorly studied value of the amount of food harvested but not consumed, anywhere along the value chain. Anecdotally, it is mostly between farm and market in developing countries, and retail or post-consumer in wealthy countries. If you change the `Food waste` setting, the new value is reached in 2100 with a linear path.

Food consumption for both crop and animal products is the product of population, food per person, and percent from livestock. Accounting for waste gives production needed to meet that consumption. An additional factor `Livestock feed multiplier` gives how much plant matter (feed, fodder, grazing vegetation, etc.) it takes to produce each kilogram of animal product. For now that is fixed at 10 kg plant / kg animal product. Farmland desired is then those needs for plant matter divided by yield.

Yield is the global aggregate production of crops, animal feed, pasture vegetation, etc., per year per hectare. The crop yield structure is designed to (1) have Baseline food demand result in land use changes matching LUH projections (2) allow for other yield growth scenarios (3) allow a feedback from temperature to yield (4) have lower yield growth if pressure on food demand is low.

In the data model and supporting files, we find the regression fit to FAO food balance data and use that along with the baseline assumptions to find baseline food demand. The rate of change in implied yield gives a baseline for the potential yield increase over time. The potential is modified up or down by the action of the Crop yield growth slider. The closure of the gap between the potential yield and maximum yield reduces the crop yield growth. The default of the maximum yield set to 2.5 times the 2020 yield implies a comparable growth rate observed since 1960.

The two endogenous reductions to crop yield are low food pressure and high temperature change. Food pressure requiring farming intensity to exceed normal intensity, defaulted to be 0.7, increases the rate of crop yield growth; the converse is true of farming intensity less than normal. It is measured by the ratio of crops needed relative to the crops produced under normal intensity of the farmland, defaulted to 0.7. The integral of crop yield growth is then reduced by the Effect of temperature on crop yield, defaulted to the mean of 4% decrease per degree C, consistent with the Zhao et al (2017) used for the impact table. However, the user may adjust this strength in Assumptions.

Farmland Expansion and Contraction

Farmland expansion occurs when the ratio of crops produced to the crops that could be produced at maximum intensity given the current farmland area exceeds the normal farmland intensity. Conversely, if that ratio is less than the normal farmland intensity, then what is not needed is converted to forest land via natural regrowth, whereas the rest degrades to other land.

Other Land Decreases and Increases

Afforestation policy, i.e. the action depending on the Afforestation slider of En-ROADS, is implemented as the conversion of other land to forest land, since the land identified to be available for afforestation, excludes existing forests and agricultural land and falls into the other land category. Afforestation, as a policy implementation, is formulated based on a user-defined fraction of the full potential of afforestable land, and its delayed conversion to afforested land, which results in the land flux of Land afforestation rate. This flux is then incorporated into the land use change module as a chain of conversions from the other land to young forests and then aging to medium and mature forests. Deforestation from afforested land to farmland and other land affects the efficacy of this policy. The model captures historical regrowth of other land to nonAF young forest. Other land also decreases with farmland expansion, as only a fraction of the expansion comes from forests.

Model Structure

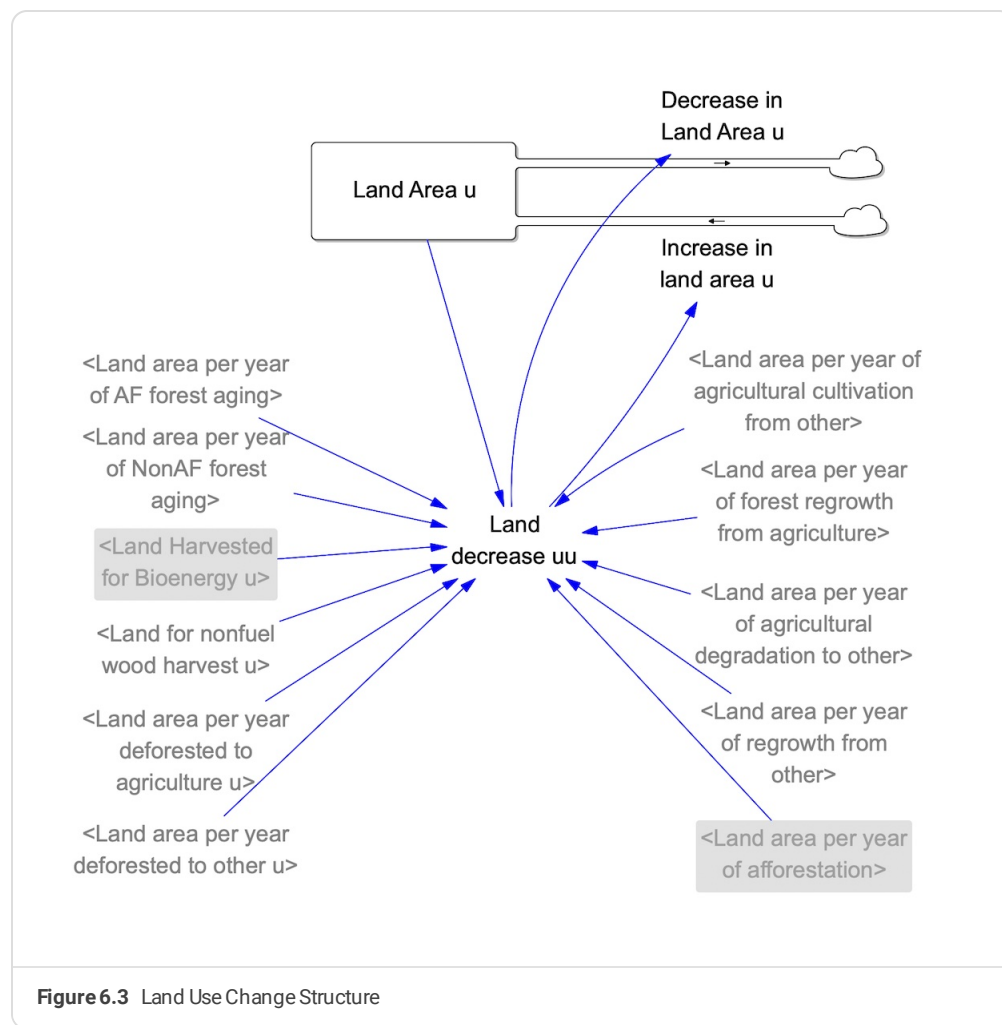


Figure 6.3 Land Use Change Structure

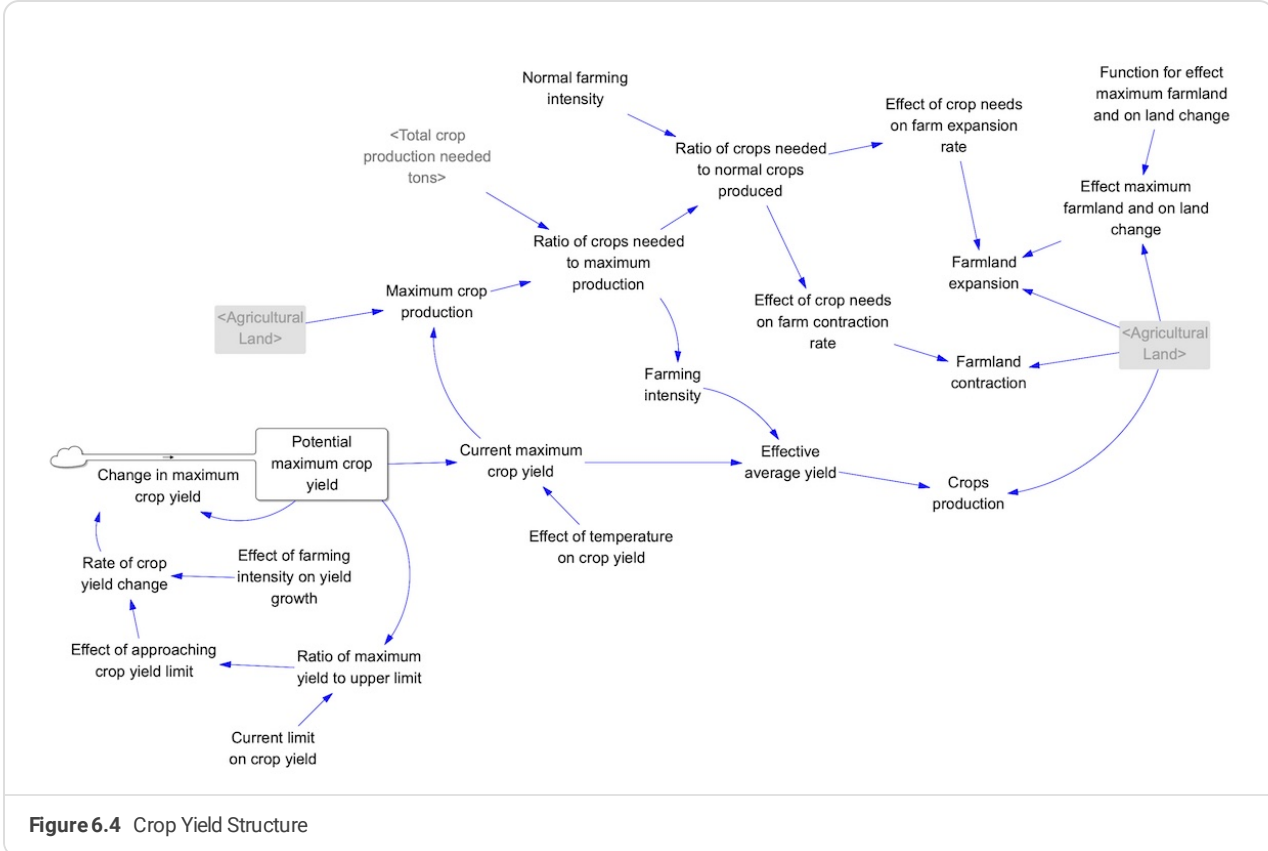


Figure 6.4 Crop Yield Structure

Terrestrial Biosphere Carbon Cycle

The terrestrial biosphere carbon (TBC) cycle reflects the primary productivity of biomass, removing carbon from the atmosphere as it grows, the natural and anthropogenic carbon fluxes from biomass and soil stocks, the flux from biomass carbon to soil carbon, and the fluxes of biomass and soil carbon as methane to the methane cycle. These fluxes by land type are summed together to feed into the carbon cycle.

The Goudriaan and Ketner (1984) and [IMAGE](#) models have detailed biospheres, partitioned into leaves, branches, stems, roots, litter, soil, and charcoal. To simplify the model, these categories are aggregated into stocks of biomass (leaves, branches, stems, roots) and soil (litter, soil). First-order time constants were calculated in C-ROADS assuming equilibrium in 1850 for each category land type and C-ROADS region and aggregated across regions for use in En-ROADS. Charcoal is neglected due to its long lifetime. The results are reasonably consistent with other partitionings of the biosphere and with the one-box biosphere of the Oeschger model (Oeschger, Siegenthaler et al., 1975; Bolin, 1986).

Net Primary Productivity (NPP)

The natural ability of biomass to sequester carbon from the atmosphere provides a key sink in the carbon cycle. NPP is the gross primary productivity minus the autotrophic respiration. Forest, agricultural land, other land, and tundra all have primary production and respiration. Furthermore, all primary production is affected by the level of CO₂ in the atmosphere (the fertilization effect). Carbon stored in biomass and soil is also released through heterotrophic aerobic and anaerobic respiration, which increases with higher temperature (increased fire, pests, decay). With the major exception of forests, all land reaches equilibrium quickly. Accordingly, calibrating in C-ROADS, the initial unit NPP of each non-forest land type is set assuming equilibrium in 1850. The flux into the biomass is equal to the flux out from aerobic and anaerobic respiration and transfer to soil is divided by the land area.

Unlike the other land types, forests have the most complex growth and the most biomass, so are treated in the most detail. Trees take up carbon through photosynthesis / primary production, and lose it through respiration, fire, being eaten by animals, decay, etc. Some of the carbon lost from biomass ends up in the soil through decomposition. The net of these carbon flows is that forests grow in an S-shaped pattern, slowly at first, at a high rate in middle age, and then reach an equilibrium where very high primary production is balanced by very high respiration. The growth curves, primary production, respiration and soil transfer rates are initialized and calibrated with Land Use Harmonization (LUH) and OSCAR modeling output, and compared against Global Carbon Budget (2023), Houghton and Nassikas (2017), and SSP IAMs. The process involves determining the regional growth curves in C-ROADS and then aggregating to global inputs for En-ROADS.

- Initialize carbon in stocks of forest, farmland, tundra, and other biomass and soil from OSCAR 1850 output by 10 regions, disaggregated and re-aggregated to fit our 7 regions.
- Initialize fractional rate of biomass and soil C respiration and transfer biomass to soil from OSCAR 1850 output.
- Determine forest unit NPP Richard's growth curve parameters for each of 7 regions.
 - Set Test Pulse scenario in which all LULUCF is set to 0 EXCEPT for a pulse of 95 of mature forest in 1900; when Test Pulse = 1, all fertilization and temperature feedbacks are turned off.
 - Set unit NPP inputs within ranges determined from forest analyses and assure unit NPP curves are reasonable given the types of forests in each region, e.g., more tropical in India and Other Developing A and B and more temperate in Developed.
 - Iteratively adjust parameters to achieve near equilibrium prior to pulse and assure regrowth is reasonable given the types of forests in each region.
 - Determine forest unit NPP Richard's growth curve parameters for global aggregation.
- Create global TBC cycle in C-ROADS
 - Using land fluxes as sum of regional fluxes, set unit NPP inputs within ranges determined from forest analyses such that the global forest carbon aligns with sum of regional forest carbon.
 - vTest pulse
 - vTest Baseline
 - Unit NPP from all other land types remain constant
 - Use global rates calculated from 1850 output of OSCAR model of biomass to soil transfer, biomass to atm respiration and soil to atmosphere respiration.
 - Iteratively adjust parameters to achieve comparable global results as from C-ROADS.

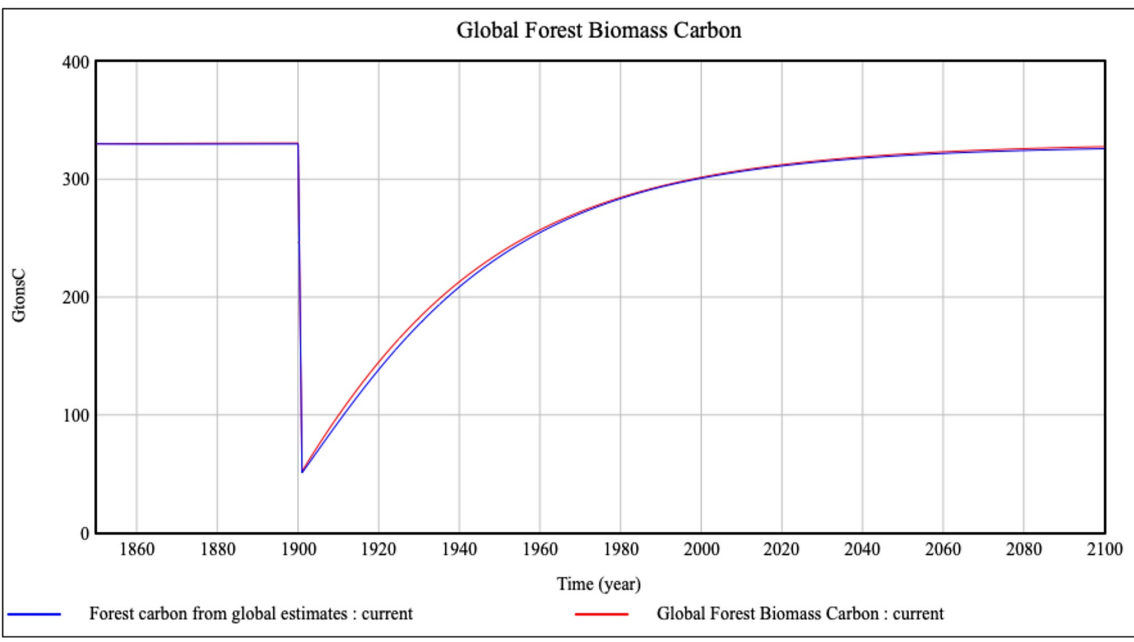


Figure 7.1 Regrowth After Instant Deforestation

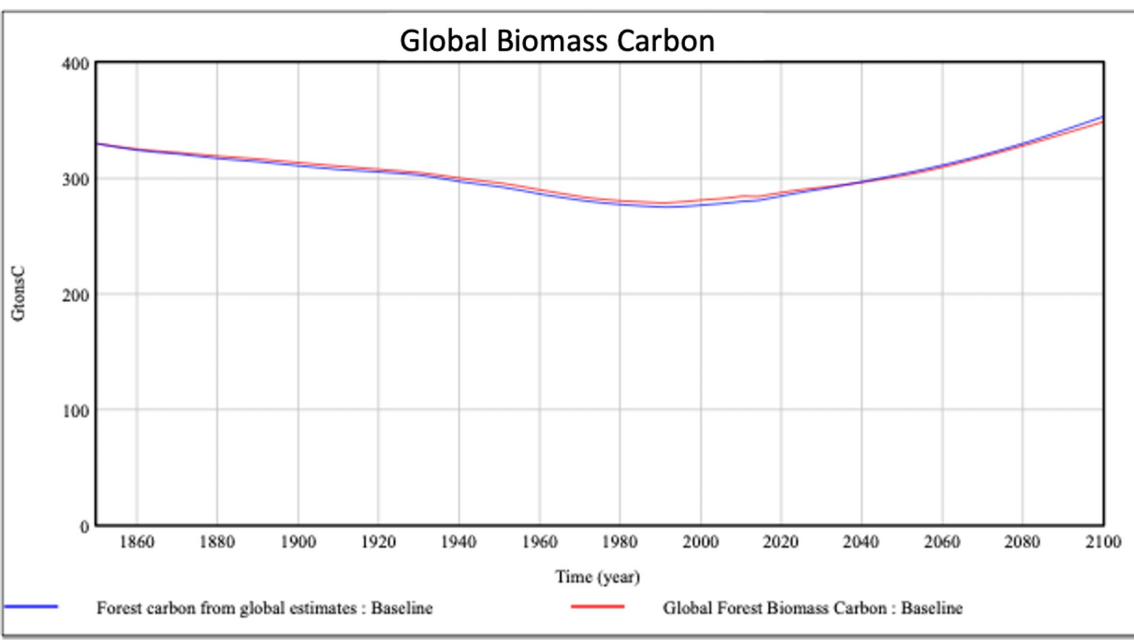


Figure 7.2 Baseline Forest Biomass

Increasing forest biomass carbon from 1980s despite decreasing forest area due to fertilization effect. Supported by data, e.g., Table 1 in [Xu et al. \(2021\)](#) shows that tropical moist forests is the only biome that has had a decrease from 2000 to 2019, but that is outweighed by the forest C increase everywhere else. "Globally, woody carbon stocks are increasing slowly with an average annual gain of $0.23 \pm 0.09 \text{ PgC year}^{-1}$."

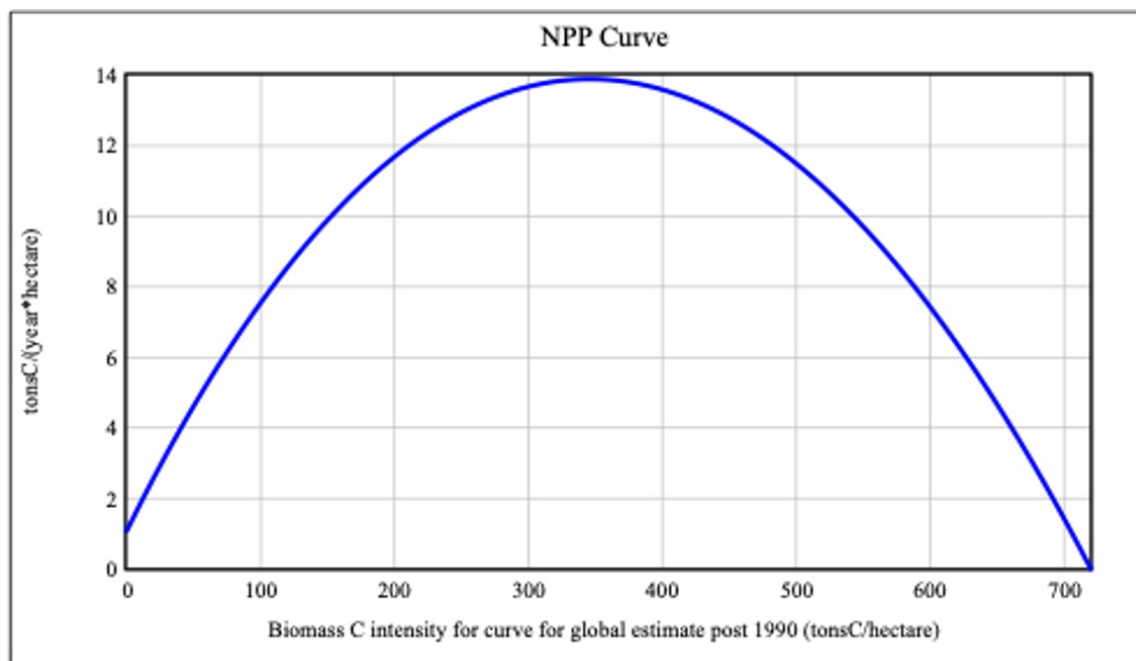


Figure 7.3 Net Primary Productivity versus Biomass Density

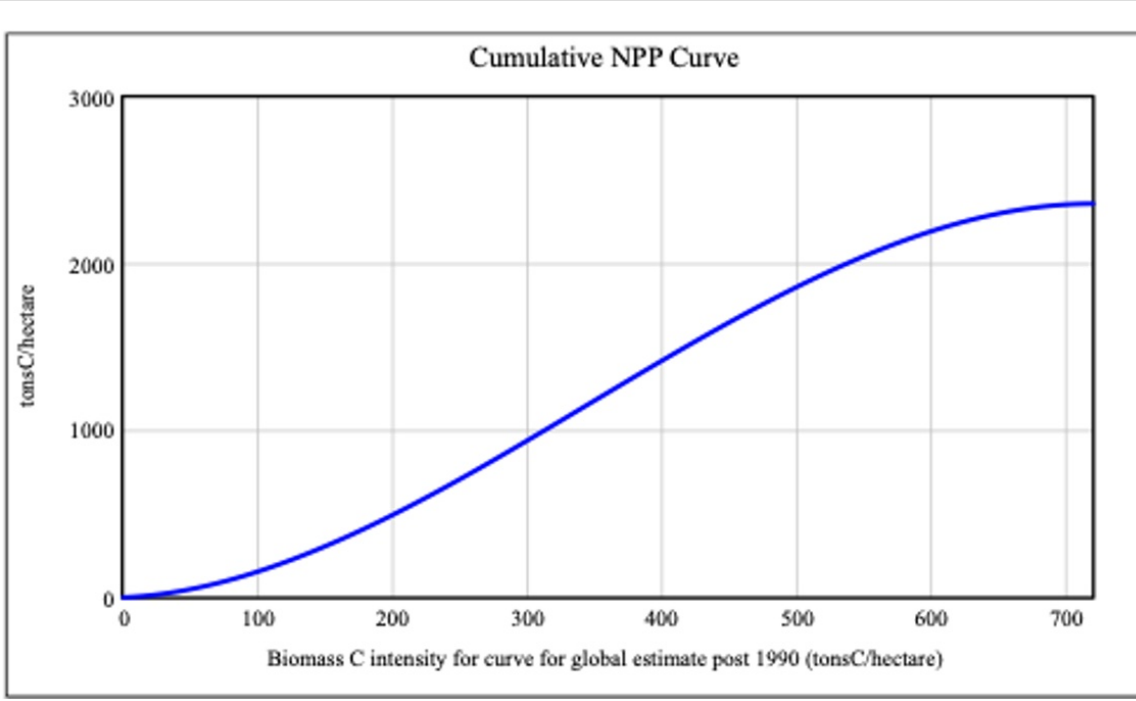


Figure 7.4 Biomass Density Growth over Time

The logarithmic relationship of the uptake of C by the biosphere reflects the fact that the uptake is less than proportional to the increase in atmospheric C concentration (Wullschleger, Post et al., 1995). This formulation, though commonly used, is not robust to large deviations in the atmospheric concentration of C. As the atmospheric concentration of C approaches zero, net primary production approaches minus infinity, which is not possible given the finite positive stock of biomass. As the concentration of C becomes very high, net primary production can grow arbitrarily large, which is also not possible in reality. Accordingly, we instead use a CES production function, which exhibits the following: 1) the slope around the preindustrial operating point is controlled by the biostimulation coefficient, which can be loosely interpreted as CO₂'s share of plant growth (at the margin), with the balance due to other factors like water and nutrients; 2) there is a finite slope at zero CO₂, such that there are no singularities; and 3) it controls saturation at high CO₂.

$$NPP = NPP_0 \left(1 - \beta_b + \beta_b \frac{C_a}{C_{a,0}} \right)^{\frac{1}{CO_2 \cdot sat}}$$

NPP = net primary production

NPP_0 = reference net primary production

β_b = biostimulation coefficient

C_a = C in atmosphere

$C_{a,0}$ = reference C in atmosphere

$CO_2 \cdot sat$ = coefficient that determines the rate of CO₂ saturation

Natural Losses

Carbon stored in biomass and soil is lost due to fire and microbial/fungal respiration. Rates of the release from each carbon stock is increased with increasing temperature change.

Carbon in both biomass and soil is also released as natural methane, entering into the methane cycle as such. The fractional rates of these releases also increase with temperature change. We assume a linear relationship, likely a good approximation over the typical range for warming by 2100. The sensitivity parameter, set by the user, governs the strength of the effect. The default sensitivity of 1 yields the average value found in Friedlingstein et al., 2006. Additionally, the rate of methane from tundra increases as temperature exceeds a threshold, representing a tipping point in the model.

Anthropogenic Carbon Fluxes

[Land Use, Land Use Change, and Forestry](#) explains the land use changes and uses. Carbon emitted from LUC is a coflow of each land change, driven by the Fraction biomass C emitted and Fraction soil C emitted. The remaining carbon, i.e., 1 minus that fraction, drives the carbon transferred to the new land type.

Net removals from regrowth after harvesting and from afforestation account for the net primary productivity (NPP) and also for the carbon lost back to the atmosphere from aerobic and anaerobic respiration and to the carbon and methane cycles, respectively. In order to isolate the removals due to land changes, the model simultaneously calculates the removals for the counterfactual scenario of no land changes. Corresponding coflows, aerobic and anaerobic respiration, and transfers from biomass to soil drive the TBC cycle without harvesting and regrowth. Accordingly, the net removals due to land changes are taken as difference in net removals with and without the land changes.

The net carbon emissions from LULUCF are the gross emissions, i.e., the LULUCF released to the atmosphere from biomass and soil, minus the net removals due to the land changes.

A reduction in converting forests and in harvesting mature trees leads to a reduction in net emissions from LULUCF, eventually meaning negative emissions. Part of this is because demand for bioenergy from wood falls; the young and medium forests cannot make up for the reduced availability of biomass from mature forests, which makes wood more expensive. Increases from the other sources of biomass (crops and waste) only partially cover the reduction from wood.

Bioenergy

The amount of bioenergy used and the investment in bioenergy infrastructure is endogenously determined by cost and other attractiveness, along with all other energy sources. Within bioenergy, there are three feedstocks (wood, energy crops, and waste) likewise determined by cost. The basic structure is market clearing / market share / logit structures for both electricity and thermal use. The various components have independent learning curves.

Bioenergy markets interact with the land structure because flow constraints, and therefore costs, depend on the carbon and land available in the appropriate land use areas. In turn, harvesting for bioenergy removes the indicated carbon, converting any age of forest into new forest with low carbon content, or increasing the desired farmland.

The costs, learning curves, sensitivities and other parameters are set to be reasonable compared to IEA WEO scenarios.

LULUCF net emissions are reported in two ways, including those resulting from bioenergy and also excluding those when reporting bioenergy emissions are reported separately. Regardless of reporting, bioenergy emissions and resulting net removals are appropriately included in the TBC cycle and included as such in the main carbon cycle. Although reported as part of the energy emissions, bioenergy net emissions are not included with the Global C energy and industry emission flux of carbon into the atmosphere.

Emissions from bioenergy are a function of the fraction coming from each feedstock, i.e., wood, crops, and waste/other non-crop fast-growing feedstocks. The carbon intensity of each feedstock (GtonsC/EJ) and the fraction of bioenergy emissions that are captured through bioCCS before entering the atmosphere also affect emissions into the atmosphere. The available bioenergy feedstock can constrain the extracted bioenergy supply.

All forests supply bioenergy and wood for non-fuel products according to their carbon content. To isolate the removals due to harvesting for bioenergy, the model also calculates the counterfactual land areas and terrestrial biosphere carbon resulting from all fluxes excluding harvest and regrowth for bioenergy.

Model Structure

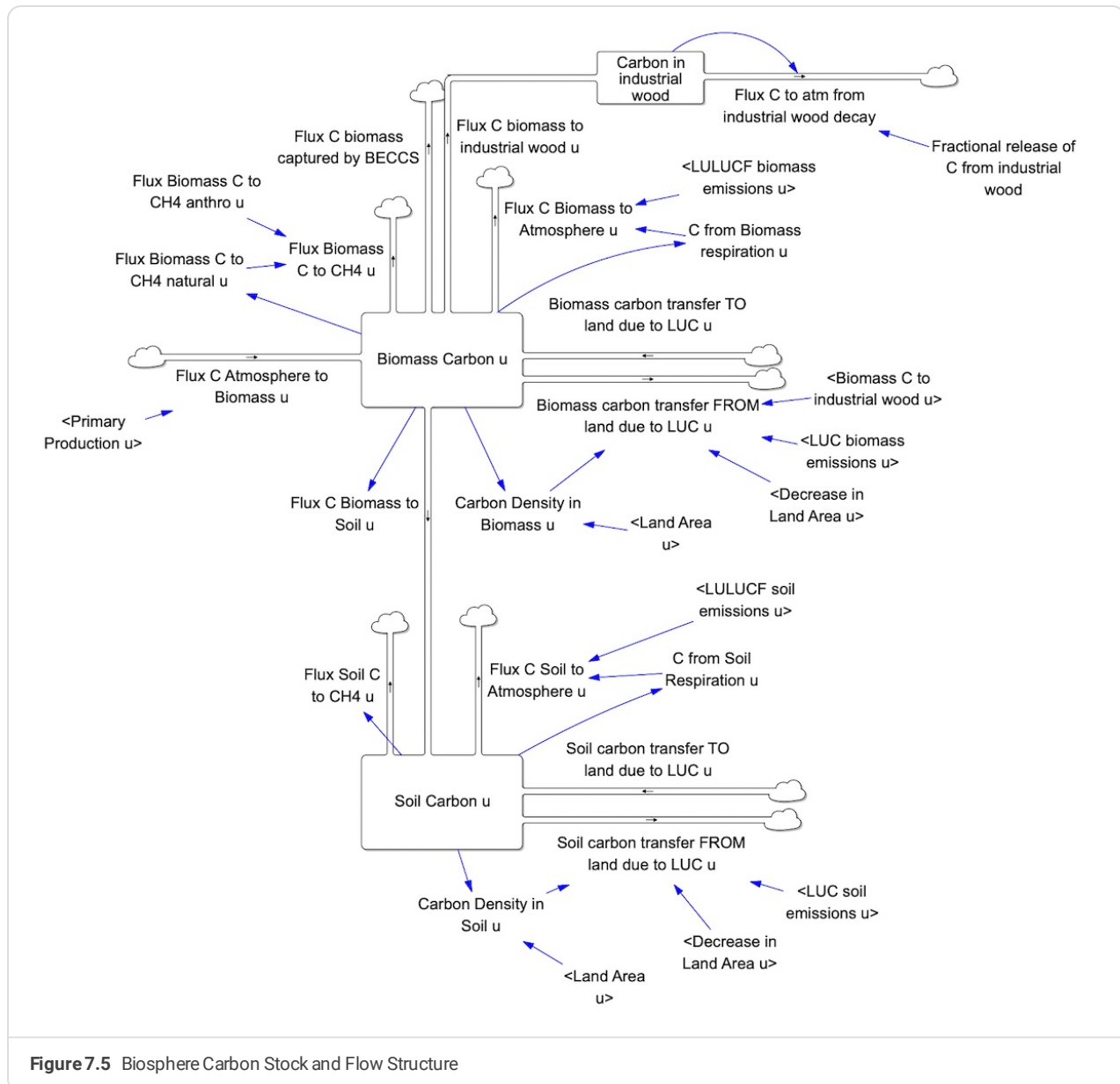


Figure 7.5 Biosphere Carbon Stock and Flow Structure

Emissions

En-ROADS models the emissions of well-mixed greenhouse gases (GHGs), including CO₂, CH₄, N₂O, PFCs, SF₆, HFCs, CFCs and HCFCs. For each gas, each potential source is modeled: energy production, energy-consuming capital, agriculture, and waste. CO₂ from energy is the largest source of total equivalent annual emissions, driven by total energy demand, energy choices, and energy supply infrastructure constructed to meet that demand. Other emission sources are ultimately driven by demand along with technology and practices which determine the emissions intensity of each activity for each gas.

Data for calibrating emissions are found under [Initialization, Calibration, Model Testing](#). In particular, initial values for the non-CO₂ GHGs are taken from 1990 data from PRIMAP 2021, assuming Agriculture includes PRIMAP MAG and LU categories, and Waste includes PRIMAP Waste and Other categories. Values for CO₂ are calibrated to multiple sources.

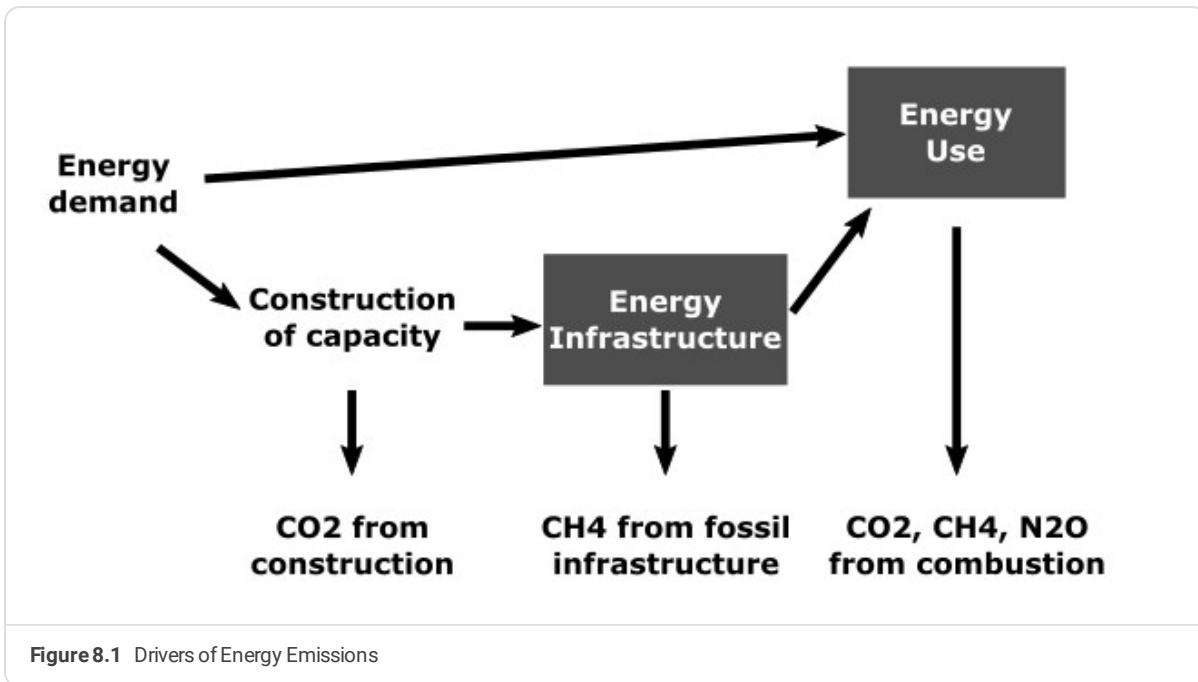
Land use CO₂ emissions are a function of the land use changes and uses as defined in [Land Use, Land Use Change, and Forestry](#) and [Terrestrial Biosphere Carbon Cycle](#).

Emissions from Energy Production

Energy production emissions include those from production capacity (infrastructure), construction of that production capacity, and from energy use. Emissions from each stage are calculated for electricity generation and non-electric use from each power source.

Energy use of fossil fuels and bioenergy produce the largest share of emissions. These depend on the GHG intensity of each source and use, and the primary energy used. Primary energy in turn depends on demand for each fuel, efficiency, and losses. Fossil fuels produce mostly CO₂ in every application; a small amount of CH₄ and N₂O are produced in some non-electric applications from incomplete combustion. Bioenergy produces CO₂, CH₄, and N₂O when burned.

Construction of all energy infrastructure, including renewable energy, produces CO₂ reflecting the energy used for construction and materials, modeled as a constant amount per unit of electricity or fuel capacity. Fossil fuel infrastructure produces CH₄ from off-gassing and leaks, the rate of which can be affected by policy controls.



Emissions from Energy Consuming Capital

End use capital represents all the constructed and manufactured materials that use energy or cause emissions. Capital is modeled in three economic sectors (residential & commercial, industry, transport) and three ages (vintage 1, 2, 3). CO₂ is emitted when new capital is constructed, similar to energy infrastructure, a fixed amount per unit of capital. Besides the energy used by capital and the emissions calculated under energy use above, there are direct emissions specific to each sector.

Industrial capital emits F-gases (PFCs, SF₆, and HFCs), N₂O, and a tiny amount of CH₄ as a byproduct of some processes. Byproduct emissions are modeled as directly proportional to total industrial capital. The ratios are subject to changes in practices and technology. Included in these calculations are the emissions of F-gases used as propellants in foams, aerosols, fire extinguishers, etc - they might be emitted in any sector but are produced by industrial capital. Industry also uses F-gases as solvents, insulating gases, etc. This application is modeled as a stock of each F-gas in use which can leak, and will be discarded, recycled, or destroyed at end of life. The fractions for each flow are subject to changes in practices and technology, and the demand for F-gases for these applications can change if alternatives are adopted.

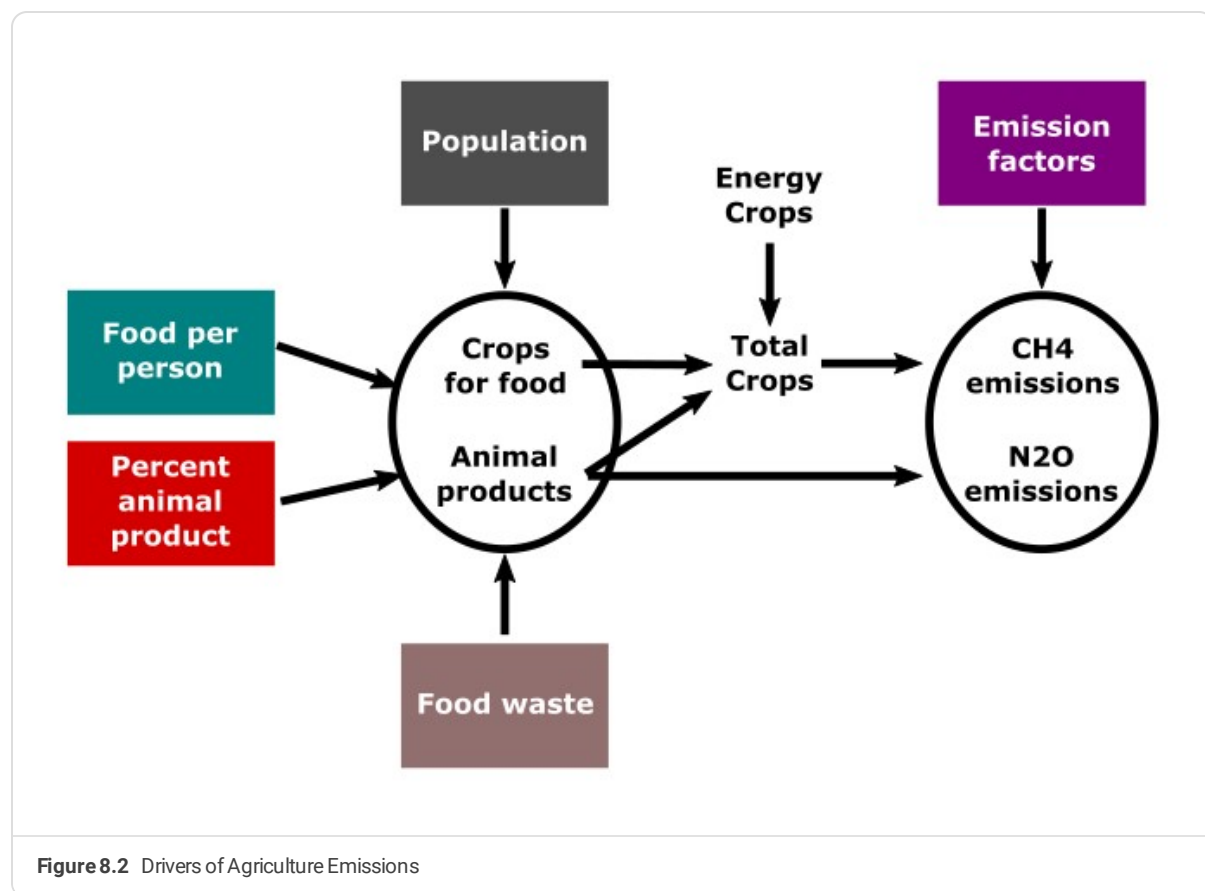
The largest emissions source from capital is refrigerants in cooling systems: refrigerators, heat pumps, air conditioners, etc. Demand for cooling (in GW capacity) is estimated from electric demand in the residential and commercial sector, and total energy demand in the transportation and industry sectors. The ratio of HFCs as refrigerants per GW of cooling demand is estimated from initial emissions rates and trends, and can change if alternatives are adopted. There are stocks of HFCs in current equipment and in discarded equipment, which emit depending on leak, recycling, and destruction rates, subject to changes in practices and technology.

Finally, ozone-depleting substances (ODSs, also called “Montreal gases”, principally CFCs and HCFCs) are modeled as an aggregate group with averaged characteristics. There is an exogenous emission - calibrated to observed atmospheric concentrations - plus a user-adjustable assumed stock representing the uncertain remaining chemicals in stockpiles and obsolete equipment. ODS leak rates are fixed, but the stocks of ODS can be destroyed before they leak if action is taken.

Emissions from Agriculture

Agriculture is the largest sector source of both methane and nitrous oxide, as well as the largest driver of deforestation. Emissions from livestock and crops are modeled individually. The demand as described in the [Land Section](#) determines the amount of animal product, and crop production, including the crops grown for energy and livestock feed. The emission factors for CH₄ and N₂O for both crops and livestock have base improvement rates as observed from production and emission data. Policies to lower emissions from agriculture are modeled as an adoption process of best practices, such as better feed and manure management, fertilizer runoff reduction and so on. This brings the emission factors towards their minimum practical values.

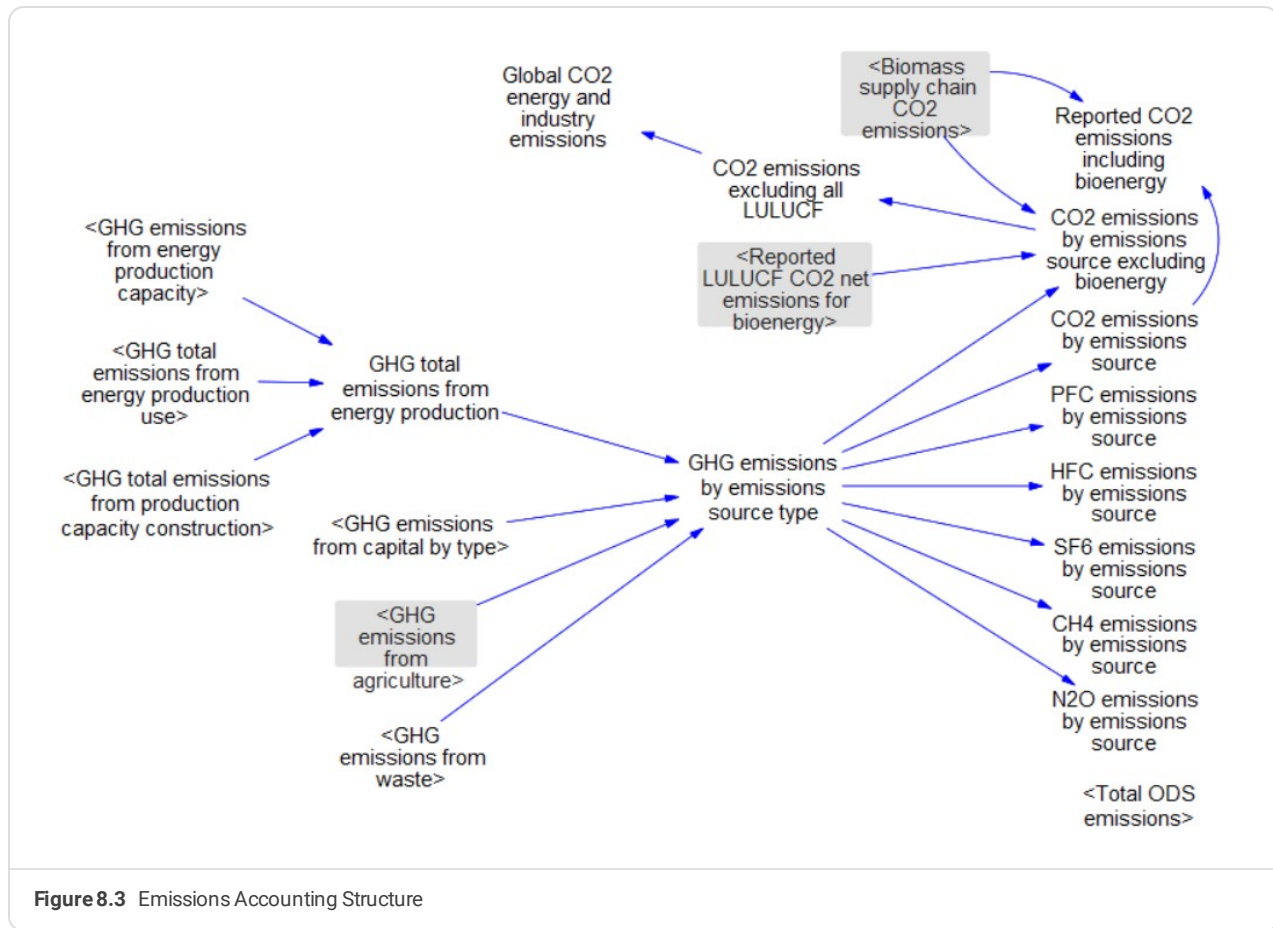
Actions in the food and agriculture system also affect emissions from agriculture. Reducing the trend towards greater consumption of food from animals lowers emissions in two ways: by shifting some demand to crops, which have lower emission factors; and by reducing the need for crops for animal feed. Reducing food waste lowers the production needed to meet food demand, lowering the activity that produces emissions in both crops and livestock.



Emissions from Waste

The waste sector represents both landfill (garbage / trash / municipal solid waste) and wastewater (sewage). Both subsectors emit both CH₄ and N₂O. The production of waste is modeled as a ratio of waste per person, representing only the waste relevant for emissions. Waste per person follows a declining trend. The emission factors for waste are calculated from initial data. Both the production ratio and the emission factors are reduced by policy, as many actions (such as recycling and composting) overlap in their effects.

Model Structure



Carbon Dioxide Removal (CDR)

The carbon dioxide removal (CDR) submodel governs the storage of carbon by biological, chemical, and industrial means. It includes both CDR proper, and Carbon Capture and Storage (CCS). CDR refers to methods that take CO₂ from the atmosphere and sequester it as carbon somewhere else. The CDR methods we include are afforestation, soil carbon management, biochar, enhanced mineralization, direct air carbon capture and storage (DACCs), and bioenergy with carbon capture and storage (BECCS). CCS refers to methods that capture carbon from a fuel before or after combustion, so that less CO₂ is released to the atmosphere. CCS is modeled for fossil fuels (coal and gas) and bioenergy. There is overlap between CCS, BECCS, and DACCs including common technologies, storage sites, economic drivers, and infrastructure.

CCS and CDR methods are modeled at various degrees of detail. The amount and timing of removals are either set by, calibrated to, or grounded in a synthesis of literature, most frequently the [Royal Society Report](#).

The carbon flows calculated by CCS and CDR structures are passed to the [Carbon Cycle](#) model and flow into biomass, soil, or sequestration stocks as appropriate. Each storage stock is subject to a leak or loss rate, adjustable in assumptions. In addition to carbon flows, this sector calculates the expenditures, energy needs, material flows, and land needs to show the impacts of relying on these techniques.

CDR Methods

Afforestation includes the land deliberately planted with trees as a means of carbon sequestration. Additional new forests might occur endogenously if farmland is abandoned, but that is not counted as "afforestation". Afforestation is specified by the user as a percent of the maximum area available for planting, adjustable as an assumption, and potentially limited by the area of Other Land available. Once the land is specified as afforested land, the growing forests sequester and store carbon according to the NPP and respiration drivers defined in [Terrestrial Biosphere Carbon Cycle](#).

Agricultural soil carbon refers to techniques that increase the amount of carbon in farmland soil. It is specified as a percent of the peak rate of CO₂ removal, adjustable in the assumptions. The farmland carbon transfer parameters in the [Terrestrial Biosphere Carbon Cycle](#) submodel are then adjusted to achieve that rate, potentially limited by land availability. The assumption on soil carbon loss rate adjusts the parameters of the Terrestrial Biosphere Carbon Cycle as well.

Biochar refers to turning biomass into charcoal then burying the carbon in farmland as a soil amendment. It is specified as a percent of the peak rate of CO₂ removal, adjustable in the assumptions, subject to a loss rate.

Mineralization is a chemical process, also called enhanced weathering, where certain kinds of rock are spread onto farmland, where they absorb CO₂. This also has a beneficial effect on agriculture if the soil is too acidic. The user input sets the percent of suitable farmland (adjustable in the assumptions) and the rate of CO₂ absorption the amount of rock applied and the specific absorption potential. Gross absorption is adjusted by a loss rate (default zero) and the emissions from the energy used to mine, grind and transport the necessary rock.

Direct air carbon capture and storage (DACCs) (sometimes called DAC) is a function of the capture equipment and the capacity to transport the captured CO₂, which is shared with CCS. The desired DACCs capacity is a function of the target percent of maximum Gtons CO₂ per year, which results in funding for DACCs infrastructure. DACCs capacity model has orders, completions and retirement, subject to delays and limits on construction capability. The amount of CO₂ captured is the lower of DACCs capacity and available CO₂ transport capacity. The cost of DACCs declines over time with learning, but can increase if CO₂ transport and storage constraints are exceeded. The energy required to operate DACCs equipment increases the energy demand for **electricity**, potentially increasing emissions. The gross capture by DACCs is stored in geological formations; an estimate of CO₂ emitted by its energy demand is subtracted to plot net removals.

Bioenergy with CCS (BECCS) is modeled under the CCS section below. It responds to price signals, i.e. carbon price, rather than having a user input under the CDR section.

Carbon Capture and Storage (CCS)

Both fossil and bioenergy CCS are modeled as stocks of transport capacity (shared with DACCs), and individual capture capacities for each fuel, for industry and electric sectors. Completion is subject to both development and construction delays, with a limit on overall growth rates as construction capability itself takes time to construct. The time delays on transport capacity are assumed to set the limit on deploying capture capacity as well. The amount of CO₂ captured for each fuel and application is the least of: CO₂ created in combustion, capture capacity, and available transport capacity. If transport capacity is limiting, it is shared in proportion to capture capacity.

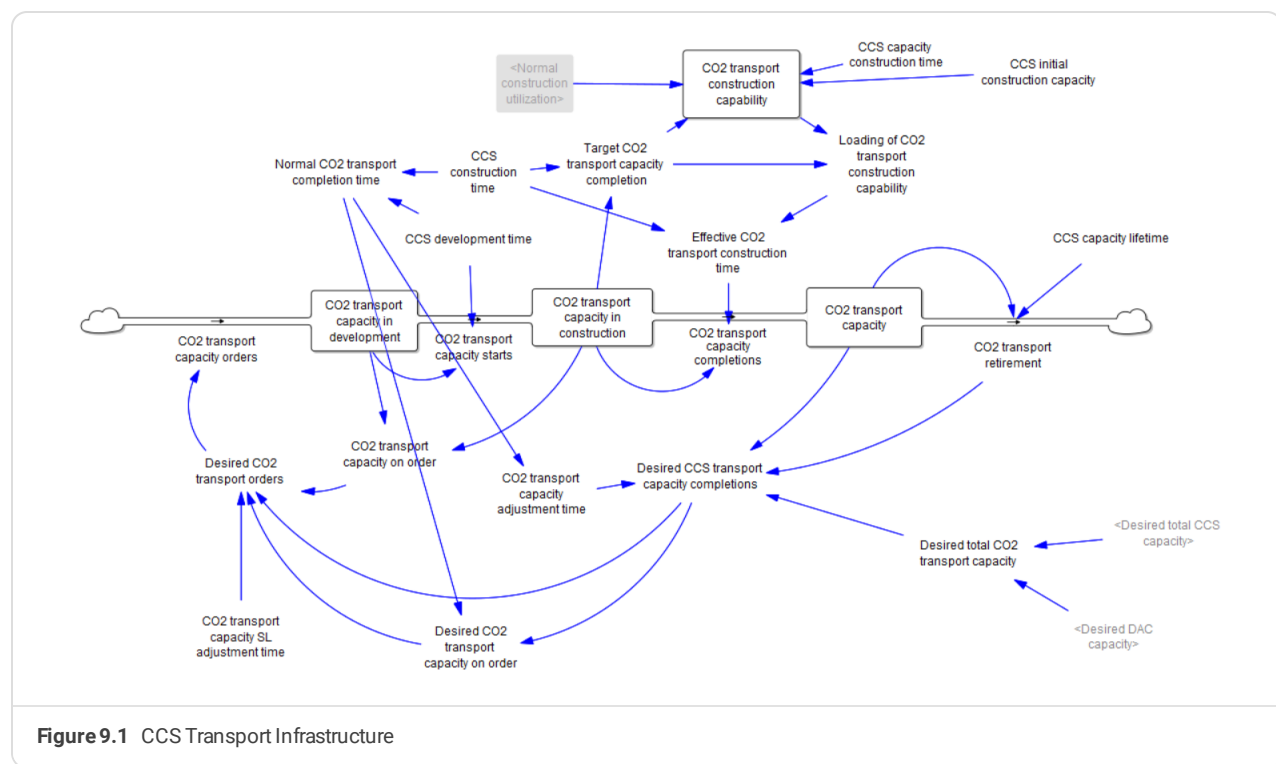
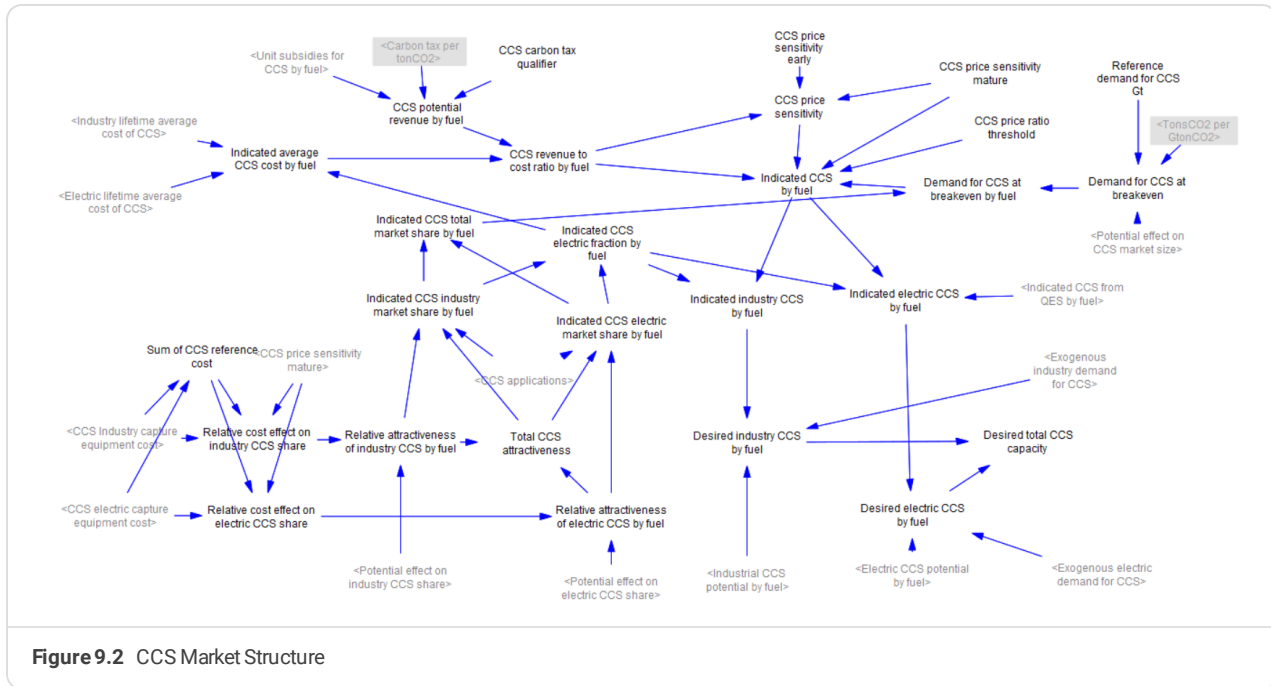


Figure 9.1 CCS Transport Infrastructure

CCS capacity adjusts over time to the amount indicated by a simple economics model. The available revenue for CCS can come from a carbon price or the incentive of a clean electricity standard. The market is defined by price sensitivity and a reference demand - the demand for CCS when its cost equals available revenue. There is additional exogenous construction of CCS representing the historical and expected construction for R&D, demonstration projects and the like, calibrated to historical CCS data. The cost of CCS capture and transport equipment costs, which follow endogenous learning curves, and the cost of energy assumed to equal the market price of electricity from the [Market Clearing sector](#). Costs also increase as constraints on storage and transport capacity are reached. Within the overall market size, the different fuels and applications of CCS compete on price and remaining potential.



Well-Mixed Greenhouse Gas Cycles

Carbon Cycle

Introduction

The carbon cycle sub-model is adapted from the FREE model (Fiddaman, 1997). While the original FREE structure is based on primary sources that are now somewhat dated, we find that they hold up well against recent data. Calibration experiments against recent data and other models do not provide compelling reasons to adjust the model structure or parameters, though in the future we will likely do so.

Other models in current use include simple carbon cycle representations. Nordhaus' DICE models, for example, use simple first- and third-order linear models (Nordhaus, 1994, 2000). The first-order model is usefully simple, but does not capture nonlinearities (e.g., sink saturation) or explicitly conserve carbon. The third-order model conserves carbon but is still linear and thus not robust to high emissions scenarios. More importantly for education and decision support, neither model provides a recognizable carbon flow structure, particularly for biomass.

Socolow and Lam (2007) explore a set of simple linear carbon cycle models to characterize possible emissions trajectories, including the effect of procrastination. The spirit of their analysis is similar to ours, except that the models are linear (sensibly, for tractability) and the calibration approach differs. Socolow and Lam calibrate to Green's function (convolution integral) approximations of the 2x CO₂ response of larger models; this yields a calibration for lower-order variants that emphasizes long-term dynamics. Our calibration is weighted towards recent data, which is truncated, and thus likely emphasizes faster dynamics. Nonlinearities in the C-ROADS carbon uptake mechanisms mean that the 4x CO₂ response will not be strictly double the 2xCO₂ response.

Structure

The adapted FREE carbon cycle is an eddy diffusion model with stocks of carbon in the atmosphere, biosphere, mixed ocean layer, and three deep ocean layers. The model couples the atmosphere-mixed ocean layer interactions and net primary production of the Goudriaan and Kettner and IMAGE 1.0 models (Goudriaan and Ketner 1984; Rotmans 1990) with a 5-layer eddy diffusion ocean based on (Oeschger, Siegenthaler et al., 1975) and a 2-box biosphere based on (Goudriaan and Ketner 1984).

The global terrestrial biosphere carbon cycle fluxes and initial biomass and soil stocks are the sum of those by land type as defined in [Terrestrial Biosphere Carbon Cycle](#).

The interaction between the atmosphere and mixed ocean layer involves a shift in chemical equilibria (Goudriaan and Ketner, 1984). CO₂ in the ocean reacts to produce HCO₃⁻ and CO₃⁼. In equilibrium,

$$C_m = C_{m,0} \left(\frac{C_a}{C_{a,0}} \right)^{\frac{1}{\zeta}}$$

C_m = C in mixed ocean layer

$C_{m,0}$ = reference C in mixed ocean layer

C_a = C in atmosphere

$C_{a,0}$ = reference C in atmosphere

ζ = buffer factor

The atmosphere and mixed ocean adjust to this equilibrium with a time constant of 1 year. The buffer or Revelle factor, ζ , is typically about 10. As a result, the partial pressure of CO₂ in the ocean rises about 10 times faster than the total concentration of carbon (Fung, 1991). This means that the ocean, while it initially contains about 60 times as much carbon as the preindustrial atmosphere, behaves as if it were only 6 times as large.

The buffer factor itself rises with the atmospheric concentration of CO₂ (Goudriaan and Ketner, 1984; Rotmans, 1990) and temperature (Fung, 1991). This means that the ocean's capacity to absorb CO₂ diminishes as the atmospheric concentration rises. This temperature effect is another of several possible feedback mechanisms between the climate and carbon cycle. The fractional reduction in the solubility of CO₂ in ocean falls with rising temperatures. Likewise for the temperature feedback on C flux to biomass, we assume a linear relationship, likely a good approximation over the typical range for warming by 2100. The sensitivity parameter that governs the strength of the effect on the flux to the biomass also governs the strength of the effect on the flux to the ocean. For both effects, the default sensitivity of 1 yields the average values found in Friedlingstein et al., 2006.

$$\zeta = \zeta_0 + \delta_b \ln\left(\frac{C_a}{C_{a,0}}\right)$$

ζ = buffer factor

ζ_0 = reference buffer factor

δ_b = buffer CO₂ coefficient

C_a = C in atmosphere

$C_{a,0}$ = reference C in atmosphere

The deep ocean is represented by a simple eddy-diffusion structure similar to that in the Oeschger model, but with fewer layers (Oeschger, Siegenthaler et al., 1975). Effects of ocean circulation and carbon precipitation, present in more complex models (Goudriaan and Ketner, 1984; Björkstrom, 1986; Rotmans, 1990; Keller and Goldstein, 1995), are neglected. Within the ocean, transport of carbon among ocean layers operates linearly. The flux of carbon between two layers of identical thickness is expressed by:

$$F_{m,n} = \frac{(C_m - C_n)^e}{d^2}$$

$F_{m,n}$ = carbon flux from layer m to layer n

C_k = carbon in layer k

e = eddy diffusion coefficient

d = depth of layers

The effective time constant for this interaction varies with d , the thickness of the ocean layers. To account for layer thicknesses that are not identical, the time constant uses the mean thickness of two adjacent layers. The following table summarizes time constants for the interaction between the layers used in C-ROADS, which employs a 100 meter mixed layer, and four deep ocean layers that are 300, 300, 1300, and 1800 meters, sequentially deeper. Simulation experiments show there is no material difference in the atmosphere-ocean flux between the five-layer ocean and more disaggregate structures, including an 11-layer ocean, at least through the model time horizon of 2100.

Table 10.1 Effective Time Constants for Ocean Carbon Transport

Layer Thickness	Time Constant
100 meters	1 year
300 meters	14 years
300 meters	20 years
1300 meters	236 years
1800 meters	634 years

The sum of carbon removals by non-land based CDR, defined in [Carbon Dioxide Removal](#), is another flux from the carbon in the atmosphere, which increases the stock of carbon sequestered. Carbon captured from CCS also increases that stock. The sum of carbon from that stock that is lost re-enters the atmosphere.

Other greenhouse gases

Other GHGs included in CO₂equivalent emissions

The basis for emissions is described in the [Emissions](#) section. En-ROADS explicitly models other well-mixed greenhouses gases, including methane (CH₄), nitrous oxide (N₂O), and the fluorinated gases (PFCs, SF₆, and HFCs). PFCs are represented as CF₄-equivalents due to the comparably long lifetimes of the various PFC types. HFCs, on the other hand, are represented as an array of the nine primary HFC types, each with its own parameters. Ozone-depleting substances (ODSs, also called “Montreal gases”, principally CFCs and HCFCs) are represented as an aggregated stock with averaged parameters. The structure of each GHG’s cycle reflects first order dynamics, such that the gas is emitted at a given rate and is taken up from the atmosphere according to its concentration and its time constant. Initialization is based on 1990 levels of data from GISS for CH₄ and N₂O and according to C-ROADS (2023) for F-gases. The remaining mass in the atmosphere is converted, according to its molecular weight, to the concentration of that gas. The multiplication of each gas concentration by the radiative coefficient of the gas yields its instantaneous radiative forcing (RF). This RF is included in the sum of all RFs to determine the total RF on the system.

For those explicitly modeled GHGs, the CO₂ equivalent emissions of each gas are calculated by multiplying its emissions by its 100-year Global Warming Potential. Time constants, radiative forcing coefficients, and the GWP are taken from the IPCCs Fifth Assessment Report (AR5) Working Group 1 Chapter 8. (Table 8.A.1. Lifetimes, Radiative Efficiencies and Metric Values GWPs relative to CO₂).

In addition to the anthropogenic emissions considered as part of the CO₂ equivalent emissions, CH₄, N₂O, and PFCs also have a natural component. The global natural CH₄ emissions are from the anaerobic respiration of biomass, soil, and oceans. The global natural N₂O emissions are based on MAGICC output, using the remaining emissions in their “zero emissions” scenario. The global natural PFC emissions are calculated by dividing Preindustrial mass of CF₄ equivalents by the time constant for CF₄. The units of each gas are: MtonsCH₄, MtonsN₂O-N, tonsCF₄, tonsSF₆, and tonsHFC for each of the primary HFC types. To calculate the CO₂ equivalent emissions of N₂O, the model first converts the emissions from MtonsN₂O-N/year to Mtons N₂O/year.

The sensitivity of this release defaults to 0.1% per degree Celsius over a threshold, defaulted to 2 Degrees Celsius; the user may change these assumptions.

Cumulative Emissions

En-ROADS calculates the cumulative CO₂ with the initial value taken as the 1990 C-ROADS value starting in 1870. Cumulative emissions are determined through the simulation. The trillionth ton is a marker of cumulative emissions above which a two degree future is far less likely. Budgets are also presented from 2011 and from 2018, based on IPCC thresholds.

Model Structure

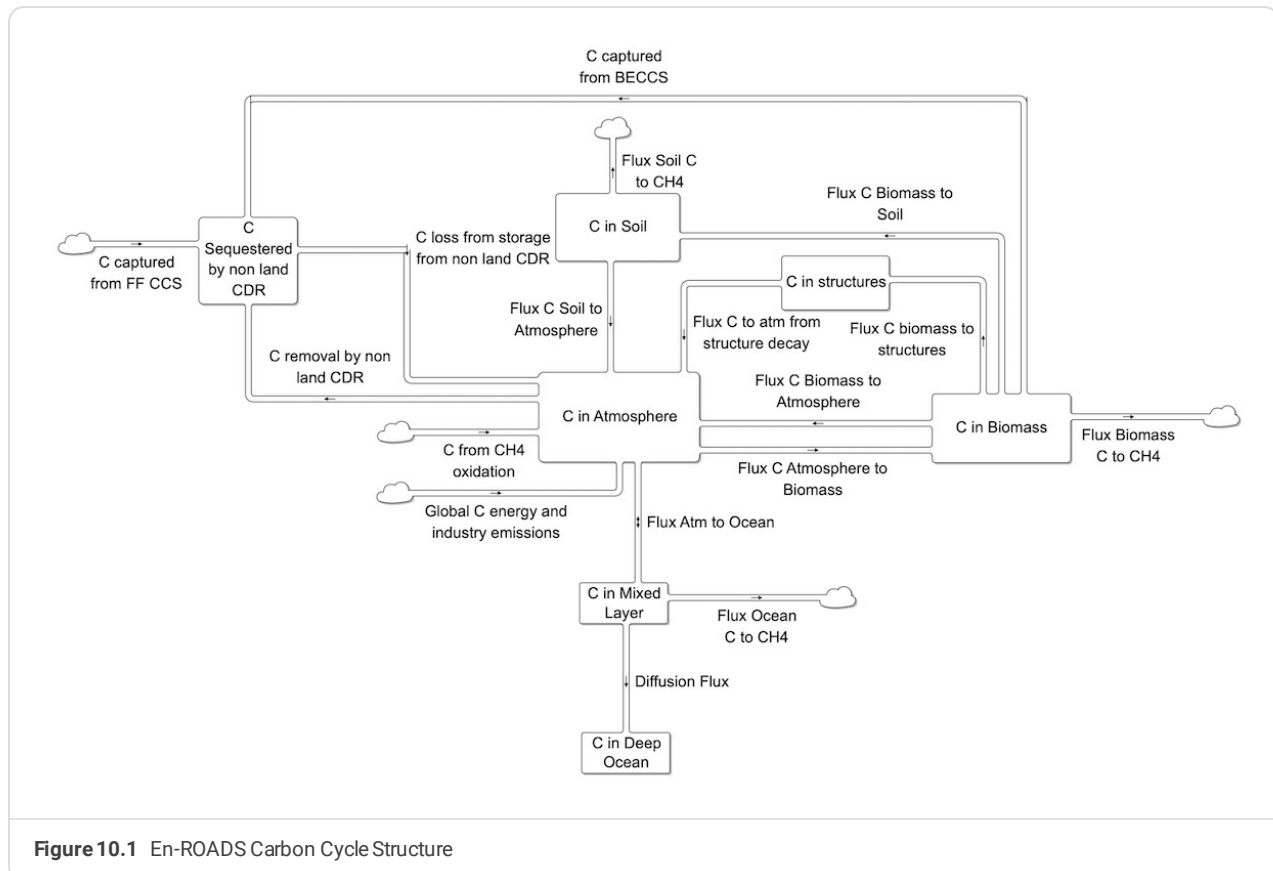


Figure 10.1 En-ROADS Carbon Cycle Structure

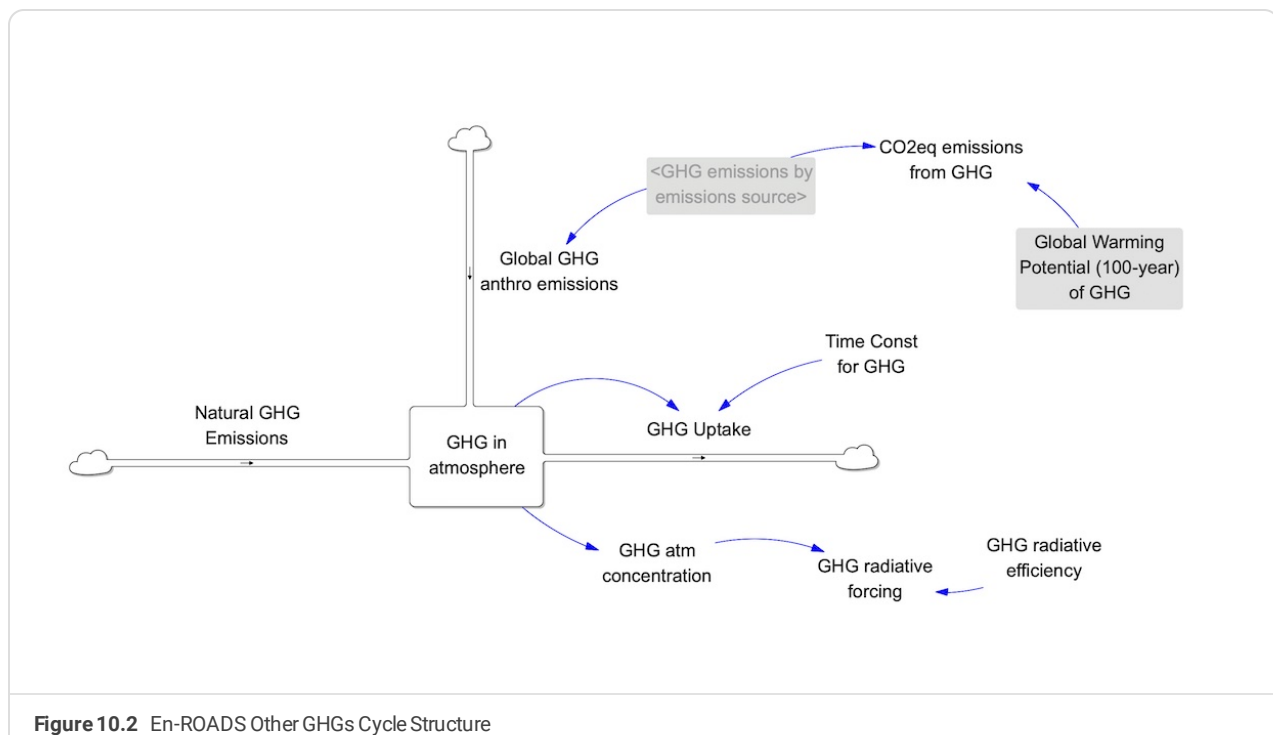


Figure 10.2 En-ROADS Other GHGs Cycle Structure

Climate

Introduction

Like the carbon cycle, the climate sector is adapted from the FREE model, which used the DICE climate sector without modification (Nordhaus 1994). The DICE structure in turn followed Schneider and Thompson (1981).

The model has been recast in terms of stocks and flows of heat, rather than temperature, to make the physical process of accumulation clearer to users. However, the current model is analytically equivalent to the FREE and DICE versions. While FREE and DICE used exogenous trajectories for all non-CO₂ radiative forcings, this version adds endogenous forcings from all well-mixed GHGs, i.e., CO₂, CH₄, N₂O, PFCs, SF₆, and each HFC type.

Structure

The climate is modeled as a fifth-order, linear system, with three negative feedback loops. Two loops govern the transport of heat from the atmosphere and surface ocean, while the third represents warming of the deep ocean. Deep ocean warming is a slow process, because the ocean has such a large heat capacity. If the deep ocean temperature is held constant, the response of the atmosphere and surface ocean to warming is first-order.

Temperature change is a function of radiative forcing (RF) from greenhouse gases and other factors, feedback cooling from outbound longwave radiation, and heat transfer from the atmosphere and surface ocean to the deep ocean layer.

$$\begin{aligned} T_{\text{surf}} &= \frac{Q_{\text{surf}}}{R_{\text{surf}}} \\ T_{\text{deep}} &= \frac{Q_{\text{deep}}}{R_{\text{deep}}} \\ Q_{\text{surf}} &= \int (RF(t) - F_{\text{out}}(t) - F_{\text{deep}}(t)) dt + Q_{\text{surf}}(0) \\ Q_{\text{deep}} &= \int F_{\text{deep}}(t) dt + Q_{\text{deep}}(0) \end{aligned}$$

T = temperature of surface and deep ocean boxes

Q = heat content of respective boxes

R = heat capacity of respective boxes

RF = radiative forcing

F_{out} = outgoing radiative flux

F_{deep} = heat flux to deep ocean

$$F_{\text{out}}(t) = \lambda T_{\text{surf}}$$

$$F_{\text{deep}}(t) = R_{\text{deep}} \cdot \frac{T_{\text{surf}} - T_{\text{deep}}}{\tau}$$

λ = climate feedback parameter

τ = heat transfer time constant

Radiative forcing from CO₂ is logarithmic of the atmospheric CO₂ concentration, but also dependent on the N₂O concentration (IPCC AR6, 2023; NOAA, 2023). Forcing from CH₄ and N₂O is less than the sum of RF from each individually to account for interactions between both gases; CO₂ concentrations also affect forcings from N₂O. Forcing from each F-gas is the product of its concentration and its radiative forcing coefficient; the total forcings of F-gases is the sum of these products, as are the forcings from MP gases derived. The sum of other forcings, which include those from aerosols (black carbon, organic carbon, sulfates), tropospheric ozone, defaults to an exogenous time-varying parameter. The values use a composite of AR6 history 1750-2019 and their projections for SSP4 6.0 through 2100. The equilibrium temperature response to a change in radiative forcing is determined by the radiative forcing coefficient, κ , and the climate feedback parameter, λ . Equilibrium sensitivity to 2xCO₂eq forcing is 3°C in the base case. The plot of that relationship is shown as Figure 11.1.

$$T_{\text{equil}} = \frac{\kappa \cdot \ln\left(\frac{C_a}{C_{a,0}}\right)}{\lambda \cdot \ln(2)}$$

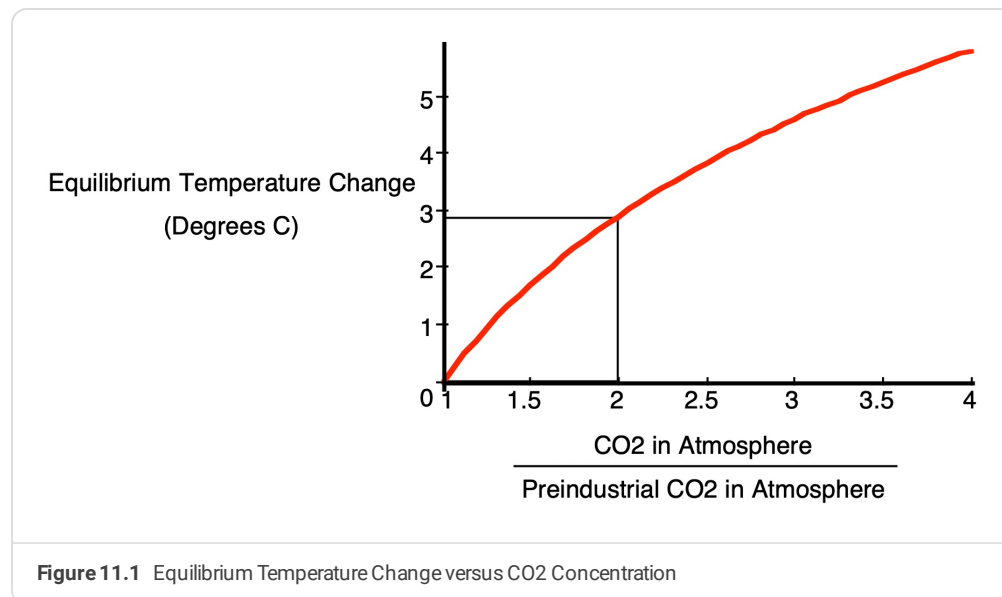
T_{equil} = equilibrium temperature

C_a = atmospheric CO₂ concentration

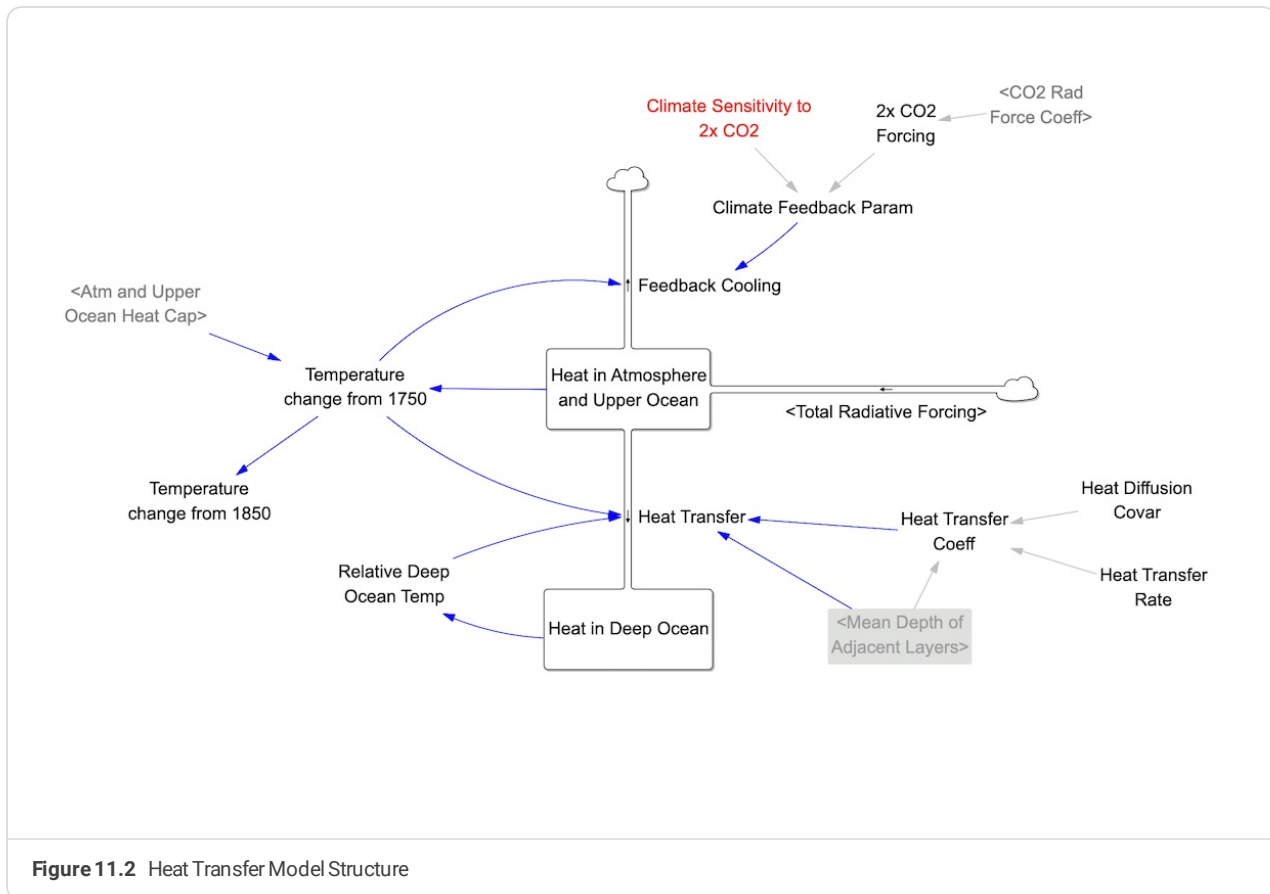
$C_{a,0}$ = preindustrial atmospheric CO₂ concentration

κ = radiative forcing coefficient

λ = climate feedback parameter



Model Structure



Sea Level Rise

Sea Level Rise (SLR) is modeled by extending the semi-empirical approach proposed by Vermeer and Rahmstorf (2009) in a way to accommodate the water impoundment by artificial reservoirs and to experiment with higher levels of contribution to SLR from ice sheet melting in Antarctica and Greenland than already assumed. The model is estimated from historical data 1900-2021, a period with low levels of warming that therefore may underestimate future sea level rise from the faster-than-historical rates of melt of the Greenland and Antarctic ice sheets. “Contribution to SLR from Ice Melt in Antarctica by 2100” and “Contribution to SLR from Ice Melt in Greenland by 2100” sliders allow users to capture these effects. Sliders are initialized with the mid-range estimates for the contribution of ice sheet melting in Antarctica/Greenland in the IPCC AR6 report.

Model Structure

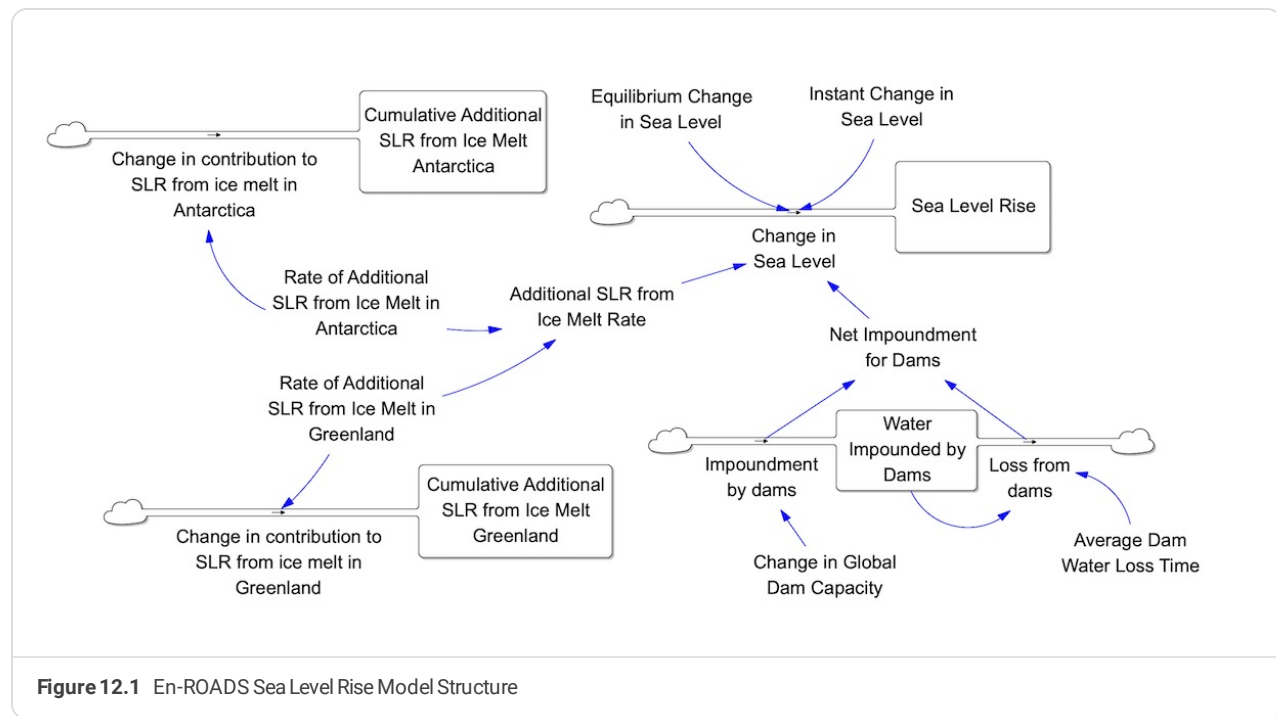


Figure 12.1 En-ROADS Sea Level Rise Model Structure

Damage to GDP

In En-ROADS, economic growth can be reduced from what it would otherwise be, due to the effects of climate change on human activity. En-ROADS uses temperature change as a proxy for the multiple effects of shifting patterns of temperature, rainfall, disease, etc., that might affect the economy. Economists refer to these effects as the "damage function" and measure the net present value of potential damage as the social cost of carbon.

Literature on damage function

In the scientific literature, aggregate economic impact of climate change is expressed as a fraction of 'annual income', global GDP or GDP per capita. It is formulated as an increasing function of global mean temperature change from preindustrial times. Extensive research into the literature shows the vast disparity between estimates of damage at varying temperature changes. See Damage Function References.

We assessed the very low estimates (Nordhaus, 2007, 2013, and 2016; Weitzman, 2012), ranging from 1% at 2°C, 2-3% at 3°C, and 4-9% at 4°C, and 6-25% at 5°C, to be unrealistic.

The four sources we deemed most credible and covering a range of rates of increasing damage with increasing temperature change are:

- Burke *et al.* (2018)
- Burke *et al.* (2015)
- Dietz and Stern (2015)
- Howard and Sterner (2017)

Burke et al. (2015) estimate the macro impacts of climate change from micro impacts based on an extensive empirical study (e.g. daily temperature effect on labor productivity per person scaled up to annual and global). They conclude that, taking nonlinearities into account, the damage is much higher than the earlier estimates, which is 21% of GDP per capita by 2100 on average. Wealthy countries are not unaffected. Their estimates take different responses by countries into account. In the 'pooled response' formulation, rich and poor countries are assumed to respond identically to the temperature change. Short run estimates account for 1 year of temperature, whereas long run estimates account for 5 years of temperature change.

In their 2018 study where they focus on the impact of mitigation targets, they estimate 15%–25% loss in GDP per capita by 2100 for 2.5–3°C warming, and more than 30% for 4°C. Their damage function is widely used in recent studies that analyze the social cost of carbon (Ricke et al., 2018; Taconet et al., 2020; Glanemann et al., 2020). Dietz and Stern follow the formulation of Weitzman (2012), yet assume 50% damage at 4°C.

Through a meta-analysis, Howard and Sterner (2017) determined quadratic equations to define the damage function with varying assumptions:

- Preferred model for non-catastrophic damage
- Preferred model for total (non-catastrophic plus catastrophic) damages
- Preferred model for total damages plus productivity

Modelling the damage function in En-ROADS

The literature has a variety of damage function forms and values. In En-ROADS, we would like to capture all these, and to allow users explore a wider variety of damage values while keeping the model robust. Accordingly, there are five options in the model, four presets using the equations to reflect the chosen literature and one to customize the damage function with a logistic equation with user specified parameters. There is also an additional option to turn off the damage entirely.

For each source, the model uses the exact formula given, or determined if not provided, to capture the preset. Burke *et al* (2015 and 2018) do not define a damage function but instead show curves of damage vs. temperature change. Accordingly, we digitized the graphs and assessed regression analyses Ω with cubic, quadratic, and linear equations for $\Omega = \text{Damage function} = 1 - 1/(1+D)$. Cubic regression, i.e., $\Omega = 1 - 1/(1+\alpha*T + \beta*T^2 + \gamma*T\delta)$, best captures the fit for all relevant temperatures. Unlike Dietz and Stern (2015) and Burke *et al* (2015 and 2018), Howard and Sterner (2017) define $\Omega = D$ as noted below.

Burke et al, 2018 SR Pooled

$$\alpha = 0.3079; \beta = -0.0532; \gamma = 0.004; \delta = 3$$

Burke et al, 2015 LR Pooled

$$\alpha = 0.3074; \beta = 0.0144; \gamma = 0.0168; \delta = 3$$

Dietz and Stern, 2015

$$\alpha = 0; \beta = 1/18.82; \gamma = 4\delta; \delta = 6.754$$

Howard and Sterner, 2017

$\Omega = D$ "Preferred model for total damages plus productivity"

$$\Omega = 1.145 * T^2$$

For the customized damage function, we use a logistic function formulation with three parameters, L , k and x_0 , where L is the maximum damage, k refers to the steepness of the damage curve and x_0 is the inflection point.

$$D(t) = \frac{L}{1 + e^{-k(T(t) - x_0)}} \quad (1)$$

This allows for a function form that captures the damage function shapes and values presented in the literature and allows parameterization based on easily understandable user inputs (sliders) such as "the damage % at 1.5°C warming" and/or the "maximum damage" saturates at the maximum damage value entered by the users or at 100% so that the damage and GDP values are kept in realistic ranges for extreme temperatures.

Social Cost of Carbon

Social cost of carbon (SCC) is the marginal cost of emitting one extra tonne of CO₂ in a given year. It is a commonly used metric in US administration and climate policy debate. En-ROADS shows the SCC in the present year (i.e. 2023) calculated according to the emission trajectory in the baseline scenario, and the subsequent economic damage of this emission trajectory which depends on the user inputs for the damage function, Social Discount Rate, and climate sensitivity assumptions.

To calculate SCC in En-ROADS, we adopt the approach followed by United States Interagency Working Group (IWG) (Greenstone et al., 2013), which calculated the SCC values used by the US government. This approach involved simulating the integrated assessment models until 2300, since atmospheric CO₂ has a very long lifetime and the economic damages from today's emissions are observed for centuries. Therefore, even though the normal time horizon of En-ROADS is until 2100, for SCC calculation it is extended until 2300. In other words, all scenarios displayed by En-ROADS cover the horizon through 2100, yet SCC is calculated based on two additional simulations run upon demand (when users click on the SCC table on UI) through 2300. For the post-2100 period in these simulations to 2300, we make the following assumptions following IWG:

- IWG assumes that population growth rate declines linearly after 2100, reaching zero in the year 2200, hence a stable population after 2100. In the En-ROADS population stabilizes by 2100 already in the baseline scenario.
- GDP per capita growth rate is assumed to decline linearly after 2100, from whatever value it takes in 2100 based on user inputs and damage, reaching zero in the year 2300.
- The rate of decline in the Carbon intensity of GDP (CO₂ emissions from energy / GDP) between 2090 and 2100 is maintained from 2100 through 2300. To formulate this assumption,
 - We calculate the average rate of change of the Carbon intensity of GDP in 2090-2100.
 - We compute the Post-2100 carbon intensity of GDP according to this new constant rate of change.
 - We calculate the post-2100 CO₂ emissions from energy as the multiplication of this Post-2100 carbon intensity of GDP * Global GDP.
- Net land use CO₂ emissions (LULUCF net emissions) are assumed to decline linearly after 2100, from any value they take in a scenario in 2100, reaching zero in the year 2200.
- Non-CO₂ GHG emissions (that of CH₄, N₂O, SF₆, PFC and HFC) are assumed to follow the same rate of change as CO₂ emissions. In other words, the post-2100 trajectory of all these GHG gases are set to follow the trajectory of CO₂.

With these assumptions for the 2100-2300 period, SCC is calculated with the following three main steps:

Step 1: Run a baseline damage scenario through 2300 and calculate the present value of damage

With any user-set assumptions for the economic impact of temperature rise (damage function) and other climate system assumptions, the damage, i.e. the percentage of global GDP loss (D) is calculated as in Equation 1 above. From there, annual Global GDP Loss (L) is calculated as the corresponding fraction of Global GDP (Gross World Product, GWP), Equation 2. These losses over time are discounted to the present year with the variable Present Value of Global GDP Loss (PVL) based on the user-set Social Discount Rate (r) as in Equation 3, where t_p is the present year. Present Value of Cumulative Damage until time is the accumulation of PVL as denoted in Equation 4 where t_0 and t_f are the initial and final time, respectively, i.e. 1990 and 2300.

$$L(t) = D(t) \cdot GWP(t) \quad (2)$$

$$PVL(t) = L(t) \cdot \frac{1}{(1+r)^{\max\{0, t-t_p\}}} \quad (3)$$

$$CPVL(t) = \int_{t_0}^{t_f} PVL(t) dt \quad (4)$$

Step 2: Run an emission shock scenario through 2300 and calculate the present value of damage

The same scenario as in Step 1 is simulated with an additional 1 Gton of CO₂ emissions in the present year. In other words, the trajectory of CO₂ emissions is perturbed with the pulse of 1 GtonCO₂ yr⁻¹ in the present year.

Step 3: Calculate SCC as the marginal damage between the two simulations

The difference between the Present Value of Cumulative Damage by 2300 in the two simulations yields the social cost of carbon. This formulation is denoted in Equation 5:

$$SCC(t_p) = \frac{CPVL^2(t_f) - CPVL^1(t_f)}{e} \quad (5)$$

$CPVL^1(t_f)$ = Present Value of Cumulative Damage in the baseline damage scenario in the final time (2300)

$CPVL^2(t_f)$ = Present Value of Cumulative Damage in the emission shock scenario in the final time (2300)

e = amount of the emission shock (1 GtonCO₂ yr⁻¹)

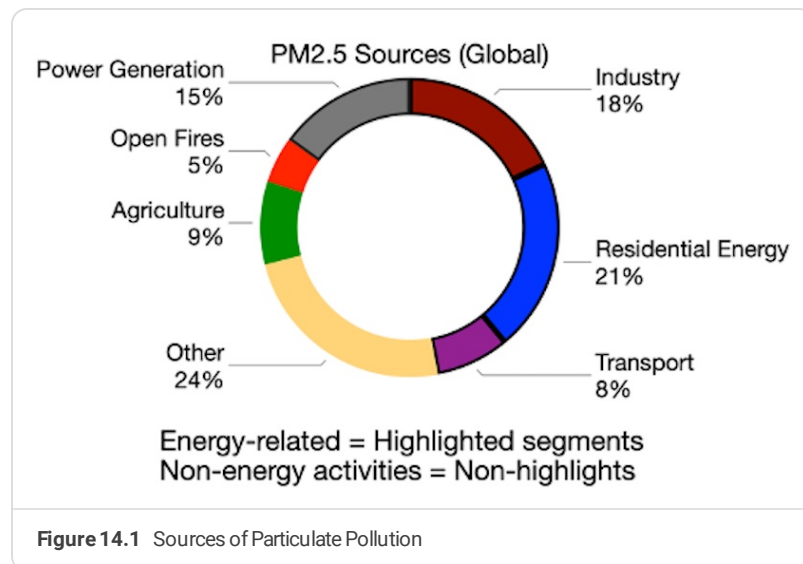
Damage Function References

- IPCC. (2014). Summary for policymakers. in Climate Change 2014: Impacts, Adaptation, and Vulnerability. Part A: Global and Sectoral Aspects. Contribution of Working Group II to the Fifth Assessment Report of the Intergovernmental Panel on Climate Change (eds. Field, C.B., V.R. Barros, D.J. Dokken, K.J. Mach, M.D. Mastrandrea, T.E. Bilir, M. Chatterjee, K.L. Ebi, Y.O. Estrada, R.C. Genova, B. Girma, E.S. Kissel, A.N. Levy, S. MacCracken, & P.R. Mastrandrea, and L.L. White) 1–32 Cambridge University Press.
- Nordhaus, W. D. (2007). Accompanying notes and documentation on development of DICE-2007 model: Notes on DICE-2007. v8 of September 21, 2007. N. Hav. CT Yale Univ.
- Ackerman, F. & Stanton, E. (2012). Climate risks and carbon prices: Revising the social cost of carbon. *Econ. Open-Access Open-Assess. E-J.* 6, 10.
- Nordhaus, W. & Sztorc, P. (2013). DICE 2013R: Introduction and user's manual.
- Tol, R. S. (2009). The economic effects of climate change. *J. Econ. Perspect.* 23, 29–51.
- Nordhaus, W. D. (2017). Revisiting the social cost of carbon. *Proc. Natl. Acad. Sci.* 114, 1518–1523.
- Keen, S. (2020). The appallingly bad neoclassical economics of climate change. *Globalizations* 1–29.
- Weitzman, M. L. (2012). GHG targets as insurance against catastrophic climate damages. *J. Public Econ. Theory* 14, 221–244.
- Hanemann, W. M. (2008). What is the economic cost of climate change?
- Dietz, S. & Stern, N. (2015). Endogenous growth, convexity of damage and climate risk: how Nordhaus' framework supports deep cuts in carbon emissions. *Econ. J.* 125, 574–620.
- Burke, M., Hsiang, S. M. & Miguel, E. (2015). Global non-linear effect of temperature on economic production. *Nature* 527, 235–239.
- Burke, M., Davis, W. M. & Diffenbaugh, N. S. (2018). Large potential reduction in economic damages under UN mitigation targets. *Nature* 557, 549–553.
- Ricke, K., Drouet, L., Caldeira, K. & Tavoni, M. Country-level social cost of carbon. *Nat. Clim. Change* 8, 895–900 (2018).
- Taconet, N., Méjean, A. & Guiavarch, C. (2020). Influence of climate change impacts and mitigation costs on inequality between countries. *Clim. Change* 1–20.
- Glanemann, N., Willner, S. N. & Levermann, A. (2020). Paris Climate Agreement passes the cost-benefit test. *Nat. Commun.* 11, 1–11.
- Greenstone, M., Kopits, E. & Wolverton, A. (2013). Developing a Social Cost of Carbon for US Regulatory Analysis: A Methodology and Interpretation. *Review of Environmental Economics and Policy* 7, 23–46.

Other Impacts

Air Quality—PM2.5

The air quality sector simulates annual global emissions of PM2.5. En-ROADS estimates annual global emissions from three sources: energy generation (electricity), energy generation (non electricity), and other sources (including agriculture and open fires).



Ambient PM2.5 is considered the leading environmental health risk factor globally and is a top 10 risk factor in countries across the economic development spectrum. PM2.5 is fine particulate matter as defined by the mass per cubic meter of air of particles with a diameter of ≤ 2.5 micrometers (μm).

The components of PM2.5 are solid and liquid particles small enough to remain airborne and are defined as two forms:

1. Solids/liquid particles directly emitted to the atmosphere (primary PM).
2. Solids/liquid particles formed from gaseous precursors (secondary PM).

Components of PM2.5 may include (some of) the following:

- Carbons
- Sulfates
- Nitrates
- Chlorides
- Iron
- Calcium
- Other Organics (solid/liquid)

Sources of PM2.5 in En-ROADS – Overview

PM2.5 is generated from multiple sources. The chart was from research Global Sources of Fine Particulate Matter: Interpretation of PM2.5 Chemical Composition Observed by SPARTAN using a Global Chemical Transport Model (Weagle et al 2018).

En-ROADS aggregates these sources into the following sources:

1. Energy generation a. Electricity production b. Energy (non electricity) production
2. Non-energy generation a. agriculture, b. open fires, c. other sources.

PM2.5 from Energy Generation

En-ROADS calculates energy generated PM2.5 emissions by applying an emissions factor (EF) (in million metric tons (Mtons) emitted per exajoule (EJ)) for each fuel source to the annual rate of energy produced (in EJ/year).

$$Emission\ Rate[Fuel] = EF[Fuel] \times Electricity\ Production[Fuel]$$

EFs for fuel sources are calculated in several input-output models. En-ROADS applies EFs estimated from analysis by the International Institute for Applied Systems Analysis (IIASA). The EFs for coal, oil, and gas were calculated using the GAINS model (IIASA) to estimate emissions/year from G20 countries/regions and then averaged. Countries included the United States, several EU countries, India (2 regions) and China (3 different regions). The EF for bio was calculated from the RAINS model (IIASA).

Estimates for EFs were not significantly different between electricity and non electricity (which includes industry). En-ROADS applies the same EFs to electricity and non electricity. Users can vary the EF assumption across a range (by source), with a range of 50% to 150% of the base EF (shown in the table below).

Table 14.1 Emission Factors by Fuel

Source	EF (Mtons/EJ)
Coal	0.1200
Oil	0.0050
Gas	0.0001
Bio	0.0400

PM2.5 from Non Energy Sources

Non-energy sources of PM2.5 are estimated by applying a per capita EF (Mtons/year/billion people) to global population (billion people). The per capita EF is set at the start of the scenario year.

In 2015, non-energy sources of PM2.5 accounted for 35% total PM2.5 emissions. En-ROADS uses that 35% as an estimate of the non-energy contribution to total prior to 2015.

The per capita PM_{2.5} is calculated in 2015 (Scenario Year) by dividing global non-energy PM_{2.5} (Mtons/year) by global population in billions (2015). For 2015 and remaining simulated years, non-energy PM_{2.5} (Mtons/year) is calculated by multiplying global population (billions) by the 2015 emissions factor.

pH

The pH sector of En-ROADS reflects the empirical function presented by Bernie et al. (2010). As the atmospheric concentration in the atmosphere increases, the pH of the ocean decreases by a third order response.

Other Impacts from Warming

The continuous increase in the global temperature is expected to cause a variety of impacts on ecology and human activities – in addition to sea level rise, increased ocean acidity and the loss in global GDP discussed in previous sections. More frequent and intense extreme weather events, major reduction in global crop yield and biodiversity loss are some examples of the other anticipated impacts of climate change. En-ROADS simulates five categories of such climate impact metrics (some categories containing more than one metric):

- Population Exposed to Sea Level Rise
- Probability of Ice-free Arctic Summer
- Decrease in Crop Yield from Warming
- Species Losing More than 50% of Climatic Range
- Additional Deaths from Extreme Heat

Building on the findings of five peer-reviewed climate studies, we formulated the relationship between global mean temperature (as well as sea level rise) and these metrics (primarily through interpolation and extrapolation).

Nature Impacts from Warming

Drawing on the IPCC's Sixth Assessment Report, we identified and formulated relationships between global mean temperature and impacts on ecosystems.

Ecosystem Shifts from Warming

A notable projected impact of climate change is the risk of ecosystem shift which was presented in Ostberg et al. (2013) and expanded in Warszawski et al. (2013). Climate change is expected to cause biogeochemical changes in land, which would affect flora and fauna and their interactions, thus impacting ecosystems. The assumption is the larger biogeochemical changes are, the higher the risk of ecosystems being disrupted.

Global land was classified into 16 categories as follows:

Table 14.2 Land Type Classification

Land types	
Tropical rainforest	Warm woody savanna, woodland & shrubland
Tropical seasonal & deciduous forest	Warm savanna & open shrubland
Temperate broadleaved evergreen forest	Warm grassland
Temperate broadleaved deciduous forest	Temperate woody savanna, woodland & shrubland
Mixed forest	Temperate savanna & open shrubland
Temperate coniferous forest	Temperate grassland
Boreal evergreen forest	Arctic tundra
Boreal deciduous forest	Desert

Warszawski et al. (2013) used an ensemble of global vegetation models to estimate the percentage of global land area at risk of experiencing ecosystem shifts, from one land type to another, under different temperature scenarios. We digitized the S-shaped relationship from Warszawski et al. (2013) Figure 3 into En-ROADS and linked it to our temperature projections to enable the user to track the impact of different policy scenarios on ecosystems. We converted the percentage to area in million hectares to make it more relevant to En-ROADS users.

Arid Land Expansion from Warming

One worrisome land type change is desertification as increased aridity can change an area's capacity to supply ecosystem services or host biodiversity. Increased aridity is often associated with desertification, although recent studies show the relationship is not one-to-one. We used a bias-corrected estimate from the CMIP5 model ensemble from Huang et al. (2016) Figure 2 to link temperature rise to the increased area of arid lands globally. Digitizing the relationship over time under two RCP scenarios, we estimated an exponential relationship between global arid land area and temperature over the 21st century.

Initialization, Calibration, Model Testing

En-ROADS initializes and calibrates to available historical data, primarily provided by the following sources:

Energy and Emissions

- Energy Information Administration (EIA) (2019)
- International Energy Agency (IEA) World Energy Balances and World Energy Statistics (2024)
- Energy Institute (EI) Statistical Review of World Energy (2024)
- Global Carbon Budget (2023) (CO₂ Energy Emissions and Land Use Change Emissions)
- PRIMAP 2.4.2 (2023) (Non-CO₂ GHG Emissions only)
- Houghton and Nassikas (2017) (CO₂ Land Use only)

Land Areas

- Land Use Harmonization (LUH2) data (Hurt et al., 2018)

GHG Concentrations, Radiative Forcings, Temperature Change, Sea Level Rise

- National Oceanic and Atmospheric Administration (NOAA) concentrations (2024) and radiative forcings (2023)
- Goddard Institute for Space Studies (GISS) GISTEMP4 Global Mean Estimates based on Land and Ocean Data 1880-2023 (2024)
- Met Office Hadley Centre HadCRUT5.0.1.0 temperature 1850-2023 (2024)
- National Aeronautics and Space Administration (NASA) satellite sea level rise (2023)

En-ROADS calibrates to projected values provided by the following sources:

- International Energy Agency (IEA) WEO (2023)
- Network for Greening the Financial System (2023)
 - GCAM 6.0 (U.S.)
 - MESSAGEix-GLOBIOM 1.1-M-R12 (IIASA)
 - REMIND-MAgPIE 3.2-4.6 (Germany)
- SSP Version 2.0 scenarios (2018 - Available at: <https://tntcat.iiasa.ac.at/SspDb>)
 - Netherlands Environmental Assessment Agency (PBL). Integrated Model to Assess the Global Environment (IMAGE): Detlef van Vuuren, David Gernaat, Elke Stehfest
 - International Institute for Applied Systems Analysis (IIASA). Model for Energy Supply Strategy Alternatives and their General Environmental Impact - GLobal BIOsphere Management (MESSAGE-GLOBIOM): Keywan Riahi, Oliver Fricko, Petr Havlik
 - National Institute for Environmental Studies (NIES). Asia-Pacific Integrated Model (AIM): Shinichiro Fujimori
 - Pacific Northwest National Laboratory (PNNL). Global Change Assessment Model (GCAM): Kate Calvin and Jae Edmonds
 - Potsdam Institute for Climate Impact Research (PIK). REMIND-MAGPIE: Elmar Kriegler, Alexander Popp, Nico Bauer
 - European Institute on Economics and the Environment (EIEE). World Induced Technical Change Hybrid-GLobal BIOsphere Management (WITCH-GLOBIOM): Massimo Tavoni, Johannes Emmerling

“Calibration and validation comparisons.xlsx” and “Calibration and validation comparisons.pptx” provide output and figures demonstrating the strong fit to history and other modeling groups’ projections. Key comparison measures include GDP, total and source energy use and cost measures, GHG emissions and concentrations, and temperature change. Noteworthy, comparisons of primary energy of renewables depend on conversion assumptions which vary dramatically between sources.

Our default settings are guided primarily by history, WEO Current Policies, and NGFS Current Policies projections.

Land Calibration

The land use change module is calibrated in the regional C-ROADS based on the Land Use Harmonization (LUH2) data prepared for the Climate Research Program Coupled Model Intercomparison Project (CMIP6). Our output for each land type strongly aligns with historical data. However, our projections suggest more farmland and less forest than do the LUH projections and those of the NGFS models. The differences are due to our accounting for the temperature effect on reducing crop yield, which translates to more farmland expansion to meet food demands. The other models do not account for that feedback.

Response to Actions

Importing as data variables, En-ROADS also uses various scenario projections for model validation. Accordingly, there are necessary files, generated from data models, which must accompany the model. We test the model against the NGFS projections for their 6 scenarios. We set population and GDP per capita controls to follow the given NGFS trajectories and exogenously use the average of the models’ carbon price values for the given NGFS scenario, and assess the model output versus the IAMs’ results.

An important caveat is that these other IAMs’ assumptions other than carbon pricing are unknown. Accordingly, we force CDR and other GHG action to align with the NGFS projections for carbon removal and other GHG emissions. Reliably, for each scenario, the model captures the key dynamics of the NGFS models.

Although outdated now, we ran comparable assessments against all of the Shared Socioeconomic Pathway (SSP) of the IPCC’s AR5 scenarios. Comparisons were against the output of 6 models for 5 SSP scenarios, each with up to 6 radiative forcing options, i.e., 1.9, 2.6, 3.4, 4.5, 6.0, and Baseline. Reliably, for each SSP storyline and RF level, the model captures the key dynamics of the SSP models.

Sensitivity Analyses

Extreme Testing

Sensitivity analyses provide insight into model robustness. Using a Latin grid, two tests for extreme conditions, one with standard controls and another with advanced controls, varied key actions. The extreme values for some variables are beyond the ranges available on the app but are tested for model robustness in Vensim. Output measures for each simulation were exported as a .csv file and assessed using an Excel workbook created to confirm reasonable model behavior.

Table 15.1 Sensitivity Analysis Definition (see Table 15.2 for normal slider ranges)

Variable	Min	Max*
Basic Controls		
Source tax delivered coal tce	0	1000
Source tax delivered oil boe	0	1000
Source tax delivered gas MCF	0	20
Source tax delivered bio boe	0	1000
Source tax renewables kWh	-0.1	0
Carbon tax initial target	0	1000
Annual improvement to energy efficiency of new capital stationary	-1	5
Annual improvement to energy efficiency of new capital transport	-1	5
Electric carrier subsidy stationary	0	100
Electric carrier subsidy with required comp assets	0	100
Percent available land for afforestation	0	100
Non afforestation Percent of max CDR achieved	0	100
Advanced Controls		
Damage function on	0	1
No new coal	0	100
No new oil	0	100
No new gas	0	100
Utilization adjustment factor delivered coal	0	100
Utilization adjustment factor delivered oil	0	100
Utilization adjustment factor delivered gas	0	100

Table 15.2 Actual En-ROADS slider ranges (some values in Table 15.1 go beyond these limits)

Variable	Min	Max
Basic Controls		
Source subsidy delivered coal tce	0	110
Source subsidy delivered oil boe	0	100
Source subsidy delivered gas MCF	0	5
Source subsidy delivered bio boe	0	30
Source subsidy renewables kWh	-0.03	0
Carbon tax initial target	0	250
Electric carrier subsidy stationary	0	50
Electric carrier subsidy with required comp assets	0	50

Output variables for the sensitivity analyses include:

- Final energy by each carrier for each end use[EndUseSector, Carrier]
- Total Primary Energy Demand
- Primary energy demand of coal
- Primary energy demand of oil
- Primary energy demand of gas
- Primary energy demand of bio
- Primary energy demand of nuclear
- Primary energy demand of renewables
- Primary energy demand of hydro
- Market price of electricity
- Market price of delivered fuels for nonelec carriers[Primary Fuels]
- Adjusted cost of energy per GJ
- CO2 emissions from energy
- Temperature change from 1850

Varying Key Assumptions

Additionally, using random triangular distribution, another set of sensitivity analyses tested the effects of varying key assumptions with actions. Results indicate that, regardless of these assumptions, the relative effect these actions have on the system are robust.

References

Climate Interactive Data Files: Data.vdfx, Created from En-ROADS data model (Data.mdl). Global-RS GHG.vdfx, from C-ROADS.mdl. EnROADS-Calc.vdfx, Created from (En-ROADS-RS.mdl). NGFS-Scenarios.vdfx, Created from NGFS data model, dated 11/11/2023. SSP v2 Global Data, Created from SSP v2 data model, dated 11/08/2019.

Ackerman, F. & Stanton, E. (2012). Climate risks and carbon prices: Revising the social cost of carbon. *Econ. Open-Access Open-Assess. E-J.* 6, 10.

Albertus, P. (2020). Long-Duration Electricity Storage Applications, Economics, and Technologies, 2020 [https://www.cell.com/joule/pdf/S2542-4351\(19\)30539-2.pdf](https://www.cell.com/joule/pdf/S2542-4351(19)30539-2.pdf).

Bastin, J.-F., et al. (2020). Erratum for the Report: "The global tree restoration potential" by J.-F. Bastin, Y. Finegold, C. Garcia, D. Mollicone, M. Rezende, D. Routh, C. M. Zohner, T. W. Crowther and for the Technical Response "Response to Comments on 'The global tree restoration potential'" by J.-F. Bastin, Y. Finegold, C. Garcia, N. Gellie, A. Lowe, D. Mollicone, M. Rezende, D. Routh, M. Sacande, B. Sparrow, C. M. Zohner, T. W. Crowther, . *Science*, 368(6494): eabc8905.

Bernie, D., Lowe, J., Tyrrell, T., Legge, O. (2010). Influence of Mitigation Policy on Ocean Acidification. *Geophysical Research Letters*, 37:L15704.

Björkström, Anders. (1986). One-Dimensional and Two-Dimensional Ocean Models for Predicting the Distribution of CO₂ Between the Ocean and the Atmosphere. 10.1007/978-1-4757-1915-4_14.

Burke, M., Hsiang, S. M. & Miguel, E. (2015). Global non-linear effect of temperature on economic production. *Nature* 527, 235–239.

Burke, M., Davis, W. M. & Diffenbaugh, N. S. (2018). Large potential reduction in economic damages under UN mitigation targets. *Nature* 557, 549–553.

Caldecott, Ben, Lomax, Guy, & Workman, Max. (2015). Stranded Carbon Assets and Negative Emission Technologies (Working Paper). University of Oxford Stranded Assets Programme. Retrieved from <http://www.smithschool.ox.ac.uk/research-programmes/stranded-assets/Stranded%20Carbon%20Assets%20and%20NETs%20-%2006.02.15.pdf>

Covington, H. and R. Thamotheram. (2015). The Case for Forceful Stewardship (Part 1): The Financial Risk from Global Warming. Available at SSRN: <https://ssrn.com/abstract=2551478> or <http://dx.doi.org/10.2139/ssrn.2551478>

Dietz, S. & Stern, N. (2015). Endogenous growth, convexity of damage and climate risk: how Nordhaus' framework supports deep cuts in carbon emissions. *Econ. J.* 125, 574–620.

EDGAR (Emissions Database for Global Atmospheric Research) Community GHG Database, a collaboration between the European Commission, Joint Research Centre (JRC), the International Energy Agency (IEA), and comprising IEA-EDGAR CO₂, EDGAR CH₄, EDGAR N₂O, EDGAR F-GASES version 7.0, (2022) European Commission, JRC (Datasets). The complete citation of the EDGAR Community GHG Database is available in the 'Sources and References' section.

Energy Institute. (2024). Statistical Review of World Energy, 73rd Edition. <https://www.energyinst.org/statistical-review>.

Erb, K.-H., Kastner, T., Plutzar, C., Bais, A. L. S., Carvalhais, N., Fetzl, T., Gingrich, S., Haberl, H., Lauk, C., Niedertscheider, M., Pongratz, J., Thurner, M., & Luyssaert, S. (2018). Unexpectedly large impact of forest management and grazing on global vegetation biomass. *Nature*, 553(7686), 73–76.
<https://doi.org/10.1038/nature25138>.

Fares, R.L. and C.W. King. (2016). Trends in Transmission, Distribution, and Administration Costs for U.S. Investor Owned Electric Utilities. White Paper UTEI/2016-06-1.
https://energy.utexas.edu/sites/default/files/UTAustin_FCe_TDA_2016.pdf.

Fiddaman, T. (1997). Feedback complexity in integrated climate-economy models.
<https://dspace.mit.edu/handle/1721.1/10154>

Fiddaman, T., L.S. Siegel, E. Sawin, A.P. Jones, and J. Sterman. (2023). C-ROADS Technical Reference.
<https://www.climateinteractive.org/c-roads-technical-reference>

Food and Agriculture Organization of the United Nations (FAO). FAOStat Database.
<https://www.fao.org/faostat/en/#data>.

Friedlingstein, P., O'Sullivan, M., Jones, M. W., Andrew, R. M., Bakker, D. C. E., Hauck, J., Landschützer, P., Le Quéré, C., Luijkx, I. T., Peters, G. P., Peters, W., Pongratz, J., Schwingshackl, C., Sitch, S., Canadell, J. G., Ciais, P., Jackson, R. B., Alin, S. R., Anthoni, P., Barbero, L., Bates, N. R., Becker, M., Bellouin, N., Decharme, B., Bopp, L., Brasika, I. B. M., Cadule, P., Chamberlain, M. A., Chandra, N., Chau, T.-T.-T., Chevallier, F., Chini, L. P., Cronin, M., Dou, X., Enyo, K., Evans, W., Falk, S., Feely, R. A., Feng, L., Ford, D. J., Gasser, T., Ghattas, J., Gkritzalis, T., Grassi, G., Gregor, L., Gruber, N., Gürses, Ö., Harris, I., Hefner, M., Heinke, J., Houghton, R. A., Hurtt, G. C., Iida, Y., Ilyina, T., Jacobson, A. R., Jain, A., Jarníková, T., Jersild, A., Jiang, F., Jin, Z., Joos, F., Kato, E., Keeling, R. F., Kennedy, D., Klein Goldewijk, K., Knauer, J., Korsbakken, J. I., Kötzinger, A., Lan, X., Lefèvre, N., Li, H., Liu, J., Liu, Z., Ma, L., Marland, G., Mayot, N., McGuire, P. C., McKinley, G. A., Meyer, G., Morgan, E. J., Munro, D. R., Nakaoka, S.-I., Niwa, Y., O'Brien, K. M., Olsen, A., Omar, A. M., Ono, T., Paulsen, M., Pierrot, D., Pocock, K., Poulter, B., Powis, C. M., Rehder, G., Resplandy, L., Robertson, E., Rödenbeck, C., Rosan, T. M., Schwinger, J., Séférian, R., Smallman, T. L., Smith, S. M., Sospedra-Alfonso, R., Sun, Q., Sutton, A. J., Sweeney, C., Takao, S., Tans, P. P., Tian, H., Tilbrook, B., Tsujino, H., Tubiello, F., van der Werf, G. R., van Oijen, E., Wanninkhof, R., Watanabe, M., Wimart-Rousseau, C., Yang, D., Yang, X., Yuan, W., Yue, X., Zaehle, S., Zeng, J., and Zheng, B.: Global Carbon Budget 2023, *Earth Syst. Sci. Data*, 15, 5301–5369, <https://doi.org/10.5194/essd-15-5301-2023>, 2023.

Fung, I. et al. (1991). Three-dimensional model synthesis of the global methane cycle. *J. Geophys. Res.*, 96, 13033–13065, doi:10.1029/91JD01247.

Gasser, T., Crepin, L., Quilcaille, Y., Houghton, R. A., Ciais, P., and Obersteiner, M.: Historical CO₂ emissions from land use and land cover change and their uncertainty, *Biogeosciences*, 17, 4075–4101,
<https://doi.org/10.5194/bg-17-4075-2020>, 2020. Plus direct communication on March 24, 2022 by the lead author, Thomas Gasser.

Gaunt, J. L., & Lehmann, J. (2008) Energy Balance and Emissions Associated with Biochar Sequestration and Pyrolysis Bioenergy Production. *Environmental Science & Technology*, 42(11), 4152–4158.
<https://doi.org/10.1021/es071361i>

Gitz, V., and P. Ciais (2003), Amplifying effects of land-use change on future atmospheric CO₂ levels, *Global Biogeochem. Cycles*, 17, 1024, doi:10.1029/2002GB001963, 1.

Glanemann, N., Willner, S. N. & Levermann, A. (2020). Paris Climate Agreement passes the cost-benefit test. *Nat. Commun.* 11, 1–11.

Global Carbon Budget (GCB). (2022) Pierre Friedlingstein, Michael O'Sullivan, Matthew W. Jones, Robbie M. Andrew, Luke Gregor, Judith Hauck, and many others. Global Carbon Budget 2022, Earth Syst. Sci. Data, 2022. https://globalcarbonbudget.org/wp-content/uploads/GCB2022_ESSD_Paper.pdf.

Goddard Institute for Space Studies (GISS) (2024) GISTEMP4 Global Mean Estimates based on Land and Ocean Data 1880-2023.

Goudriaan, J. and Ketner, P. (1984) A Simulation Study for the Global Carbon Cycle, Including Man's Impact on the Biosphere. Climatic Change, 6:167-192.

Greenstone, M., Kopits, E. & Wolverton, A. (2013). Developing a Social Cost of Carbon for US Regulatory Analysis: A Methodology and Interpretation. Review of Environmental Economics and Policy 7, 23–46.

Gütschow, J.; Pflüger, M. (2023): The PRIMAP-hist national historical emissions time series v2.4.2 (1750-2021). zenodo. doi:10.5281/zenodo.7727475.

Gütschow, J., Jeffery, L., Gieseke, R., Gebel, R., Stevens, D., Krapp, M., Rocha, M. (2016). The PRIMAP-hist national historical emissions time series, Earth Syst. Sci. Data, 8, 571-603, <https://dx.doi.org/10.5194/essd-8-571-2016>.

Hanemann, W. M. (2008). What is the economic cost of climate change?.

HDR GSFC. 2021. Global Mean Sea Level Trend from Integrated Multi-Mission Ocean Altimeters TOPEX/Poseidon, Jason-1, OSTM/Jason-2, and Jason-3 Version 5.1. Ver. 5.1 PO.DAAC, CA, USA.

<https://doi.org/10.5067/GMSLM-TJ151>. Dataset accessed 07/12/2023.

https://archive.podaac.earthdata.nasa.gov/podaac-ops-cumulus-protected/MERGED_TP_J1_OSTM_OST_GMSL_ASCII_V51/GMSL_TPJAOS_5.1_199209_202303.txt

Houghton, R. A., and A. A. Nassikas (2017). Global and regional fluxes of carbon from land use and land cover change 1850–2015, Global Biogeochem. Cycles, 31.doi:10.1002/2016GB005546.

Huang, J., Yu, H., Guan, X. et al. (2016). Accelerated dryland expansion under climate change. Nature Clim Change 6, 166–171. <https://doi.org/10.1038/nclimate2837>

Humpenöder, F., Popp, A., Dietrich, J. P., Klein, D., Lotze-Campen, H., Markus Bonsch, Müller, C. (2014). Investigating afforestation and bioenergy CCS as climate change mitigation strategies. Environmental Research Letters, 9(6), 064029. <https://doi.org/10.1088/1748-9326/9/6/064029>

Hunter, Chad and Penev, Michael and Reznicek, Evan P. and Eichman, Joshua and Rustagi, Neha and Baldwin, Samuel F., Techno-Economic Analysis of Long-Duration Energy Storage and Flexible Power Generation Technologies to Support High Variable Renewable Energy Grids. Available at SSRN: <https://ssrn.com/abstract=3720769> or <http://dx.doi.org/10.2139/ssrn.3720769>

Hurt, G. C., L. Chini, R. Sahajpal, S. Frolking, B. L. Bodirsky, K. Calvin, J. C. Doelman, J. Fisk, S. Fujimori, K. K. Goldewijk, T. Hasegawa, P. Havlik, A. Heinemann, F. Humpenöder, J. Jungclaus, Jed Kaplan, J. Kennedy, T. Kristzén, D. Lawrence, P. Lawrence, L. Ma, O. Mertz, J. Pongratz, A. Popp, B. Poulter, K. Riahi, E. Sheviakova, E. Stehfest, P. Thornton, F. N. Tubiello, D. P. van Vuuren, X. Zhang. (2020). Harmonization of Global Land-Use Change and Management for the Period 850-2100 (LUH2) for CMIP6. Geoscientific Model Development. DOI: 10.5194/gmd-2019-360; <https://luh.umd.edu/>

International Energy Agency (IEA). (2023). World Energy Outlook (WEO). World data for final and primary energy by source and sector, and CO₂ emissions. <https://www.iea.org/weo>

IEA. (2024). World Energy Balances and World Energy Statistics Datasets. 1990-2022. <https://www.iea.org/data-and-statistics/data-product/world-energy-statistics-balances>.

IEA. (2023). World Energy Balances. <https://www.iea.org/reports/world-energy-balances-overview>

IEA. (2020). Evolution of solar PV module cost by data source, 1970-2020, IEA, Paris. <https://www.iea.org/data-and-statistics/charts/evolution-of-solar-pv-module-cost-by-data-source-1970-2020> License: CC BY 4.0.

Intergovernmental Panel on Climate Change (IPCC). 2018. Special Report - Global Warming of 1.5o C.

Intergovernmental Panel on Climate Change (IPCC). (2023): Summary for Policymakers. In: Climate Change 2023: Synthesis Report. A Report of the Intergovernmental Panel on Climate Change. Contribution of Working Groups I, II and III to the Sixth Assessment Report of the Intergovernmental Panel on Climate Change [Core Writing Team, H. Lee and J. Romero (eds.)]. IPCC, Geneva, Switzerland, (in press).

IPCC. (2021): Climate Change 2021: The Physical Science Basis. Contribution of Working Group I to the Sixth Assessment Report of the Intergovernmental Panel on Climate Change [Masson-Delmotte, V., P. Zhai, A. Pirani, S.L. Connors, C. Péan, S. Berger, N. Caud, Y. Chen, L. Goldfarb, M.I. Gomis, M. Huang, K. Leitzell, E. Lonnoy, J.B.R. Matthews, T.K. Maycock, T. Waterfield, O. Yelekçi, R. Yu, and B. Zhou (eds.)]. Cambridge University Press, Cambridge, United Kingdom and New York, NY, USA, In press, doi:10.1017/9781009157896.

IPCC. (2021): AR6 WG1, Chapter 5. Canadell, J.G., P.M.S. Monteiro, M.H. Costa, L. Cotrim da Cunha, P.M. Cox, A.V. Eliseev, S. Henson, M. Ishii, S. Jaccard, C. Koven, A. Lohila, P.K. Patra, S. Piao, J. Rogelj, S. Syampungani, S. Zaehle, and K. Zickfeld, 2021: Global Carbon and other Biogeochemical Cycles and Feedbacks. In Climate Change 2021: The Physical Science Basis. Contribution of Working Group I to the Sixth Assessment Report of the Intergovernmental Panel on Climate Change [Masson-Delmotte, V., P. Zhai, A. Pirani, S.L. Connors, C. Péan, S. Berger, N. Caud, Y. Chen, L. Goldfarb, M.I. Gomis, M. Huang, K. Leitzell, E. Lonnoy, J.B.R. Matthews, T.K. Maycock, T. Waterfield, O. Yelekçi, R. Yu, and B. Zhou (eds.)]. Cambridge University Press, Cambridge, United Kingdom and New York, NY, USA, pp. 673–816, doi: 10.1017/9781009157896.007.

IPCC. (2021): AR6 WG1, Chapter 6. Szopa, S., V. Naik, B. Adhikary, P. Artaxo, T. Berntsen, W.D. Collins, S. Fuzzi, L. Gallardo, A. Kiendler-Scharr, Z. Klimont, H. Liao, N. Unger, and P. Zanis, 2021: Short-Lived Climate Forcers. In Climate Change 2021: The Physical Science Basis. Contribution of Working Group I to the Sixth Assessment Report of the Intergovernmental Panel on Climate Change [Masson-Delmotte, V., P. Zhai, A. Pirani, S.L. Connors, C. Péan, S. Berger, N. Caud, Y. Chen, L. Goldfarb, M.I. Gomis, M. Huang, K. Leitzell, E. Lonnoy, J.B.R. Matthews, T.K. Maycock, T. Waterfield, O. Yelekçi, R. Yu, and B. Zhou (eds.)]. Cambridge University Press, Cambridge, United Kingdom and New York, NY, USA, pp. 817–922, doi: 10.1017/9781009157896.008.

IPCC. (2021): AR6 WG1, Chapter 7. Forster, P., T. Storelvmo, K. Armour, W. Collins, J.-L. Dufresne, D. Frame, D.J. Lunt, T. Mauritsen, M.D. Palmer, M. Watanabe, M. Wild, and H. Zhang, 2021: The Earth's Energy Budget, Climate Feedbacks, and Climate Sensitivity. In Climate Change 2021: The Physical Science Basis. Contribution of Working Group I to the Sixth Assessment Report of the Intergovernmental Panel on Climate Change [Masson-Delmotte, V., P. Zhai, A. Pirani, S.L. Connors, C. Péan, S. Berger, N. Caud, Y. Chen, L. Goldfarb, M.I. Gomis, M. Huang, K. Leitzell, E. Lonnoy, J.B.R. Matthews, T.K. Maycock, T. Waterfield, O. Yelekçi, R. Yu, and B. Zhou (eds.)]. Cambridge University Press, Cambridge, United Kingdom and New York, NY, USA, pp. 923–1054, doi: 10.1017/9781009157896.009.

IPCC. (2021): AR6 Technical Summary. Arias, P.A., N. Bellouin, E. Coppola, R.G. Jones, G. Krinner, J. Marotzke, V. Naik, M.D. Palmer, G.-K. Plattner, J. Rogelj, M. Rojas, J. Sillmann, T. Storelvmo, P.W. Thorne, B. Trewin, K. Achuta Rao, B. Adhikary, R.P. Allan, K. Armour, G. Bala, R. Barimalala, S. Berger, J.G. Canadell, C. Cassou, A. Cherchi, W. Collins, W.D. Collins, S.L. Connors, S. Corti, F. Cruz, F.J. Dentener, C. Dereczynski, A. Di Luca, A. Diongue Niang, F.J. Doblas-Reyes, A. Dosio, H. Douville, F. Engelbrecht, V. Eyring, E. Fischer, P. Forster, B. Fox-Kemper, J.S. Fuglestvedt, J.C. Fyfe, N.P. Gillett, L. Goldfarb, I. Gorodetskaya, J.M. Gutierrez, R. Hamdi, E. Hawkins, H.T. Hewitt, P. Hope, A.S. Islam, C. Jones, D.S. Kaufman, R.E. Kopp, Y. Kosaka, J. Kossin, S. Kravoska, J.-Y. Lee, J. Li, T. Mauritzen, T.K. Maycock, M. Meinshausen, S.-K. Min, P.M.S. Monteiro, T. Ngo-Duc, F. Otto, I. Pinto, A. Pirani, K. Raghavan, R. Ranasinghe, A.C. Ruane, L. Ruiz, J.-B. Sallée, B.H. Samset, S. Sathyendranath, S.I. Seneviratne, A.A. Sörensson, S. Szopa, I. Takayabu, A.-M. Tréguier, B. van den Hurk, R. Vautard, K. von Schuckmann, S. Zaehle, X. Zhang, and K. Zickfeld, 2021: Technical Summary. In Climate Change 2021: The Physical Science Basis. Contribution of Working Group I to the Sixth Assessment Report of the Intergovernmental Panel on Climate Change [Masson-Delmotte, V., P. Zhai, A. Pirani, S.L. Connors, C. Péan, S. Berger, N. Caud, Y. Chen, L. Goldfarb, M.I. Gomis, M. Huang, K. Leitzell, E. Lonnoy, J.B.R. Matthews, T.K. Maycock, T. Waterfield, O. Yelekçi, R. Yu, and B. Zhou (eds.)]. Cambridge University Press, Cambridge, United Kingdom and New York, NY, USA, pp. 33–144, doi:10.1017/9781009157896.002.

IPCC. (2021): AR6 Summary for Policymakers. In: Climate Change 2021: The Physical Science Basis. Contribution of Working Group I to the Sixth Assessment Report of the Intergovernmental Panel on Climate Change [Masson-Delmotte, V., P. Zhai, A. Pirani, S.L. Connors, C. Péan, S. Berger, N. Caud, Y. Chen, L. Goldfarb, M.I. Gomis, M. Huang, K. Leitzell, E. Lonnoy, J.B.R. Matthews, T.K. Maycock, T. Waterfield, O. Yelekçi, R. Yu, and B. Zhou (eds.)]. Cambridge University Press, Cambridge, United Kingdom and New York, NY, USA, pp. 3–32, doi:10.1017/9781009157896.001.

IPCC AR6 WG3. (2021).

https://github.com/chrisroadmap/ar6/blob/main/data_output/fair_wg3_natural_ch4_n2o.csv.

IRENA. (2023). Renewable Power Generation Costs in 2022, International Renewable Energy Agency, Abu Dhabi. <https://www.irena.org/Publications/2023/Aug/Renewable-power-generation-costs-in-2022>

IRENA. (2020). Taylor, Michael. Energy subsidies: Evolution in the global energy transformation to 2050, International Renewable Energy Agency, Abu Dhabi.

Keen, S. (2020). The appallingly bad neoclassical economics of climate change. Globalizations 1–29.

Keller, A.A., Goldstein, R.A. (1995). Oceanic transport and storage of carbon emissions. Climatic Change 30, 367–395. <https://doi.org/10.1007/BF01093853>

Koornneef, Joris, van Breevoort, Pieter, Hamelinck, Carlo, Hendriks, Chris, Hoogwijk, Monique, Koop, Klaas, & Koper, Michele. (2011). Potential for Biomass and Carbon Dioxide Capture and Storage. EcoFys for IEA GHG. Retrieved from https://www.eenews.net/assets/2011/08/04/document_cw_01.pdf

Kriegler, E., Edenhofer, O., Reuster, L., Luderer, G., & Klein, D. (2013). Is atmospheric carbon dioxide removal a game changer for climate change mitigation? Climatic Change, 118(1), 45–57. <https://doi.org/10.1007/s10584-012-0681-4>

Lawrence Berkeley National Laboratory. (2022). Utility-Scale Solar. <https://emp.lbl.gov/utility-scale-solar>

Lazard (2023). Lazard's Levelized Cost of Energy Analysis – Version 16.0. <https://www.lazard.com/media/2ozoovyg/lazards-lcoeplus-april-2023.pdf>

- Lenton, T. M. (2010). The potential for land-based biological CO₂ removal to lower future atmospheric CO₂ concentration. *Carbon Management*, 1(1), 145–160. <https://doi.org/10.4155/cmt.10.12>
- Maddison, A. (2008). Historical Statistics for the World Economy: 1-2006 AD. Conference Board and Groningen Growth and Development Centre, Total Economy Database, www.ggdc.net/MADDISON/oriindex.htm.
- Massachusetts Institute of Technology (MIT). (2012). Joint Program Energy and Climate Outlook. <http://globalchange.mit.edu/Outlook2012>.
- McDonald, A., Schrattenholzer, L. (2001). Learning rates for energy technologies. *Energy Policy* 29, 255-261.
- McLaren, D. (2012). A comparative global assessment of potential negative emissions technologies. *Process Safety and Environmental Protection*, 90, 489–500. <https://doi.org/10.1016/j.psep.2012.10.005>
- Meinshausen, M., S. Smith et al. (2011). "The RCP GHG concentrations and their extension from 1765 to 2300", DOI 10.1007/s10584-011-0156-z, *Climatic Change*.
- Meinshausen, M., N. Meinshausen, W. Hare, S.C.B. Raper, K. Frieler, R. Knutti, D.J. Frame, and M.R. Allen. (2009). Greenhouse-gas emission targets for limiting global warming to 20C. *Nature*. 458: 1158-1163.
- Miller, R.L., G.A. Schmidt, L.S. Nazarenko, et al. (2015). CMIP5 historical simulations (1850-2012) with GISS ModelE2. *J. Adv. Model. Earth Syst.*, 6, no. 2, 441-477, doi:10.1002/2013MS000266.
- Mo, L., Zohner, C. M., Reich, P. B., Liang, J., de Miguel, S., Nabuurs, G.-J., Renner, S. S., van den Hoogen, J., Araza, A., Herold, M., Mirzagholi, L., Ma, H., Averill, C., Phillips, O. L., Gamarra, J. G. P., Hordijk, I., Routh, D., Abegg, M., Adou Yao, Y. C., Crowther, T. W. (2023). Integrated global assessment of the natural forest carbon potential. *Nature*, 624(7990), 92-101. <https://doi.org/10.1038/s41586-023-06723-z>.
- Morice, C.P., J.J. Kennedy, N.A. Rayner, J.P. Winn, E. Hogan, R.E. Killick, R.J.H. Dunn, T.J. Osborn, P.D. Jones and I.R. Simpson (in press) An updated assessment of near-surface temperature change from 1850: the HadCRUT5 dataset. *Journal of Geophysical Research (Atmospheres)* doi:10.1029/2019JD032361 (supporting information).
- National Oceanic & Atmospheric Administration (NOAA). (2024). Lan, X., K.W. Thoning, and E.J. Dlugokencky: Trends in globally-averaged CO₂, CH₄, N₂O, and SF₆ determined from NOAA Global Monitoring Laboratory measurements. 2024-02, <https://gml.noaa.gov/ccgg/trends/>.
- National Research Council. (2015). Climate Intervention: Carbon Dioxide Removal and Reliable Sequestration. Retrieved from <https://www.nap.edu/catalog/18805/climate-intervention-carbon-dioxide-removal-and-reliable-sequestration>.
- Network for Greening the Financial System (NGFS) (2023). Version 4.1. <https://www.ngfs.net/ngfs-scenarios-portal/data-resources/> and NGFS Scenarios Technical Documentation. 2023. <https://www.ngfs.net/en/ngfs-climate-scenarios-phase-iv-november-2023>.
- Nordhaus W. D. (1994). Managing the commons: The economics of climate change. MIT Press.
- Nordhaus W. D. (2000). Warming the World: Economic Models of Global Warming. MIT Press.
- Nordhaus, W. D. (2007). Accompanying notes and documentation on development of DICE-2007 model: Notes on DICE-2007. v8 of September 21, 2007. N. Hav. CT Yale Univ.
- Nordhaus, W. & Sztorc, P. (2013). DICE 2013R: Introduction and user's manual.

Our World in Data. Primary energy and electricity generated by source. Retrieved September 2020.
<https://ourworldindata.org/grapher/global-primary-energy> and <https://ourworldindata.org/grapher/electricity-production-source-stacked?tab=table&year=latest&time=earliest..latest>.

Oeschger, Siegenthaler et al. (1975). A box diffusion model to study the carbon dioxide exchange in nature. Tellus, 27: 168-192. <https://doi.org/10.1111/j.2153-3490.1975.tb01671.x>

Ostberg, S., Lucht, W., Schaphoff, S., and Gerten, D. (2013). Critical impacts of global warming on land ecosystems. Earth Syst. Dynam., 4(2), 347–357. <https://doi.org/10.5194/esd-4-347-2013>.

Ricke, K., Drouet, L., Caldeira, K. & Tavoni, M. (2018). Country-level social cost of carbon. Nat. Clim. Change 8, 895–900.

Rotmans, J. (1990). IMAGE, An integrated model to assess the greenhouse effect. Kluwer Academic Publishers.

Royal Society Report. (2018). Greenhouse Gas Removal.

<https://royalsociety.org/~media/policy/projects/greenhouse-gas-removal/royal-society-greenhouse-gas-removal-report-2018.pdf>.

Sand, M., Skeie, R.B., Sandstad, M (2023). A multi-model assessment of the Global Warming Potential of hydrogen. Commun Earth Environ 4, 203. <https://doi.org/10.1038/s43247-023-00857-8>.

Saunois, M., Stavert, A. R., Poulter, B., Bousquet, P., Canadell, J. G., Jackson, R. B., Raymond, P. A., Dlugokencky, E. J., Houweling, S., Patra, P. K., Ciais, P., Arora, V. K., Bastviken, D., Bergamaschi, P., Blake, D. R., Brailsford, G., Bruhwiler, L., Carlson, K. M., Carroll, M., Castaldi, S., Chandra, N., Crevoisier, C., Crill, P. M., Covey, K., Curry, C. L., Etiope, G., Frankenberg, C., Gedney, N., Hegglin, M. I., Höglund-Isaksson, L., Hugelius, G., Ishizawa, M., Ito, A., Janssens-Maenhout, G., Jensen, K. M., Joos, F., Kleinen, T., Krummel, P. B., Langenfelds, R. L., Laruelle, G. G., Liu, L., Machida, T., Maksyutov, S., McDonald, K. C., McNorton, J., Miller, P. A., Melton, J. R., Morino, I., Müller, J., Murguia-Flores, F., Naik, V., Niwa, Y., Noce, S., O'Doherty, S., Parker, R. J., Peng, C., Peng, S., Peters, G. P., Prigent, C., Prinn, R., Ramonet, M., Regnier, P., Riley, W. J., Rosentreter, J. A., Segers, A., Simpson, I. J., Shi, H., Smith, S. J., Steele, L. P., Thornton, B. F., Tian, H., Tohjima, Y., Tubiello, F. N., Tsuruta, A., Viovy, N., Voulgarakis, A., Weber, T. S., van Weele, M., van der Werf, G. R., Weiss, R. F., Worthy, D., Wunch, D., Yin, Y., Yoshida, Y., Zhang, W., Zhang, Z., Zhao, Y., Zheng, B., Zhu, Q., Zhu, Q., and Zhuang, Q.: The Global Methane Budget 2000–2017, Earth Syst. Sci. Data, 12, 1561–1623, <https://doi.org/10.5194/essd-12-1561-2020>, 2020.

Shaner, M., Davis, S.J., Lewis, N.S., and Caldeira, K., (2018). Geophysical constraints on the reliability of solar and wind power in the United States. Energy & Environmental Science. Issue 4.

Shell. (2018). Sky Scenario. <https://www.shell.com/energy-and-innovation/the-energy-future/scenarios/shell-scenario-sky.html>

Schneider, S. H., and Thompson, S. L. (1981). Atmospheric CO₂ and climate: Importance of the transient response, J. Geophys. Res., 86(C4), 3135– 3147, <https://doi.org/10.1029/JC086iC04p03135>.

Smith, J. E., Heath, L. S., Skog, K. E., & Birdsey, R. A. (2006). *Methods for calculating forest ecosystem and harvested carbon with standard estimates for forest types of the United States*. U.S. Department of Agriculture, Forest Service, Northeastern Research Station.

Smith, P., Davis, S. J., Creutzig, F., Fuss, S., Minx, J., Gabrielle, B., Yongsung, C. (2016). Biophysical and economic limits to negative CO₂ emissions. Nature Climate Change, 6(1), 42–50. <https://doi.org/10.1038/nclimate2870>

Socolow, R. H. and S. H. Lam (2007). Good Enough Tools for Global Warming Policy Making. Philosophical Transactions v365 n1853. <https://www.jstor.org/stable/25190479>

Solomon, A.A., Child, M., Caldera, U. Breyer, C. 2017. How much energy storage is needed to incorporate very large intermittent renewables? Energy Procedia, Volume 135, Pages 283-293, <https://doi.org/10.1016/j.egypro.2017.09.520>. (<https://www.sciencedirect.com/science/article/pii/S1876610217346258>).

SSP Database (Shared Socioeconomic Pathways) (2018). Version 2.0. Available at: <https://tntcat.iiasa.ac.at/SspDb>.

Taconet, N., Méjean, A. & Guivarc'h, C. (2020). Influence of climate change impacts and mitigation costs on inequality between countries. Clim. Change 1–20.

Tol, R. S. (2009). The economic effects of climate change. J. Econ. Perspect. 23, 29–51.

US EIA. (2019). Levelized Cost and Levelized Avoided Cost of New Generation Resources in the Annual Energy Outlook 2020. https://www.eia.gov/outlooks/aoe/pdf/electricity_generation.pdf.

US EIA. (2019). Electricity prices reflect rising delivery costs, declining power production costs. <https://www.eia.gov/todayinenergy/detail.php?id=32812>.

US EIA. (2016). Short-Term Energy Outlook. Short-Term Energy Outlook Real and Nominal Prices. December 2016.

US EIA. (2011). Annual Energy Outlook. DOE/EIA-0383. AEO₂₀₁₁ National Energy Modeling System. www.eia.gov/aeo.

US EIA. (2009). Annual Energy Review. Historical energy for transition comparisons.

United Nations, Department of Economic and Social Affairs, Population Division (2024). World Population Prospects: The 2024 Revision. <https://population.un.org/wpp>.

UNEP. (2016). Kigali Amendment Fact Sheet. <https://multimedia.3m.com/mws/media/13659240/unep-fact-sheet-kigali-amendment-to-mp.pdf>

van Vuuren, D. P., Deetman, S., van Vliet, J., van den Berg, M., van Ruijven, B. J., & Koelbl, B. (2013). The role of negative CO₂ emissions for reaching 2 °C--insights from integrated assessment modelling. Climatic Change; Dordrecht, 118(1), 15–27. <https://doi.org/http://dx.doi.org.libproxy.tulane.edu:2048/10.1007/s10584-012-0680-5>

Vermeer, M. and S. Rahmstorf. (2009). Global sea level linked to global temperature. Proc of the Nat Acad of Sci. 106(51):21527-21532. www.pnas.org/cgi/doi/10.1073/pnas.0907765106.

Walker, W. S., Gorelik, S. R., Cook-Patton, S. C., Baccini, A., Farina, M. K., Solvik, K. K., Ellis, P. W., Sanderman, J., Houghton, R. A., Leavitt, S. M., Schwalm, C. R., & Griscom, B. W. (2022). The global potential for increased storage of carbon on land. Proceedings of the National Academy of Sciences, 119(23), e2111312119. <https://doi.org/doi:10.1073/pnas.2111312119>.

Warszawski, L., Friend, A., Ostberg, S., Frieler, K., Lucht, W., Schaphoff, S., Schellnhuber, H. J. (2013). A multi-model analysis of risk of ecosystem shifts under climate change. Environmental Research Letters, 8(4), 044018. <http://dx.doi.org/10.1088/1748-9326/8/4/044018>.

Weagle, C. L. et al. (2018). Global Sources of Fine Particulate Matter: Interpretation of PM2.5 Chemical Composition Observed by SPARTAN using a Global Chemical Transport Model. Environ Sci Technol. <https://doi.org/10.1021/acs.est.8b01658>.

Weber, T., N.A. Wiseman, N.A., and A. Kock. (2019). Global ocean methane emissions dominated by shallow coastal waters. Nat Commun 10, 4584. <https://doi.org/10.1038/s41467-019-12541-7>.

Weitzman, M. L. (2012). GHG targets as insurance against catastrophic climate damages. *J. Public Econ. Theory* 14, 221–244.

Woolf, D., Amonette, J. E., Street-Perrott, F. A., Lehmann, J., & Joseph, S. (2010). Sustainable biochar to mitigate global climate change. *Nature Communications*, 1, 1. <https://doi.org/10.1038/ncomms1053>

World Bank. (2023). World Development Indicators, 1960-2022.

<https://data.worldbank.org/indicator/NY.GDP.MKTP.PP.KD>. Constant \$ 2017 US (PPP).

Wullschleger, S.D., W.M. Post, and A.W. King. (1995). On the potential for a CO₂ fertilisation effect in forests: Estimates of the biotic growth factors based on 58 controlled exposure studies. In: *Biotic feedbacks in the global climate system: Will the warming feed the warming?*, ed. G.M. Woodwell and F.T. Mackenzie, 85–107. Oxford University Press, U.K.

Xu et al. (2021). Changes in global terrestrial live biomass over the 21st century. *Science Advances* v7 n27.

<https://www.science.org/doi/10.1126/sciadv.abe9829>



These materials are licensed under a [Creative Commons Attribution 4.0 International License](#). This license lets you remix, adapt, and build upon Climate Interactive's work, even commercially, as long as you give Climate Interactive credit for the original creation of the materials.